A STUDY OF THE PHOTOCHEMICAL STABILITY OF 3'-AZIDO-3'-DEOXYTHYMIDINE IN DIFFERENT SOLVENTS

by

LERATO JOY MOLLO

Submitted in fulfilment of the academic requirements for the degree of Master of Science in the

School of Chemistry and Physics,

University of KwaZulu-Natal,

Durban

September 2016

ABSTRACT

Acquired immunodeficiency syndrome (AIDS) is a disease that causes weakening of the human immune system which is thus unable to fight off infections initiated by the human immunodeficiency virus (HIV). HIV/AIDS is the fourth leading cause of death in the world and South Africa has one of the highest HIV infection rates in the world, with approximately 6.2 million people infected. Zidovudine (AZT) [1-[(2R, 4S, 5S)-4-azido-5-(hydroxymethyl) oxolan-2-yl]-5-methylpyrimidine-2,4-dione] was the first HIV drug approved by the US Food and Drug Administration (FDA) to treat HIV-infected patients. Its molecule consists of three photoactive groups, namely, the alkene, carbonyl and azido groups. This study focusses on the investigation of the photochemical stability of AZT in different media.

The photochemical stability of 3'-azido-3'-deoxythymidine (AZT) was investigated in different solvents, namely, water, methanol, ethanol, 2-propanol and acetonitrile. The samples were irradiated under different conditions of pH (3, 5 and 7) and concentration (5.01×10^{-2}, 4.94×10^{-4} and 2.39×10^{-4} M). The photoreactions were monitored by ultraviolet and visible (UV/Vis) spectroscopy and reversed-phase high performance liquid chromatography (RP-HPLC). Acetophenone was used as the internal standard for quantification of AZT. Photodegradation products were identified by using liquid chromatography-mass spectrometry (LC-MS).

The results show that the photodegradation of AZT is strongly dependent on the solvent, the pH of the solution as well as on the initial concentration. The UV/Vis spectra of AZT upon photolysis showed a hyperchromic effect both at 213 and 265 nm in all of the different solvents, pH and concentration conditions. However, the change in absorbance was inconsistent with respect to irradiation time. We proposed that this could be attributed to competitive absorption by the photoproducts. The hypsochromic effect was also observed

under all conditions of pH. A new absorption band at 355 nm was formed in acetonitrile which was predicted to be the result of the elimination of nitrogen to generate a nitrene as a reactive intermediate, which may further undergo intermolecular interaction with the solvent to form new photoproducts.

The photodegradation products of AZT retained almost the same retention time and UV spectra under all the different conditions of solvent, pH and concentration. This indicates that the photoproducts formed have the same chromophore as AZT, which we propose to be a thymine moiety. Three photoproducts were formed at pH 5 and 7 and two photoproducts were formed at pH 3. For the effect of the initial concentration, three photoproducts were formed at the intermediate concentration (4.94×10^{-4} M) in all the different solvents, investigated. Three photoproducts were also formed at the lowest concentration (2.39×10^{-4} M) in all solvents, except in ethanol (two photoproducts were observed). Only one photoproduct was formed at high concentration (5.01×10^{-2} M) in water and acetonitrile and two photoproducts were formed in alcoholic solutions (methanol, ethanol and 2-propanol). The HPLC peak area of AZT decreases with increase in irradiation time whereas the HPLC peak areas of the photoproducts increase with increase in irradiation time for all conditions of solvent, pH and concentration.

The photodegradation of AZT occurs faster as the dipole moment of the solvent increases in order: methanol < ethanol < water < acetonitrile, except for 2-propanol. The rate of photodegradation of AZT is more rapid at pH 7 than at pH 3 and 5. For water, methanol and 2-propanol, the rate of photodegradation was higher for the lowest concentration followed by the intermediate and then the highest concentration. For ethanol and acetonitrile, the rate of photodegradation was higher at the intermediate concentration followed by the lowest and highest concentrations. The mass spectral results revealed that the azido group was accountable for the photoreactivity of the drug. Thymine was found to be the major

photoproduct under all conditions of pH, solvent and concentration. Five photodegradation pathways were proposed to account for the photoproducts formed in protic and aprotic polar solvents.

PREFACE

The experimental work described in this dissertation was carried out in the School of Chemistry and Physics, University of KwaZulu-Natal, Westville Campus, from February 2014 to September 2016, under the supervision of Professor Bice S. Martincigh.

These studies represent original work by the author and have not otherwise been submitted in any form for any degree or diploma to any tertiary institution. Where use has been made of the work of others it is duly acknowledged in the text.

Signed: _____

Date: _____

DECLARATION 1 - PLAGIARISM

I, Lerato Joy Mollo, declare that

1. The research reported in this dissertation, except where otherwise indicated, is my original research.
2. This dissertation has not been submitted for any degree or examination at any other university.
3. This dissertation does not contain other persons' data, pictures, graphs or other information, unless specifically acknowledged as being sourced from other persons.
4. This dissertation does not contain other persons' writing, unless specifically acknowledged as being sourced from other researchers. Where other written sources have been quoted, then:
    a. Their words have been re-written but the general information attributed to them has been referenced.
    b. Where their exact words have been used, then their writing has been placed in italics and inside quotation marks, and referenced.
5. This dissertation does not contain text, graphics or tables copied and pasted from the Internet, unless specifically acknowledged, and the source being detailed in the dissertation and in the References sections.

Signed: _____

DECLARATION 2 - CONFERENCE PRESENTATIONS

Poster presentation 1

Authors: Lerato J. Mollo, Maryam A. Jordaan and Bice S. Martincigh

Title: Photochemical synthesis of derivatives of lamivudine

Conference: 5th IUPAC International Conference on Green Chemistry, 17-21 August 2014, Durban, South Africa

Poster presentation 2

Author: Lerato J. Mollo

Title: Photochemical synthesis of derivatives of lamivudine

Conference: College of Agriculture, Engineering and Science Postgraduate Research Day, 27 October 2014, University of KwaZulu-Natal, Westville Campus, Durban

Poster presentation 3

Authors: Lerato J. Mollo, Maryam A. Jordaan and Bice S. Martincigh

Title: A study of the photochemical stability of 3'-azido-3'-deoxythymidine in different solvents

Conference: 42nd National Convention of the South African Chemical Institute, 29 November – 4 December 2015, Durban, South Africa

Signed:_____

ACKNOWLEDGEMENTS

Firstly, I would like to give praise to Almighty God and my Lord Jesus Christ for the strength and perseverance throughout this study.

I would like to express my sincere gratitude to my supervisor, Prof. Bice S. Martincigh, for her help, guidance, continuous support and patience throughout the study.

I am very grateful to my family especially, to my daughter (Lubambo Malevu) and the Malevu family for their support, patience and love during difficult circumstances. I would also like to thank my family in Deeper Life Campus Church for all their support, love and care.

I give credit to my mentors and beloved pastors, Prof Aderemi Adewumi, Dr Joseph Adesina, Dr Micheal Olusanya and Dr Adebayo Adeniyi, for their guidance, support and encouragement throughout this study.

I would like to thank Dr Maryam A. Jordaan for her contribution and assistance throughout the study.

I would also like to thank my fellow colleagues, especially Dr Moses Ollengo and the lab technicians (Brian Ndlovu, Unathi Bongoza, Neal Broomhead and Anita Naidoo) for their assistance, patience and support.

Last, but not the least, I would like to thank UKZN for giving me the opportunity to register for this degree and the NRF for sponsoring me.

TABLE OF CONTENTS

CHAPTER 1

INTRODUCTION

It is well known that light and oxygen play a significant role both in our lives and the environment. However, they can change the properties of different materials and products. This is often observed as bleaching of coloured compounds or as a discoloration of colourless products. Photostability has been a main concern in the pharmaceutical industry, due to the increasing number of drugs found to be photochemically unstable. Over 250 pharmaceutical drugs have been found to be sensitive to light [1, 2]. Light acts by interacting with the drug molecules and endogenous substrates, which may further result in photodecomposition of the drugs that consequently may lead to the loss of potency and therapeutic effects. The photostabilities of several classes of drugs, such as antimalarials, phenothiazines, non-steroidal anti-inflammatory agents, etc., have been thoroughly investigated [3].

The research described in this dissertation concerns the photostability of zidovudine (AZT), commercially known as Retrovir®, that belongs to the class of nucleoside reverse transcriptase inhibitors (NRTIs). Its chemical name is 3'-azido-3'-deoxythymidine and its structure is shown in **Fig. 1.1**. It is the first human immunodeficiency virus (HIV) drug approved by the US Food and Drug Administration (FDA) to treat HIV-infected patients [4, 5]. However, its side-effects include carcinogenesis [6]. The International Agency for Research on Cancer (IARC) categorises AZT as a group 2B carcinogen, designated as possibly carcinogenic to humans [7]. Nevertheless, AZT has been shown as a telomerase inhibitor with potential anticancer properties [8]. It is used as an antitumor agent in combination with methotrexate, cisplatin, or 5-fluorouracil [9, 10].

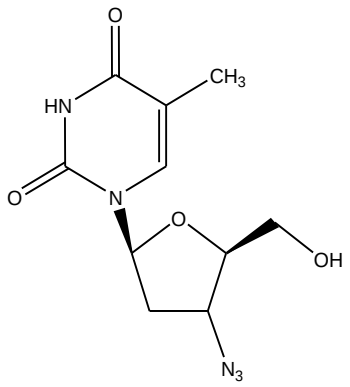

Figure 1.1: Chemical structure of zidovudine.

Zidovudine is regarded as a class 3 compound on the biopharmaceutical classification system (BCS) [11]. Its high aqueous solubility and low permeability reduces oral bioavailability. The medication does not cure HIV/AIDS but inhibits or delays the ability of HIV to replicate and spread, which lowers the viral load causing an increase in CD4+ cells. This allows the immune system to recuperate and reduces the risk of disease progression as the CD4 cells are white blood cells that maintain a healthy immune system and aid the fight against infection. Zidovudine is primarily used in combination therapy called Highly Active Antiretroviral Therapy (HAART) [12]. According to Raviolo and co-workers, the limited clinical efficacy of AZT is due to the following aspects [13]:

1. its toxicity on bone marrow,
2. hepatic anomalies,
3. inadequate brain uptake,
4. short half-life in plasma,
5. the predisposition to catabolism, and
6. rapid progress of resistance by HIV.

The consequence of these is the development of resistant viral strains, toxic side-effects and low activity. This has resulted in the development of numerous chemical approaches by

medicinal scientists to synthesize alternate analogues with less toxicity and improved properties, thereby enhancing the biopharmaceutical properties.

A possible green synthetic route involves the use of photochemistry to induce transformations. The zidovudine molecule contains three photoactive groups, namely, the alkene, carbonyl and azido groups [14]. The literature reveals that thymine and the azido group are the major cause of AZT photodegradation [15, 16]. The photolysis of the azido group is known to occur with the loss of molecular nitrogen (N_2) to yield a product derived from the corresponding nitrene or excited azide intermediates [16]. However, the photolysis of thymine is known to undergo dimerization leading to carcinogenic photoproducts [17]. In this study, the photostability of AZT was investigated in different solvents, namely, water, methanol, ethanol, 2-propanol and acetonitrile. Such information is relevant for future syntheses of novel derivatives of zidovudine (i.e. to increase cellular permeability) by utilizing green chemistry methods, such as photochemistry. These derivatives can be amalgamated within nanocarrier systems for *in vivo* drug delivery. The application of these nanocarrier systems will result in improved therapeutic efficacy and allow increased drug safety [18].

1.1. Photochemistry

Photochemistry is a branch of science concerned with the study of physical and chemical transformations induced by the absorption of light [19]. When a molecule absorbs energy in the form of light, an electron is promoted to a higher energy state or excited state. Thus, photoexcited molecules become more reactive and undergo different reactions than ground-state molecules and this can lead to several reaction pathways [20]. The part of the molecule that is responsible for the absorption of light is known as the chromophore. There are two fundamental principles of photochemical transformations [21, 22]:

- The *first law of photochemistry* states that the substrate must absorb a photon of light before it can enter an excited state.
- The *second law of photochemistry* states "that for each photon of light absorbed by a chemical system, only one molecule is activated into the excited state. This photoequivalence law was derived by Albert Eistein during his development of quantum (photon) theory of light".

The part of the electromagnetic spectrum that has sufficient energy to cause electronic transitions and the resulting chemical transformations is the ultraviolet region.

1.1.1. UV irradiation

The ultraviolet (UV) region lies between X-rays and visible light (40 and 400 nm) in the electromagnetic spectrum. The energy in this region is able to break or rearrange several types of chemical bonds in a molecule. When an organic molecule absorbs a photon of UV light different processes can result. The excited molecule can behave in two ways, either in photophysical or photochemical processes (see **Fig. 1.2**). In a photochemical process, the change can come as a result of dissociation of the absorbing molecule into reactive fragments (**process i**); or as a result of direct reaction of an excited molecule and another species (**process ii**). An excited molecule may also undergo rearrangement (or photoisomerization) (**process iii**); ionization (**process iv**); energy transfer (**process v**), luminescence (**process vi**) and physical quenching (**process vii**) which occurs when a quencher collides with the excited state molecule and causes it to lose its energy of excitation [23].

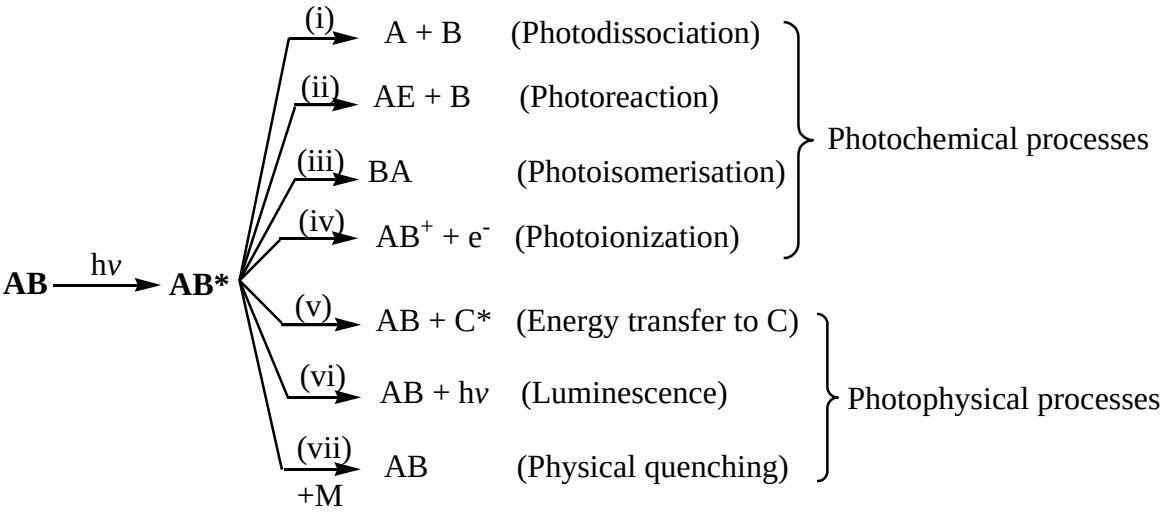

Figure 1.2: Photochemical and photophysical processes that can occur after excitation of a molecule.

In a photophysical process, the molecule returns to its ground state without any change in the structure of the molecule. This process can be well explained by a Jablonski diagram (**Fig. 1.3**) [22].

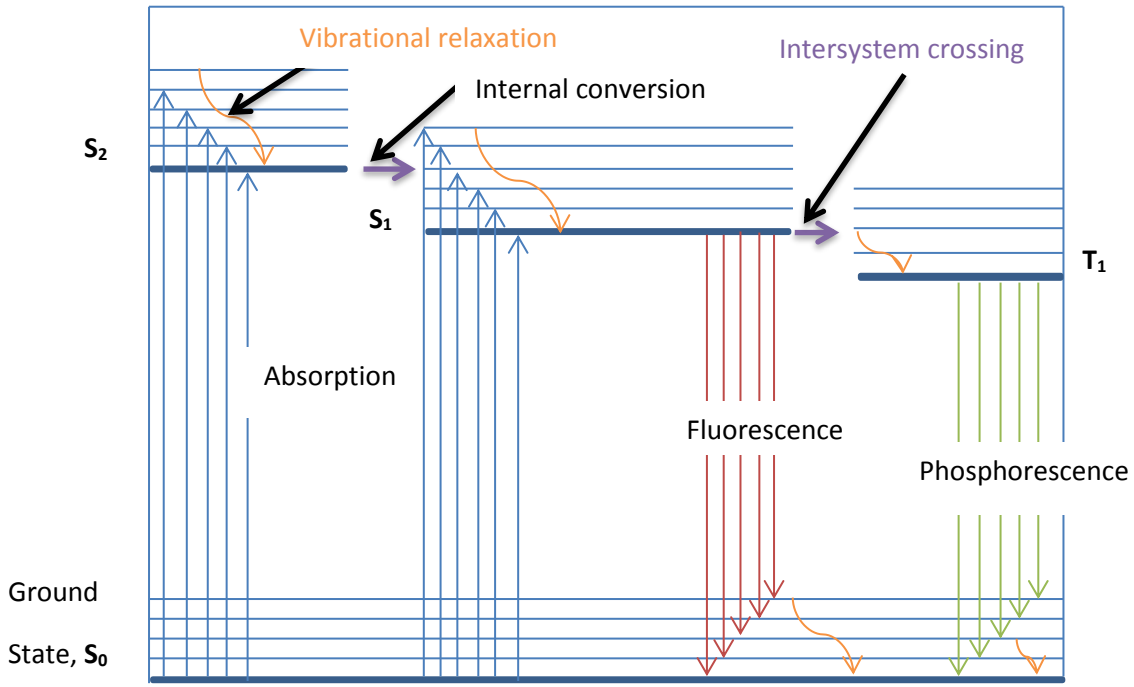

Figure 1.3: Jablonski diagram showing the transitions involved in various photophysical processes [22].

The photophysical processes include non-radiative and radiative transitions. Non-radiative transitions arise through several different mechanisms, all differently labelled in **Fig. 1.3** (vibrational relaxation, internal conversion and intersystem crossing). Vibrational relaxation occurs when the photon energy is given away to other vibrational modes as another form of energy (kinetic). This energy can either stay the same or can be transferred to other molecules around the excited molecule, largely depending on the phase of the probed sample. Internal conversion processes occur between two excited singlet states (e.g. $S_2 \rightarrow S_1$), whereas intersystem crossing occurs between an excited singlet state and a triplet state (e.g. $S_1 \rightarrow T_1$).

Radiative transitions involve the absorption (blue arrows **Fig. 1.3**) and emission (fluorescence and phosphorescence) of radiation. Fluorescence occurs between states of the same spin (e.g. $S_1 \rightarrow S_0$) while phosphorescence occurs between different spin states (e.g. $T_1 \rightarrow S_0$). The lifetimes of fluorescent states are very short (1×10^{-5} to 10^{-8} seconds) as compared with phosphorescence states that are somewhat longer (1×10^{-4} seconds).

The absorption of UV light by organic molecules can also lead to the generation of radicals.

1.1.2. Photogeneration of radicals

A radical is an atom, molecule, or ion containing one or more unpaired electrons. These unpaired electrons make free radicals highly chemically reactive towards other substances, or even towards themselves: these species will often spontaneously dimerize or polymerize if they come in contact with each other. Compounds that generate radicals are called free radical initiators. Most radicals are stable only at very low concentrations in inert media or in a vacuum. Organic radicals are normally formed via homolytic cleavage of a single covalent bond, induced by thermolysis, radiolysis or photolysis [24]. The radicals produced by photolysis can either initiate chain or non-chain reactions. In a chain reaction, a radical formed by absorption of one photon produces many product molecules whereas in a non-

chain reaction the number of photons absorbed typically must be at least equal to the number of molecules reacted. Many radical reactions involve the loss of a small, stable molecule such as CO_2, N_2 or CO. Such processes are called fragmentations.

1.2. Azide photochemistry

Organic azides have long been used in the study of nucleic acids as photo-affinity labelling reagents [25]. They are widely used as a reactive intermediate for the synthesis of heterocycles such as triazoles and tetrazoles [26]. However, they are also known as explosive substances under heat and when shaken. In the 19th century, Tiemann first proposed that the photolysis and thermolysis of organic azides undergo dissociation of N-N, which leads to the formation of nitrene intermediates [25].

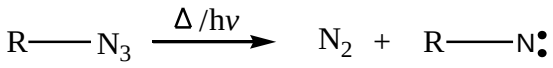

Nitrenes are a reactive intermediate containing neutral, monovalent nitrogen atoms [26]. They have a complex and fascinating chemistry that depends on the multiplicity, mode of formation as well as on the environment [27].

Nitrenes can either undergo triplet or singlet electronic transitions (**Fig. 1.4**), depending on the nature of the nitrene and on the reaction conditions [28]. Singlet nitrenes are only observed in the presence of strongly electron-withdrawing groups such as nitrogen-hydrogen or oxygen-hydrogen bonds. They are arranged as two lone pairs in each orbital. Triplet nitrenes show diradical behaviour and have two electrons in separate orbitals with their spins unpaired. The nitrenes are unstable in both cases and cause the molecules to move freely and react very easily with a great variety of organic substrates. Nitrenes have triplet ground states consistent with Hund's rule.

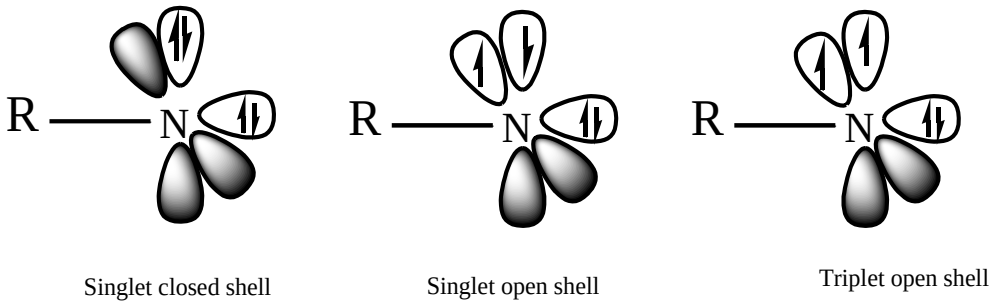

Singlet closed shell Singlet open shell Triplet open shell

Figure 1.4: Nitrene electronic configurations [28].

Nitrenes have a short lifetime which depends on the type of nitrene and on the conditions of the reaction. Wang *et al*. reported that many singlet phenylnitrenes have a lifetime of approximately 1 ns in aprotic organic solvents at ambient temperature [29].

Nitrenes are unstable intermediates which stabilize by undergoing the following reaction routes (**Scheme 1.1**): (1) hydrogen abstraction from the α-carbon bonded to nitrogen to form an imine; (2) hydrogen abstraction from the solvent resulting in the formation of an amine; (3) double-bond insertions into C-H bonds to form tertiary amines; (4) hydrogen abstraction from the 4- or 5-position followed by ring closure to form heterocyclic compounds; and (5) dimerization with the formation of azo compounds [26, 30, 31].

Step 1

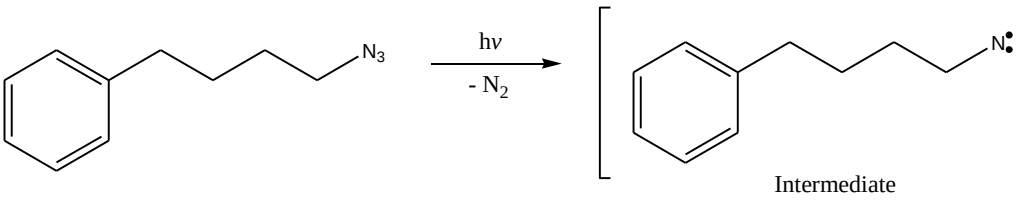

Intermediate

Step 2

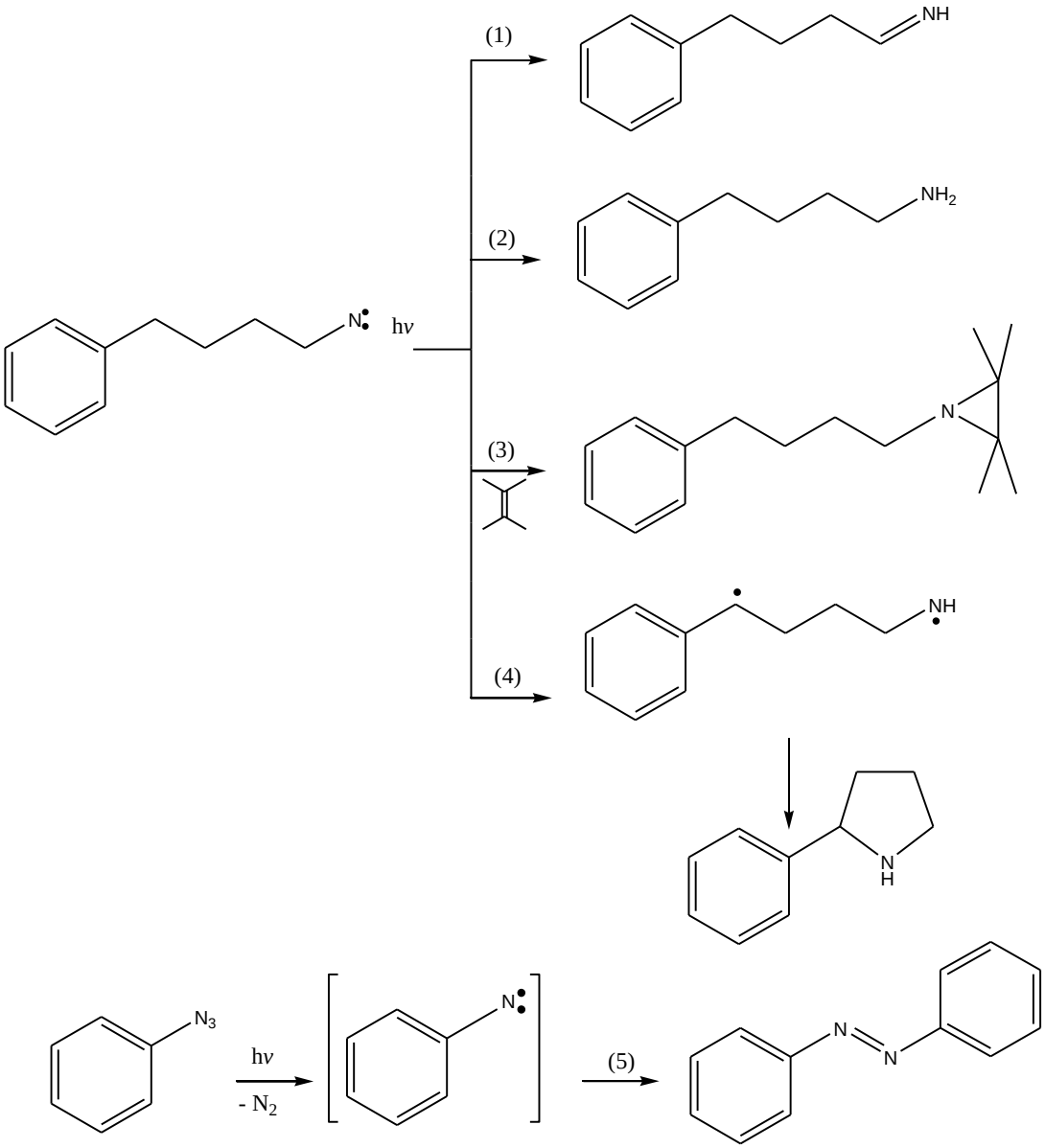

Scheme 1.1: Stabilization reactions of the nitrene intermediate [31].

1.2.1. Photochemistry of azidonucleosides

The photochemistry of azidonucleosides has been less investigated, but the photochemical transformations of various azido-substituted pyrimidine compounds have been carried out [32]. Komodziński *et al.* have studied the photochemistry of 6-azidopurine ribonucleoside **(1)** in aqueous solution (**Scheme 1.2**) [33]. The reaction undergoes only partial photoreduction to adenosine, and its dominant photo-transformation involves purine ring expansion to give a novel imidazole-fused 1,3,5-triazepinone nucleoside **(2)**. Recently, the authors investigated the photochemical behaviour of 2-azidopurine 2',3',5'-tri-O-acetylribonucleoside in aqueous solution under aerobic and anaerobic conditions [34]. The results showed that the major photochemical transformations of the 2',3',5'-tri-O-acetylated derivative of 2-azidopurine ribonucleoside in aqueous solution involve both photooxidation and photoreduction to the respective 2-nitro and 2-amino derivatives, and unprecedented formation of 1-(5'-O-acetyl-β-D-ribofuranosyl)-5-[(2-oxo-1,3,5-oxadiazocan-4-ylidene)amino]-1H-imidazole-4-carbaldehyde, depending on the irradiation conditions. Photooxidation is the major process occurring under aerobic irradiation whereas in the absence of oxygen, 2-amino-9-(2',3',5'-tri-O-acetyl-β-D-ribofuranosyl)purine is formed as the major photoproduct.

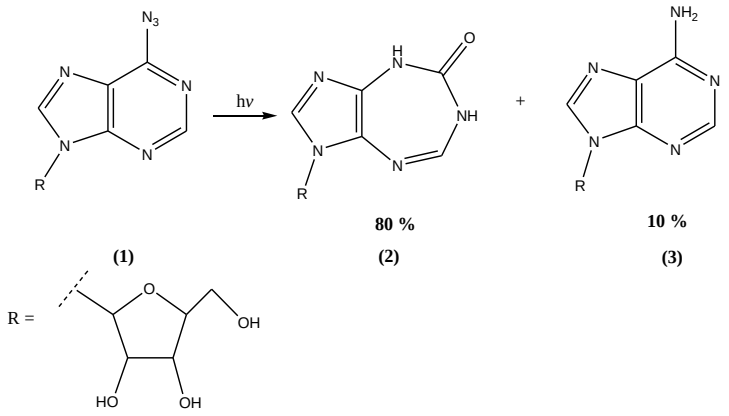

Scheme 1.2: Photochemistry of 6-azidopurine ribonucleoside in aqueous solution [33].

Polshakov *et al.* investigated the photochemistry of 8-azidoadenosine **(4)** and its derivatives in methanol [35]. The investigation was carried out by chemical trapping studies, laser flash photolysis with ultraviolet-visible spectrophotometry (UV/Vis) and infrared radiation (IR) detection, and modern computational chemistry. The reaction led to three photoproducts **(5**, **6**, **7)** with yields between 5 and 20% (**Scheme 1.3**). They concluded that photolysis of 8-azidoadenosine in methanolic solution releases the corresponding singlet nitrene which rapidly tautomerizes to form a closed adenosine diazaquinodimethane in less than 400 fs. However, its derivative cannot undergo this tautomerization, and instead, it fragments upon photolysis to form an opened adenosine diazaquinodimethane.

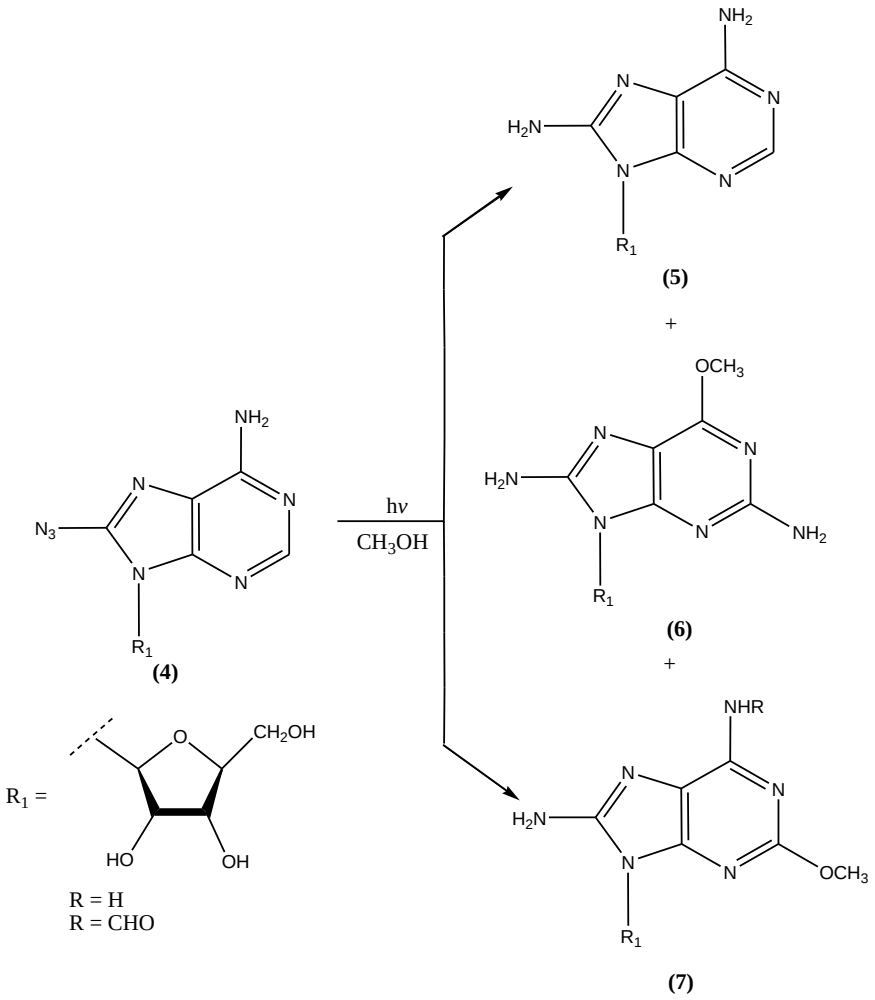

Scheme 1.3: Photochemistry of 8-azidoadenosine and its derivatives in methanol [35].

The photochemistry of 5-azido-2'-deoxyuridine **(8)** has been studied by Gourdain *et al.* [36]. The study was carried out in both aqueous and methanolic solution. The reaction in aqueous solution led to the formation of up to seven photoproducts **(9**, **11**, **12**, **15**, **17**, **19**, **20)** depending on the pH of the solution (**Scheme 1.4**). In methanolic solution the reaction led to the formation of the O^5-methyl analogue **(10)**.

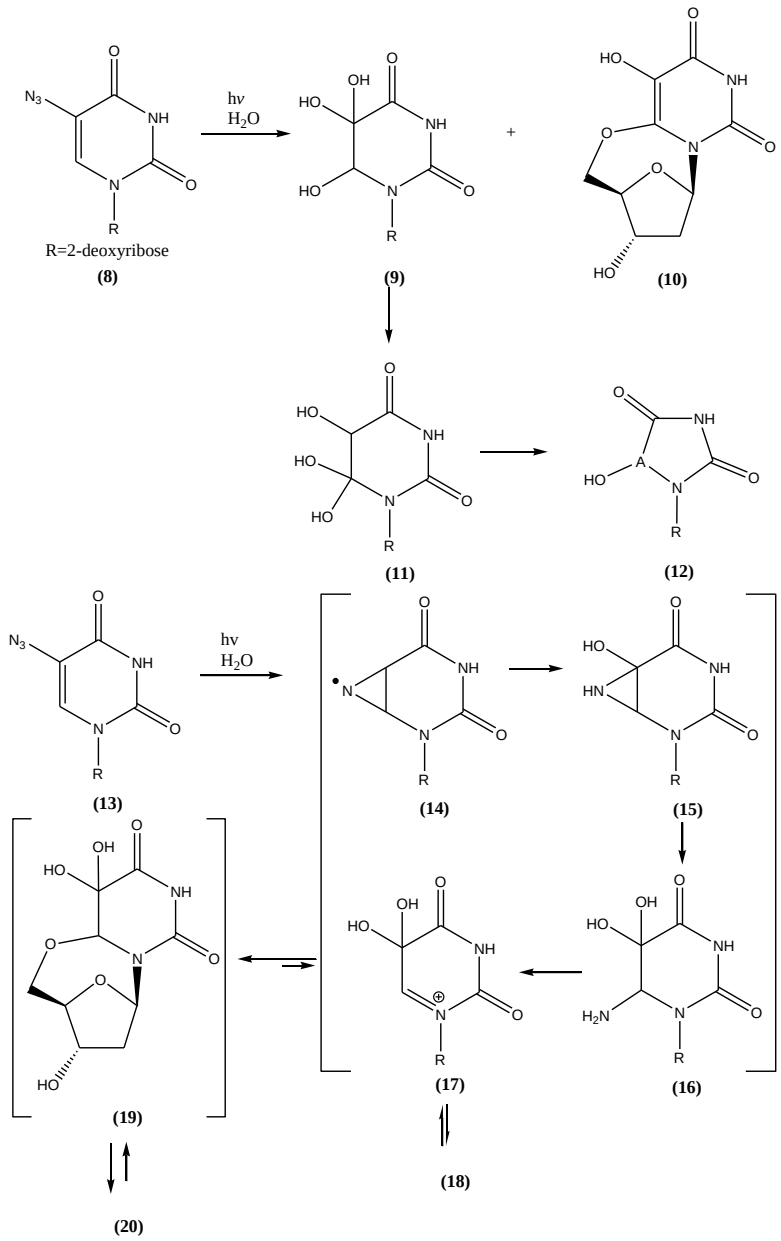

Scheme 1.4: Photochemistry of 5-azido-2'-deoxyuridine [36].

Iwamoto *et al.* reported the formation of a hydroxylamine derivative **(21)** after UVB exposure of AZT in aqueous solution (**Scheme 1.5**) [7]. Zhou *et al*. investigated the photolysis of AZT in pure water, freshwater, and seawater [37]. The reaction was carried out under sunlight. The results showed fast photodegradation of AZT in both neutral and alkaline conditions.

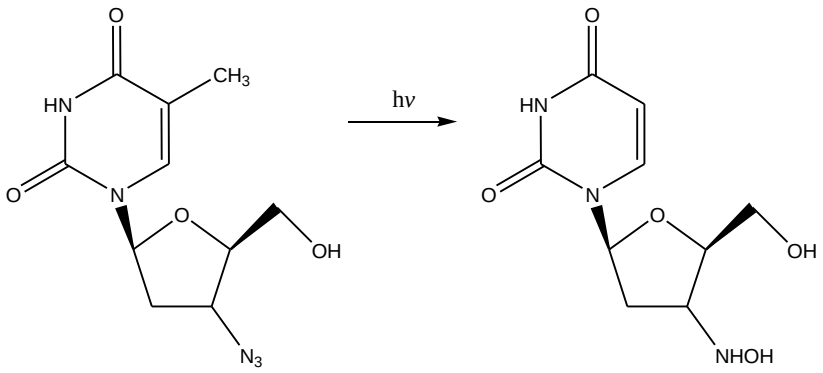

(20) **(21)**

Scheme 1.5: Photochemistry of AZT in aqueous solution [7].

Huybrechts *et al.* [16] revealed that the photolysis of 4'-azido-2'-deoxy-2'-methylcytidine hydrochloride **(22)** undergoes three main pathways (**Scheme 1.6**). The first one led to the formation of a ring-expanded imidate ester **(24)** and the other pathways involved exocyclic or endocyclic bond cleavage with imine or imino lactone formation **(26a**, **28)**.

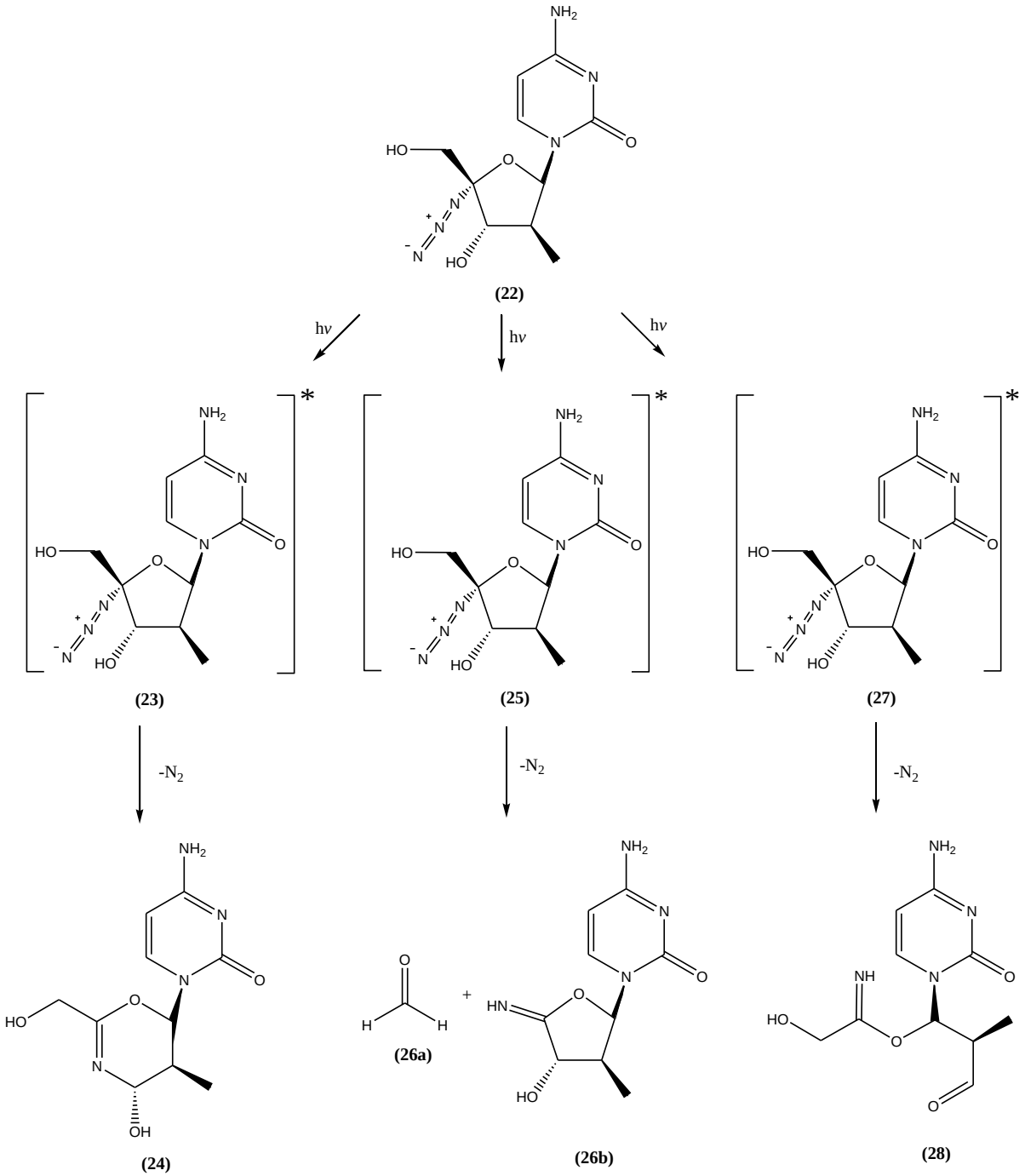

Scheme 1.6: Photodegradation of (1'R,2'S,3'S,4'R)-4'-azido-2'-deoxy-2'-methylcytidine hydrochloride [16].

Photolysis of 5-iodo-5'-azido-2',5'-dideoxyuridine **(29)** has been reported by Chen *et al.* [38].

The reaction showed the formation of free radicals and diradicals **(30)** (**Scheme 1.7**).

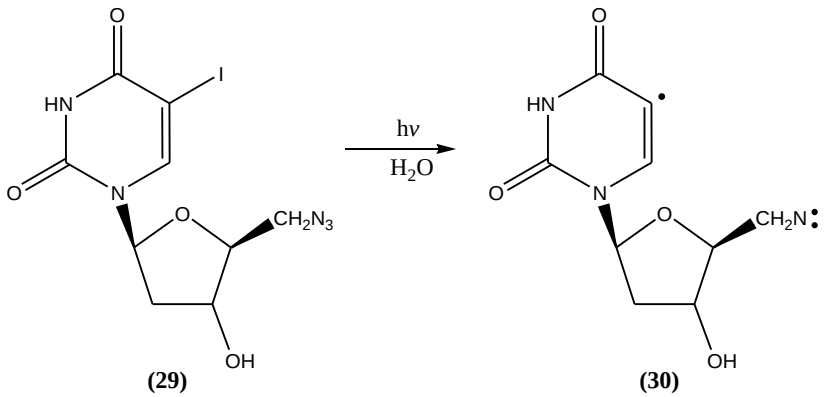

(29) **(30)**

Scheme 1.7: Photolysis of 5-iodo-5'-azido-2',5'-dideoxyuridine [38].

Peyrane *et al.* reported that the 4-azidouracil/tetrazolo[1,5-c]-pyrimidin-5(6H)-one nucleosides **(31)** undergo a photochemical nitrogen elimination and ring expansion to form 1,3,5-triazepin-2,4-dione nucleosides **(32)** in water-acetonitrile (7:3) solution (**Scheme 1.8**) [39].

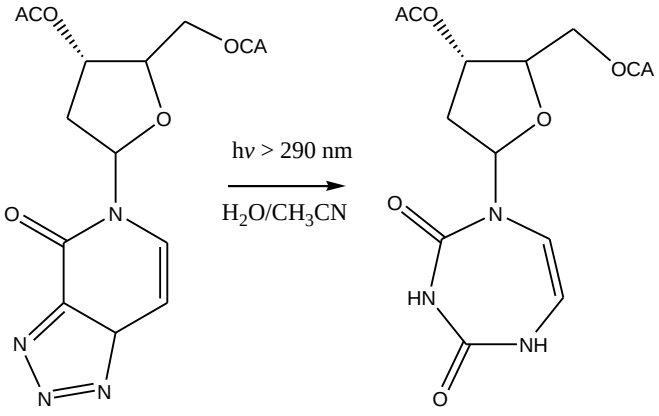

(31) **(32)**

Scheme 1.8: Photolysis of 4-azidouracil/tetrazolo[1,5-c]-pyrimidin-5(6H)-one nucleosides [39].

Hill and Platz have studied the photolysis of tetrazolo [1,5-b] pyridazine, i.e., 3-azidopyridazine **(33)**, in an argon matrix at 16 K (**Scheme 1.9**) [40]. The photolysis reaction led to nitrogen extrusion and ring opening to form E-*cis*-1-cyano-3-diazopropene 35, which further reacted to produce 3-cyanocyclopropene **(36)** *via* a vinyl carbene intermediate.

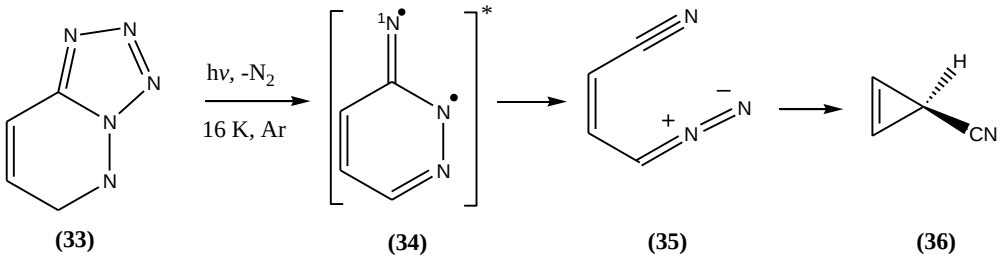

(33) **(34)** **(35)** **(36)**

Scheme 1.9: Photolysis of tetrazolo [1,5-b] pyridazine, i.e., 3-azidopyridazine, in an argon matrix at 16 K [40].

Cerro-Lopez *et al.* studied the photolysis of 2-azidopyrimidine **(37)** in glassy ethanol at low temperature (77 K) and the electron paramagnetic resonance (EPR) result showed the formation of a 2-pyrimidylnitrene **(38)** in its triplet ground state (**Scheme 1.10**) [41].

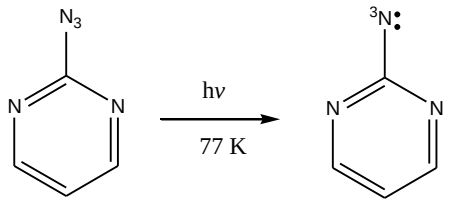

(37) **(38)**

Scheme 1.10: Photolysis of 2-azidopyrimidine [41].

1.3. Thymine photochemistry

Thymine is one of the most investigated pyrimidines in photochemistry, due to its sensitivity to light [42]. Pyrimidines are found in DNA and, upon exposure to UV light, form a number of photoproducts, including cyclobutane pyrimidine dimers (CPDs), pyrimidine pyrimidone photoproducts and photohydrates [43].

1.3.1. Cyclobutane pyrimidine dimers

Cyclobutane pyrimidine dimers (CPDs) are the most common photolesions formed in DNA and have been regarded as the origin of a range of human health problems, including cell lethality, mutagenesis, and skin cancers [44, 45]. Formation of CPDs occurs between the C5-

C6 double bonds of two adjacent pyrimidine bases in DNA. The structure of the CPD can be categorized into four types, namely, *cis-syn* **(40)**, *trans-syn* **(41)**, *cis-anti* **(42)** and *trans-anti* **(43)**, depending on the spatial alignment of the two bases (**Scheme 1.11**)**.** Among these four structures, the *cis-syn* CPD lesion has been reported as the main product and is mostly formed in double-stranded DNA, whereas *trans-syn* CPD is formed in single-stranded DNA in much less quantity [46, 47].

Over the past 30 years, the stereochemistry of CPD formation has been analyzed by using dinucleoside monophosphate [48]. *Cis-syn* and *trans-syn* CPDs have been identified in dinucleoside monophosphates containing thymine, cytosine and 5-methylcytosine. A second minor diastereoisomer of *trans-syn* TT CPD has also been isolated at the dinucleoside monophosphate level. Despite the stability of CPDs in solution, they revert to the original bases upon exposure to UVC radiation. The loss of the two double bonds of the pyrimidine bases in the formation of the CPDs results in a shift of the maximal absorption from around 260 nm to 230 nm [49]. Studies on CPDs of thymine in frozen aqueous solution have been extensively reviewed [42]. In 1993, Alderfer *et al*. reported the UV irradiation of thymidylyl-(3'-5')-deoxyfluorouridine monophosphate by using acetone as a photosensitizer [50]. The reaction was carried out under sunlamps (280-320 nm) and by varying the pH. At pH 6, *cis-syn* cyclobutane photodimers were produced as the major photoproduct whereas at high pH (8-10) a photoadduct was the major product.

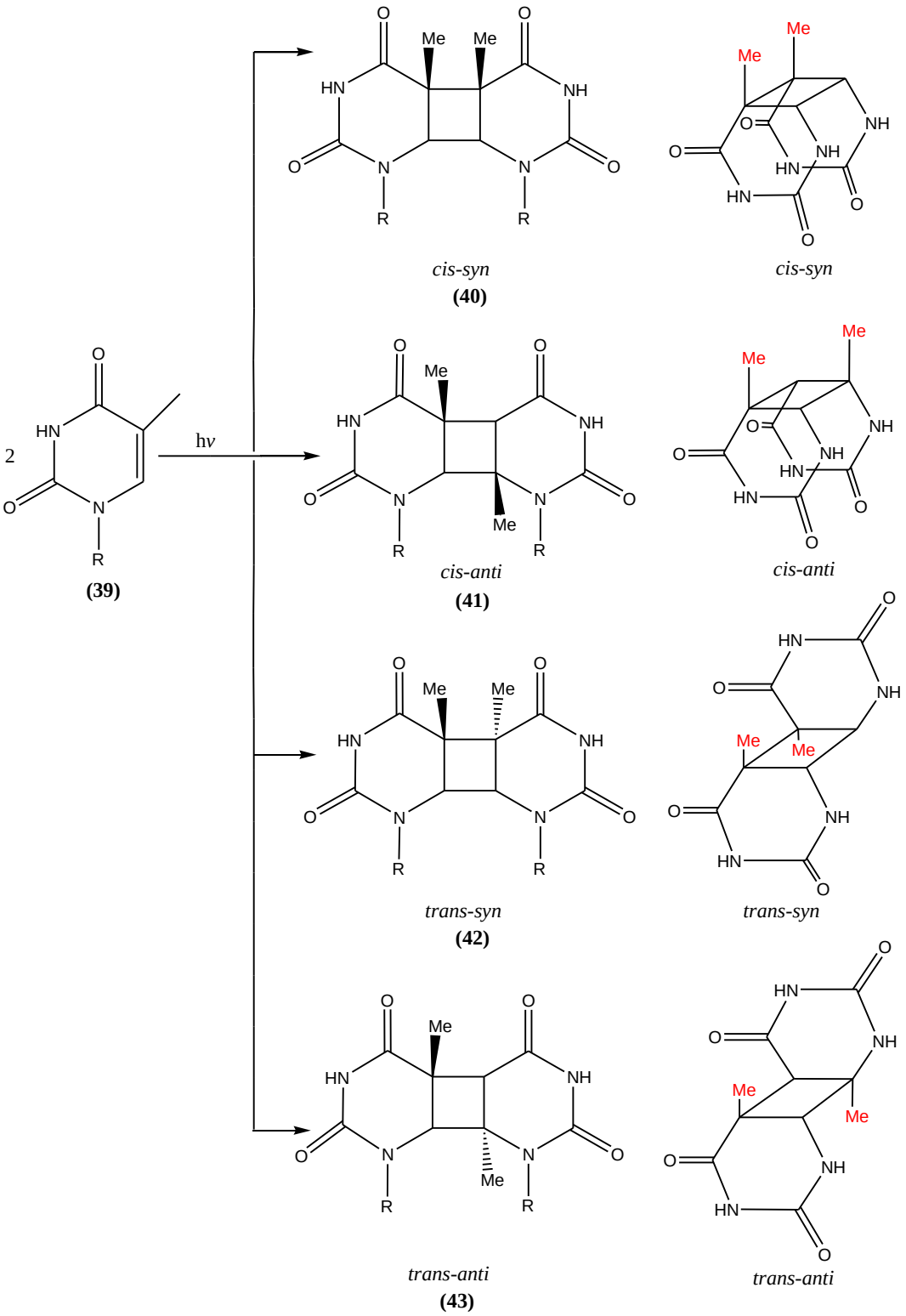

Scheme 1.11: The four stereoisomeric CPDs of thymine [48].

Recently, Shetlar and Chung reported the CPDs of 5-bromo-2'-deoxyuridine **(45)** in frozen aqueous solution (**Scheme 1.12**) [42].

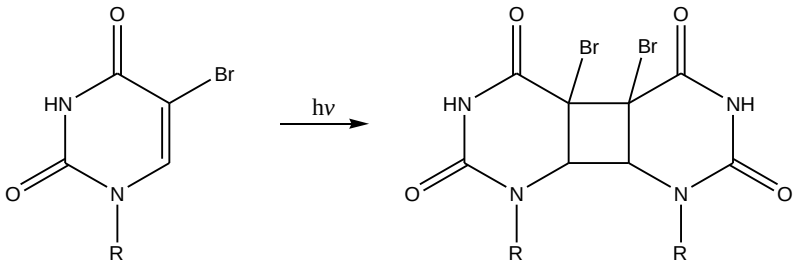

(44) **(45)**

R = H, ribosyl, 2-deoxyribosyl

Scheme 1.12: CPDs of 5-bromo uracil in frozen aqueous solution [42].

1.3.2. Pyrimidine (6-4) pyrimidone photoproducts

Formation of pyrimidine (6-4) pyrimidone adducts involves cycloaddition of the C5-C6 double bond of the 5'-end pyrimidine to the C4 carbonyl or imine group of the 3'-end pyrimidine [51, 52]. This reaction results in the formation of unstable oxetane and azetidine intermediates **(47**, **52)** which react further by ring opening to yield the (6-4) photoproducts ((6-4) PPs) **(48**, **53)** (**Scheme 1.13**). The (6-4) photoadducts occur more efficiently on TC than TT sequences. Upon exposure to UV light they undergo formal 4π electrocyclic rearrangement to give the corresponding Dewar valence isomer **(49**, **54)** [52]. The Dewar photoproducts revert to back to the (6-4) isomer upon UVC exposure [53]. Shetlar and Chung reported the (5-4) and (6-4) adducts of 1-methylthymine and their Dewar valence isomers in a frozen aqueous solution [54]. The (6-4) PP that involve a cytosine nucleobase at its 5'-end can spontaneously undergo deamination forming a more stable photo-adduct [53].

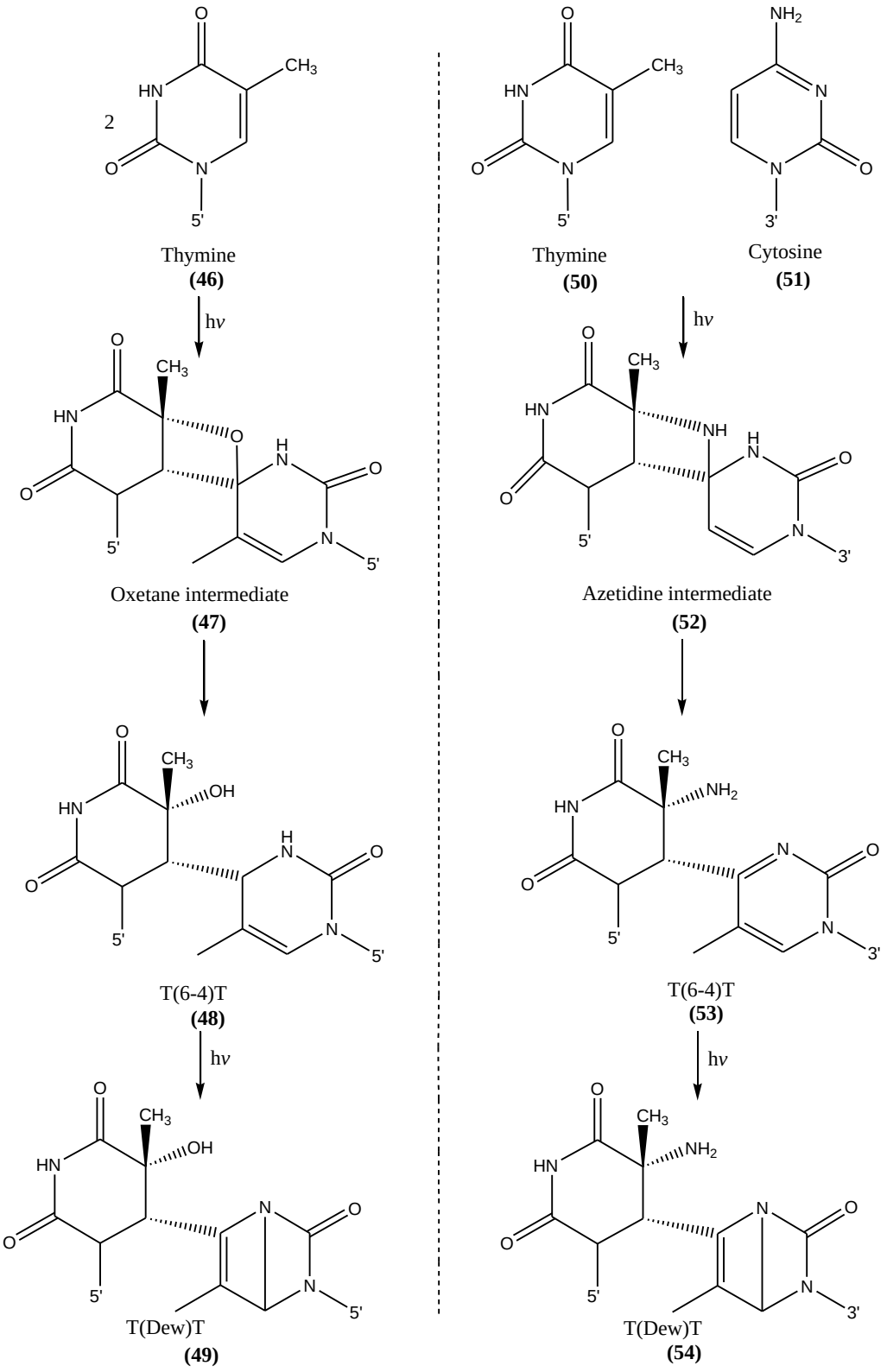

Scheme 1.13: Formation of pyrimidine (6-4) pyrimidone adducts [47].

1.3.3. Spore photoproduct

Over the past decades, the exposure of DNA extracted from bacterial spores revealed the presence of photoproducts other than CPDs. These were shown to be 5-thyminyl-5,6-dihydrothymine, which is known as the spore photoproduct (SP) [49]. The SP can be produced by UV irradiation of thymidine either in dry film or frozen solution, although its yield is much less, approximately 1% [55]. The SP consists of a chiral center at the C5 position of 5′-T **(56)** (**Scheme 1.14**). Cadet *et al.* postulated the mechanism of SP photochemistry by employing d_3-thymidine containing a deuterated methyl group for photoreaction and found that approximately 67% of the dinucleoside SP generated via UV irradiation in ice possessed a deuterium at the C6 carbon [55]. However, the result indicates a H atom transfer mechanism; the incomplete transfer observed hinders the determination of the origin of the two C6 protons on the SP. Recently, Li *et al.* examined the SP photochemistry by using the deuterium labelled dinucleotide TpT in a dry film reaction and found that the H atom on the methyl group of the 3′-T exclusively migrates to the *6proS* position of the formed SP. The SP was confirmed by ^{1}H NMR spectrometry [55].

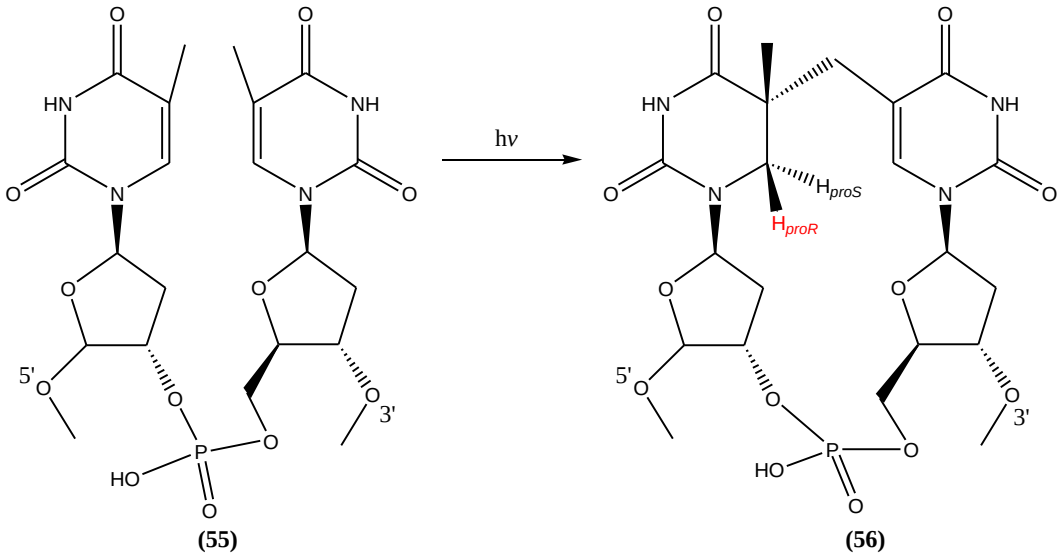

(55) **(56)**

Scheme 1.14: Formation of spore photoproduct (SP) [55].

1.3.4. Photohydration

Photohydration is defined as the photochemical reaction leading to the addition of water across a double or triple bond or to a carbonyl group. Cytosine, and its derivatives, is the most common pyrimidine base to undergo photohydration reactions (**Scheme 1.15**) and further undergoes deamination processes to form the more stable uracil hydrate **(59)** [53]. Vandana *et al.* [56] suggested that photohydration of cytosine involves the nucleophilic addition of a water molecule to form a reactive intermediate, which is likely to be either a lowest lying singlet state S_1 or a vibrationally excited state derived from S_1. There is not much information concerning the formation of cytosine photohydrates in UV-irradiated DNA due to instability of the resulting photoproduct [47].

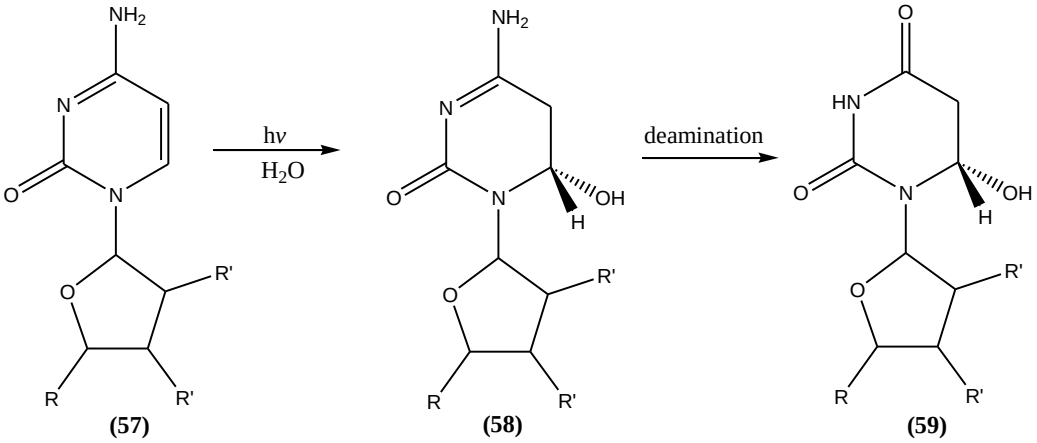

(57) **(58)** **(59)**

R = $^{-}O_3POCH_2$
R' = OH

Scheme 1.15: Photohydration of cytosine [53].

Saito *et al.* have studied the photohydrates of thymine and thymidine in the presence of amine (pH 9.5) at low temperature [57]. The reaction yields two compounds, the first one involved a ring opening in which the reactant amine (RNH_2) becomes attached to C2 in the parent pyrimidine ring while the N1 nitrogen, along with any substituent (e.g. alkyl group or sugar)

(61), is found attached to the C6 of the parent compound in the product (**Scheme 1.16**). Further treatment with base or heat caused the reaction to undergo ring closure to form photo-exchange products (PEX) **(62)**, in which the reactant amine is incorporated into the final product and the group. In 2011, Shetlar and Yang reported evidence for the opened ring of 2'-deoxycytidine photohydrates and this were confirmed by NMR spectroscopy [58].

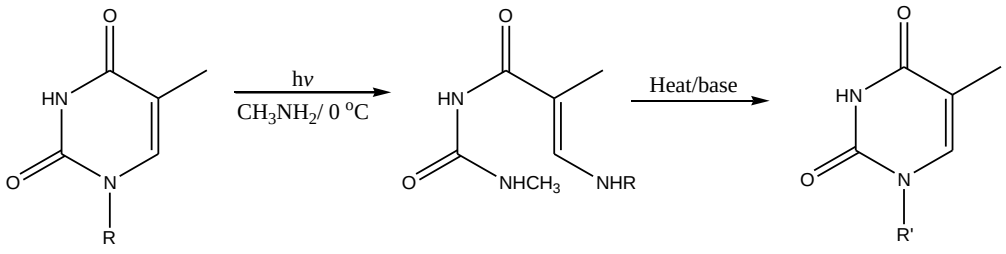

(60) **(61)** **(62)**

R = D - deoxyribofuranosyl

R' = tert-butyl

Scheme 1.16: Photohydrates of thymine and thymidine in the presence of amine [57].

Recently, Shetlar *et al.* reported the ring opening of uridine **(63)** in the presence of amine to yield an amineted product **(65)** (**Scheme 1.17**) [59]. The reaction was carried out in the cold under 254 nm UV lamps.

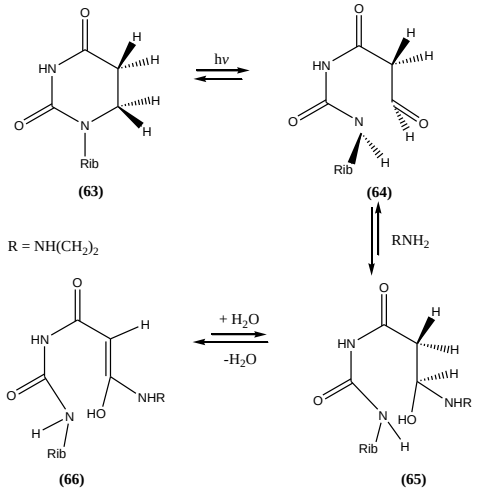

(63) **(64)** **(66)** **(65)**

R = $NH(CH_2)_2$

Scheme 1.17: Photolysis of uridine [59].

1.4. Carbonyl photochemistry

The photochemistry of ketones has been extensively investigated over the past decades [60, 61]. Ketones and aldehydes absorb UV light between 340-230 nm, which corresponds to excitation of a non-bonding 2π electron of the oxygen atom to the anti-bonding orbital of the carbon [21]. Carbonyl groups are often used as UV photo-initiators [62]. The photochemistry of carbonyls involves α-cleavage 'Norrish Type I' (**Scheme 1.18**), γ-hydrogen abstraction 'Norrish type II' (**Scheme 1.19**), cycloadditions with alkenes 'Paternò-Büchi reaction' (**Scheme 1.20**) and photoreduction (**Scheme 1.21**). The Norrish type I reaction is defined as the photochemical reaction that involves excitation of an α-carbonyl compound, where an acyl radical **(68a)** and an alkyl radical **(68b)** are formed. This reaction takes place either in the singlet or triplet excited states and can undergo several reactions, namely decarbonylation (**A**), disproportionation (**B**) and recombination (**C**) (see **Scheme 1.18**).

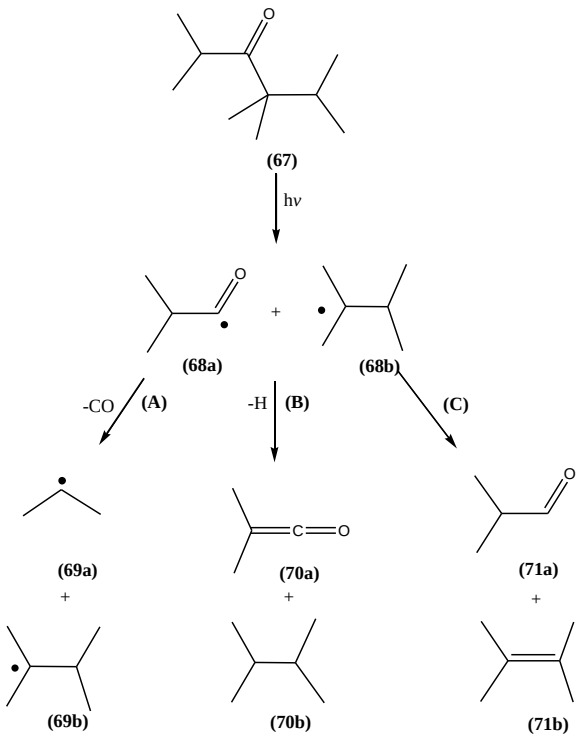

Scheme 1.18: Norrish Type I photoreaction [21].

Norrish type II reactions involve γ-hydrogen abstraction from an excited carbonyl compound to produce a 1,4-biradical (**73)**. The biradical can undergo several follow-up reactions, notably the Norrish Type II cleavage leading to the formation of cyclobutanols (**D**), as well as the formation of alkenes and enols (**E**) (see **Scheme 1.19**).

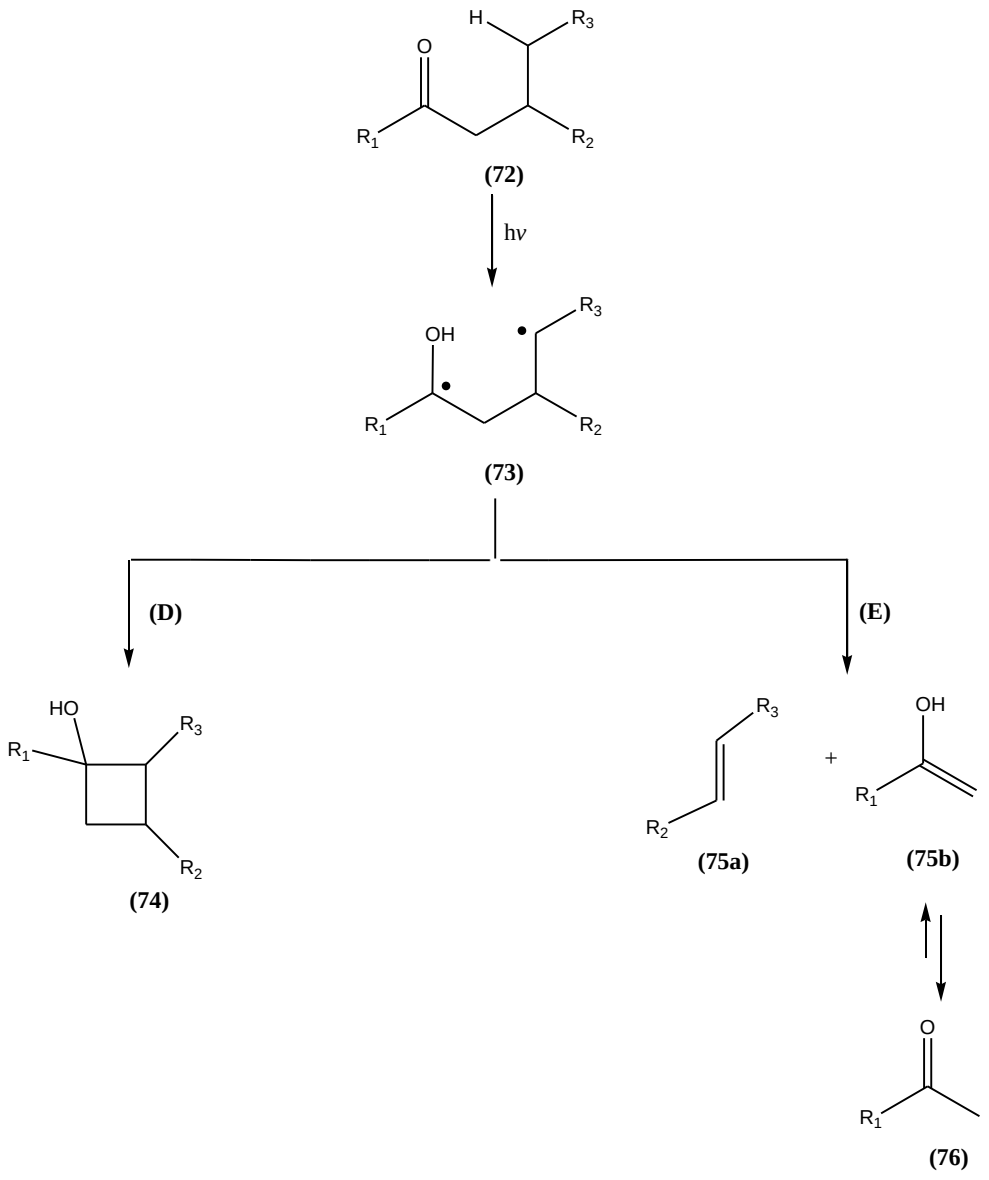

Scheme 1.19: Norrish type II photoreaction [21].

The Paternò-Büchi reaction is a [2+2] cycloaddition reaction formed between an excited carbonyl **(78)** and an alkene to yield the oxetane **(80)** (see **Scheme 1.20**).

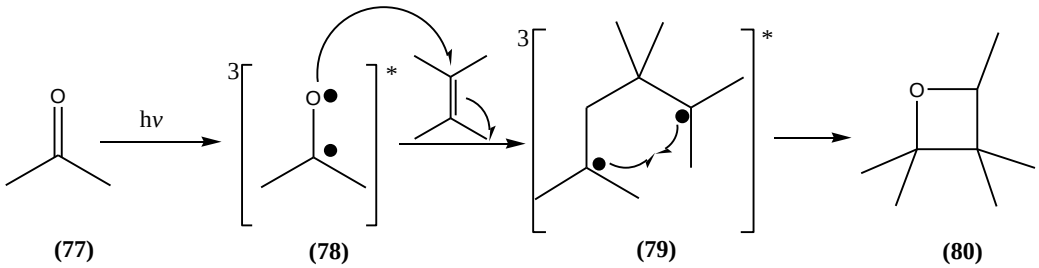

Scheme 1.20: Paternò-Büchi reaction [21].

Photoreduction of ketones involves the reaction between the photo-excited species **(82)** and a hydrogen donor (such as toluene) [21]. This reacts to form a radical which may further undergo dimerization or hydrogen-abstraction (see **Scheme 1.21**).

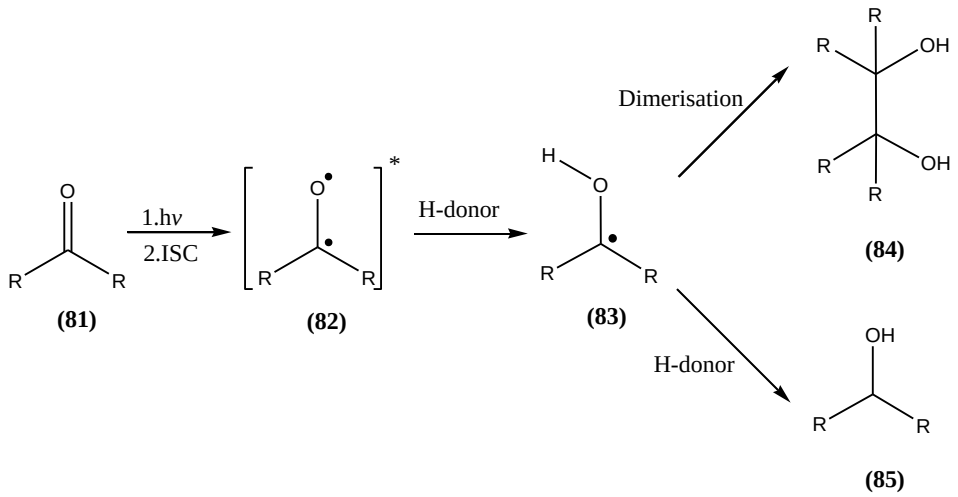

Scheme 1.21: Photoreduction of ketones [21].

1.5. Photochemistry of drugs

Photoreactions of drugs have been extensively reviewed [63]. These investigations were carried out in both the solid and solution state. The photoreactions of some drugs in different solvents are summarized in **Table 1.1.**

Table 1.1: The photoreactions of some drugs in different solvents.

Drug name	**Solvent**	**Photoreaction**	**Photoproduct**	***Ref***
Diclofenac	H_2O or Methanol	Dechlorination	Carbazole-1 acetic acids	[64]
Azathioprene	H_2O, pH 7 or 3	Fragmentaion and cyclization	6-mercaptopurine and 1-methyl-4-nitro-5-hydroxyimidazole	[65]
2-aryl propionic acid derivatives	H_2O	Decarboxylation	Benzyl radical	[66]
Indomethacin	Methanol	Decarboxylation	Methyl ester and a six membered 1,2-dioxan-3-one	[67]
Benzydamine	Methanol	Fries rearrangement	5-hydroxybenzydamine and 2-β-dimethylaminopropyl-1-benzylindalolin-3-one	[68]
Hydrocortisone 21-acetate (HCA)	Methanol	Norrish I, Rearrangement	Andro-derivative, cyclobutane adduct	[69]
Clobetasol propionate	Acetonitrile or 2-propanol	Rearrangement, H-abstraction and cyclization	21-Chloro-9-fluoro-11-hydroxy-16-methyl-17(1-oxopropoxy)-1,5-cyclopregn-3-ene-2,20-dione; 21-Chloro-9-fluoro-11-hydroxy-16-methyl-17(1-oxopropoxy)-18,20-cyclopregn-1,4-diene-3-one and 9-fluoro-17-hydroperoxy-16-methyl-17(1-oxopropoxy)androsta-1,4-diene-3-one	[70]
Diazepam	H_2O or Methanol	Cleavage of heterocyclic ring	Benzophenone, Dihydroquinazoline	[63]
Reserpine	H_2O or chloroform	Oxidation	3,4,5,6-tetradehydroreserpine	[71]
Sulfanilamide	H_2O	Oxidation	4,4'-azobenzenesulfonamide, 4-hydroxylamino- and 4-nitrobenzenesulfonamide, and 4 unidentified products	[72, 73]

Tetracycline	H_2O	Oxidation	Quinone	[74]
Chloramphenicol	H_2O	Homolytic cleavage of C-C bond.	4-nitrobenzaldehyde, glycolic aldehyde and dichloroacetamide	[75]
Metronidazole	H_2O	Rearrangement	Imino-ketone	[76]
Decarbazine	H_2O	Cyclization	2-azahypoxanthine	[77]
6-Mercaptopurine	H_2O	Oxidation	Sulfonate	[63]
Acyclovir	H_2O	Oxidation	2-hydroxyethoxy)methyl spiroiminodihydantoin,(2-hydroxyethoxy)methyl(amino)-2-imino-1,2-dihydroimidazole-5-one, and (2,2-diamino-4-[(2-hydroxyethoxy)methyl]amino)-5-[2H]-oxazolone	[78]
Clomiphene	Chloroform	Isomerization	Phenanthrenes	[79]
Hydrochloro-thiazide	H_2O and alcohol	Dechlorination	Chloro-2,4-disulphonamido-aniline	[80]
Troglitazone	H_2O	Oxidation	Quinone and quinine epoxide	[81]
Dienoestrol	H_2O, Methanol	Cyclization	4a,4b-dihydrophenanthrene	[82]
Isoniazid	Ethanol	Oxidation, C-N and N-N bond fragmentation	Hydrozone, dipyridylhydrazone and bis-pyridylhydrazide	[63]
1-hydroxy-2-thiopyridine	H_2O or chloroform	Dimerization	Disulfide di-N-oxide	[63]
Levomepromazine	Methanol, acetonitrile	Oxidation	Levomepromazine sulfoxide	[83]
Vandetanib	H_2O	Debromination, addition	(N-(2-fluorophenyl)-6-methoxy-7-((1-methylpiperidin-4 yl)methoxy)quinazolin-4-amine, FP3) and (N-(4-hydroxy-2-fluorophenyl)-6-methoxy-7-((1-methylpiperidin-4 yl)methoxy)quinazolin-4-amine, FP2)	[84]

Many drugs have been studied in aqueous solution and they tend to undergo photooxidation reactions. However, in organic solvents, the reaction differs with the type of drug.

1.6. Photostability of AZT

Apart from the study by Iwamoto *et al*. [7] that identified a hydroxylamine derivative of AZT after UVB exposure, very few other studies have been reported, particularly in solvents other than water. The studies that have been reported have been mainly directed at developing reversed-phase HPLC methods for stability-indicating studies. These involve quantifying AZT after undergoing hydrolysis, oxidation or photolysis. Dunge *et al*. investigated the degradation behaviour of AZT under hydrolytic, oxidative and photolytic conditions [85]. Thymine was formed as a major photoproduct. The degraded samples were monitored by HPLC equipped with a photodiode array (PDA) detector. The separations were achieved on a Merck C18 column (250 mm × 4.6 mm i.d. with particle size of 5 μm) by using a methanol:water (77:23) mobile phase in isocratic mode. A year later, the authors validated a specific HPLC method for the determination of AZT during stability studies [86]. However, in neither report did they identify the other degradation products of AZT besides thymine. Santos *et al.* developed a RP-HPLC method for the rapid and accurate quantification of AZT in sustained release tablets during stability testing [87]. The HPLC showed four photoproducts with a degradation percentage of 17.03±1.24% in solid state and 28.61±1.75% in solution state. Again, these photoproducts were not identified. The separations were achieved on a Waters RP-18 XTerra$^{TM®}$ column by using water:methanol (80:20, %v/v) as the mobile phase at a flow rate of 1.0 mL/min and UV detection at 266 nm. Santoro *et al.* employed a LiChrospher® 100 RP-18 (125 × 4.0 mm, 5 μm) column for the quantitative determination of AZT, stavudine and their induced degradation products in capsule

preparations [88]. The mobile phase consisted of methanol-water (25:75 v/v) at a flow rate of 1.0 mL/min.

1.7. Motivation for the project

Sunlight is responsible for the mutagenic and carcinogenic effects of drug substances. UVB radiation (280-320 nm) is the most important band because it not only causes skin cancer but is also responsible for direct mutagenic photoreactions of chemicals in natural sunlight [45]. We sought to investigate the photochemical stability of AZT as this is an important factor giving rise to the phototoxicity and photoallergy effects of this drug. Photolytic degradation causes structural modifications which could result in a change in the physicochemical properties of drugs. Light interacts with the drug molecules and endogenous substrates causing photodecomposition of the drug which leads to the loss of potency and clinical efficacy. Thus, there is a need to understand the photodegradation mechanism responsible for the phototoxicity of AZT.

In addition, AZT exhibits a number of shortcomings as regards its clinical efficacy as enumerated by Raviolo *et al*. [13]. Since AZT contains three photoactive groups in its structure, these can be utilised in photochemical synthetic methods to produce analogues with improved clinical efficacy. Therefore, there is a need to understand the photochemical behaviour of AZT in different media which this research seeks to do.

1.8. Aim and objectives

The aim of the project was to investigate the photochemical stability of AZT in different solvents. To achieve this aim the following objectives were undertaken:

- Irradiation of AZT under different conditions of pH, concentration and solvent.

- The photostability of AZT was monitored by ultraviolet and visible (UV/Vis) spectrophotometry.
- Photoproducts were separated by high performance liquid chromatography (HPLC).
- AZT was quantified by HPLC with an internal standard (acetophenone).
- Identification of photoproducts was carried out by liquid chromatography-mass spectrometry (LC-MS).

Chapter 2 contains a description of the materials, equipment and experimental methods used to undertake this research. The results obtained are presented and discussed in Chapter 3. The final conclusions reached and possible future work is discussed in Chapter 4.

CHAPTER 2

EXPERIMENTAL

This chapter describes the materials, equipment and methods used to investigate the photostability of AZT.

2.1. Materials

Zidovudine (AZT, >98.2 %) was purchased from J&H Chemical Co., Ltd (Durban, South Africa). Methanol (HPLC grade), acetonitrile (HPLC grade), ethanol (HPLC grade) and 2-propanol (CP grade) were obtained from Sigma-Aldrich (Durban, South Africa). Phosphorus pentoxide (P_2O_5), thymine, hydrochloric acid (HCl), sodium hydroxide (NaOH) and acetophenone were purchased from Saarchem (Pty) Ltd. Water was purified by a Millipore Milli-Q Elix 5 UV water purification system.

2.2. Extraction of AZT

In order to avoid the impurities from zidovudine in the high performance liquid chromatography (HPLC) analysis, the powder of zidovudine was re-extracted by dissolution in methanol and the resulting solution filtered by vacuum filtration. The filtrate was placed under air to evaporate the solvent. The product was dried in a vacuum oven for 3 hours at 60 ^{o}C with a pressure of 700 mbar. Phosphorous pentoxide (P_2O_5) was used to monitor the dryness. This purified AZT was used in all the experiments undertaken.

2.3. UV-irradiation source

A Luzchem (LZC-EDU) educational photoreactor was used as a source of UV-irradiation. The reactor was equipped with medium pressure mercury vapour lamps. The lamp emission spectrum is shown in **Fig. 2.1**.

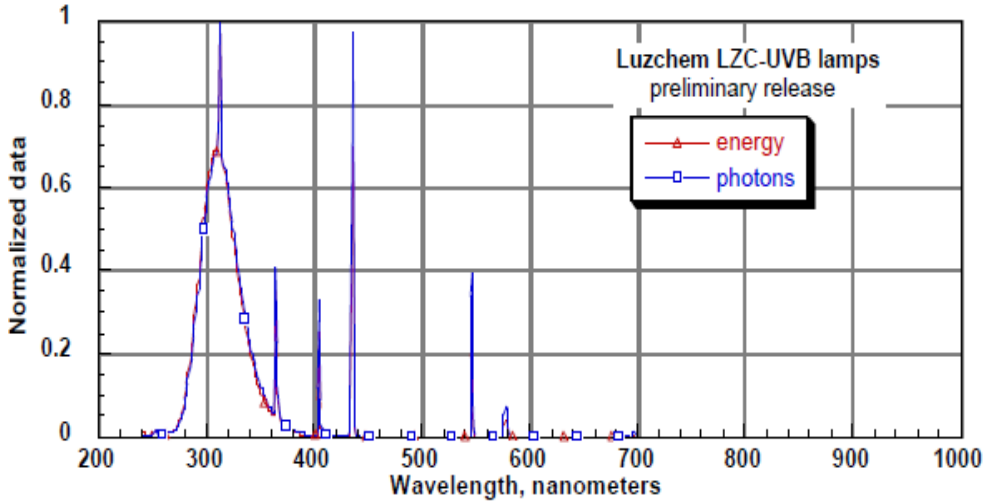

Figure 2.1: Emission spectrum of LZC-UVB lamps.

The lamps were housed (**Fig. 2.2**) in an insulated box made of mild steel and connected through a transformer (220 Volts) to the power supply. The box was fitted with a cooling fan to prevent the build-up of heat. The lamps required a 5-minute warm-up period before each experiment.

Figure 2.2: Lamp housing.

The samples to be irradiated were placed in open Pyrex® test tubes. These Pyrex® test tubes were transparent to UV radiation for wavelengths greater than 300 nm. The test tubes were placed in a carousel on top of a battery-operated turn-table. The photolysis irradiation set up is shown in **Fig 2.3**. Only side lamps were used for each experiment.

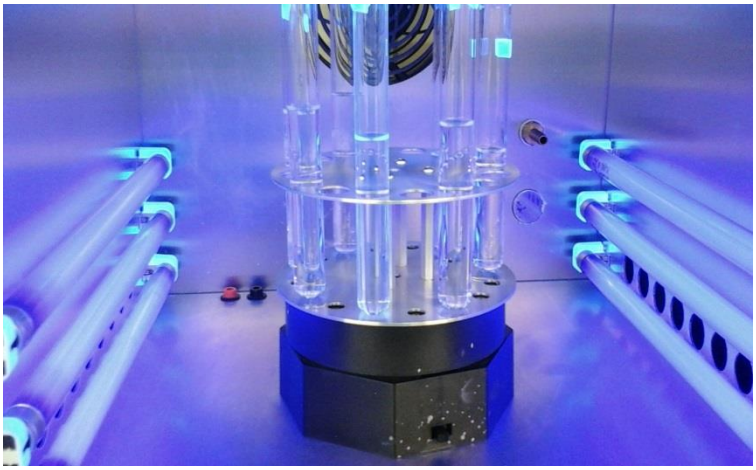

Figure 2.3: Photolysis irradiation set-up.

2.4. Photolysis experiments

UV irradiation of solutions of AZT was carried out in a Luzchem (LZC-EDU) photoreactor equipped with medium pressure mercury vapour lamps as described in **Section 2.3**. The experiments were carried out for different concentrations of AZT and pH, and for different solvents.

The effect of concentration was investigated at 5.01×10^{-2}, 4.94×10^{-4} and 2.39×10^{-4} M in different solvents (water, methanol, ethanol, 2-propanol and acetonitrile). The samples were irradiated for 1, 2, 3, 4 and 5 hours.

The effect of pH was investigated at pH 3, 5, and 7 at a concentration of 4.94×10^{-4} M AZT in aqueous solution. The pH was adjusted with either HCl (0.1 M) or NaOH (0.1 M).

The effect of solvent was investigated at a concentration of 4.94×10^{-4} M in water, methanol, ethanol, 2-propanol, as well as acetonitrile.

2.5. Ultraviolet and visible spectrophotometry

The photostability of AZT was monitored by UV/Vis spectrophotometry.

2.5.1. Theory and instrumentation

Ultraviolet and visible (UV/Vis) spectroscopy is the technique that is used to study the absorbance of a material as a function of wavelength. It is frequently referred to as electronic spectroscopy and falls between the wavelength range of 190–800 nm in the electromagnetic spectrum [89]. Four possible electronic transitions, namely $\pi \rightarrow \pi^*$, $n \rightarrow \pi^*$, $\sigma \rightarrow \sigma^*$ and $n \rightarrow \sigma^*$, can occur on absorption of a photon in the UV region. The σ-bond electrons are the most stable electrons and require the greatest amount of energy to be moved to higher energy levels. π-Bond electrons are relatively unstable and require less energy for excitation. These electrons would therefore absorb energy in the ultraviolet and visible light region. Non-bonding electrons are electrons belonging to lone pairs of atoms. They have higher energy levels than π-electrons and can also be easily excited by UV/Vis light.

The $\pi \rightarrow \pi^*$ (bonding to antibonding) and $n \rightarrow \pi^*$ (non-bonding to antibonding) electronic transitions are the most important electronic transitions in UV/Vis spectroscopy. The $\pi \rightarrow \pi^*$ transition normally occurs in conjugated molecules whereas the $n \rightarrow \pi^*$ transition occurs in carbonyl groups. Their electrons are imparted with energy in the form of light radiation which causes a jump from a lower energy to a higher energy molecular orbital. The resulting species is known as the excited state or anti-bonding state (**Fig. 2.4**).

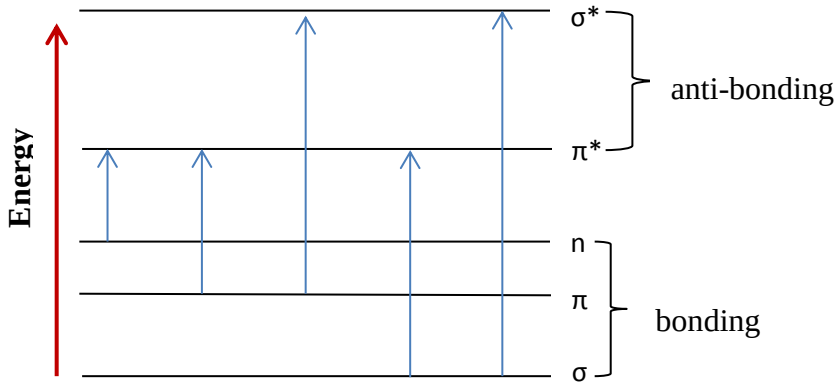

Figure 2.4: Different types of electronic transitions and their relative energies.

The n → π* transitions tend to have a low molar absorptivity (between 10-100 mol^{-1} cm^{-1}) and undergo a blue shift with polar solvent interactions (a shift to higher energy and shorter wavelengths) [90]. Such a shift is known as a hypsochromic effect and is due to the interaction between the lone pair and the solvent especially a polar solvent, such that the solvent aligns itself with the ground state. The excited state occurs in such way that the solvent molecules do not have sufficient time to rearrange in order to stabilize the excited state.

The π → π* transitions involve the movement of an electron from a bonding π orbital to an antibonding π* orbital. This transition tends to undergo a red shift in λ_{max} with solvent interactions (a shift to lower energy and longer wavelengths) and this is known as a bathochromic effect. The change could either be due to a rising of the ground state energy or lowering of the excited state energy.

Because of the distinct energy gaps between the molecular orbitals of a molecule, the UV/Vis spectrum of a substance can be used for identification of the chromophore contained within the structure. However, UV/Vis spectroscopy is mostly use for quantitative analysis of samples by making used of the Beer-Lambert law. The law states that the concentration of a substance in solution is directly proportional to the absorbance of the solution (**Fig. 2.5**).

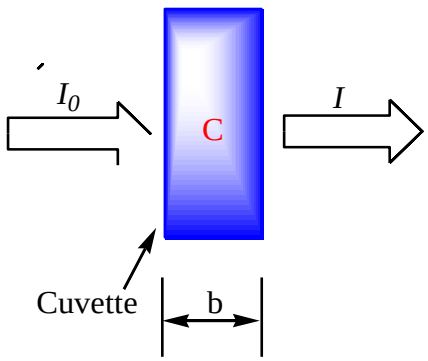

Figure 2.5: Beer-Lambert law.

When the radiation passes through a solution, the amount of light absorbed or transmitted is an exponential function of the molecular concentration of the solute and also a function of the pathlength of the radiation through the sample. Therefore,

$$A = log \frac{I_0}{I} = \varepsilon cl$$

where I_o is the intensity of the incident light, I is the intensity of light transmitted through the sample solution, c is the concentration of the solute (mol L^{-1}), l is the path length of the sample (cm) and ε is the molar absorptivity or the molar extinction coefficient of the sample (L mol^{-1} cm^{-1}).

The basic components of a UV/Vis spectrophotometer (**Fig. 2.6**) consist of a light source, a monochromator, a wavelength selector, a cuvette for the sample solution, a photoelectric detector, and a digital display or a meter. The spectrophotometer operates by passing the light from the source through the first slit of the monochromator that ensures that all the light photons are travelling on a parallel pathway. The light then strikes the prism to give different wavelengths that pass through the exiting slit to produce a single wavelength. Each monochromatic beam is then split into two equal intensity beams by a half mirror device, where one passes through the blank (solvent) and the other passes through the sample.

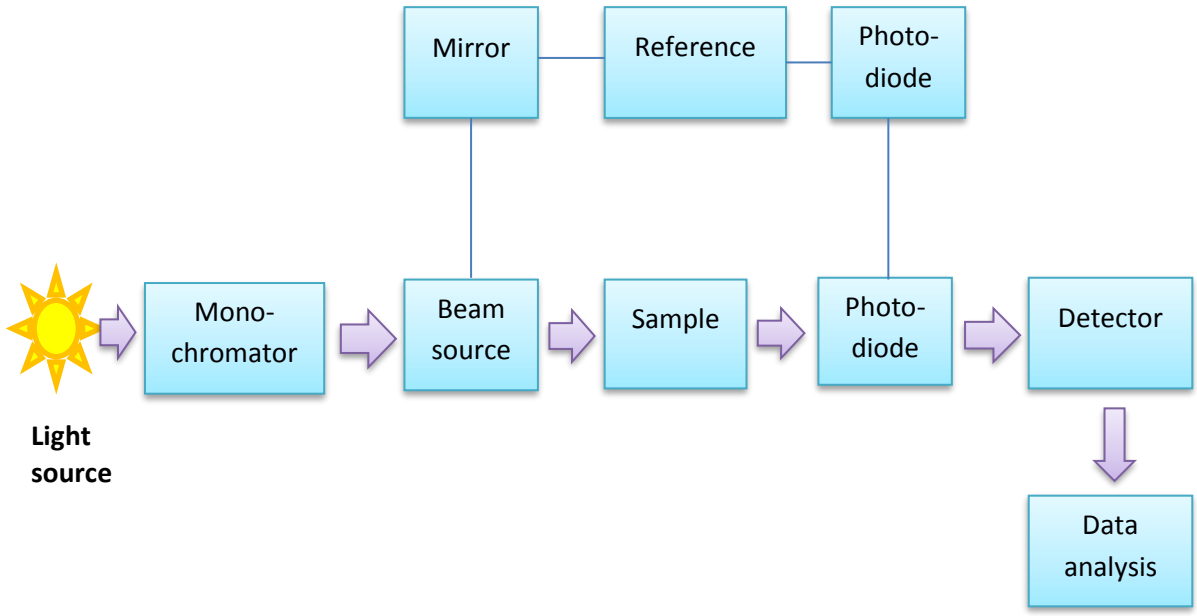

Figure 2.6: Schematic diagram of the components of a UV/Vis double-beam spectrophotometer.

2.5.2. Choice of solvent

The choice of solvent is the most important factor in UV/Vis spectroscopy. The following are the key selection criteria for the choice of suitable solvents for UV/Vis spectrometry:

1. The solvent must dissolve the reactant.
2. The solvent should be transparent at the UV irradiation wavelength.
3. The solvent should not absorb UV radiation in the same region as the substance whose spectrum is being determined.

In this work, five solvents, namely, water (**Fig. 2.7**), methanol (**Fig. 2.8**), ethanol (**Fig. 2.9**), 2-propanol (**Fig. 2.10**), and acetonitrile (**Fig. 2.11)** were investigated. All solvents showed a UV cut-off wavelength similar to that found in literarure (see **Table 3.2**), excluding 2-propanol which showed a UV cut-off wavelength different from literature (see **Table 3.2**). The UV cut-off wavelength obtained was 225 nm. This could be due to the low grade of 2-

propanol used. The UV spectra of each of these solvents measured against air are shown in **Fig 2.7 to 2.11**.

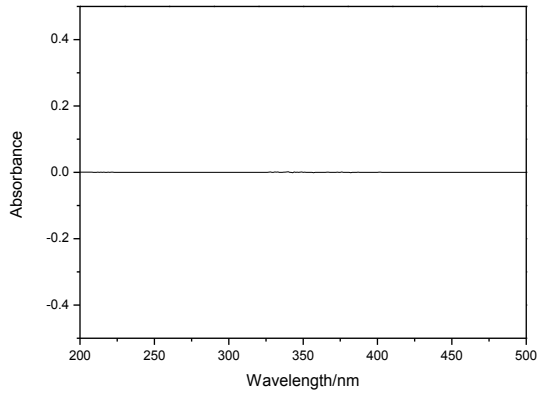

Figure 2.7: UV absorption spectrum of water measured in a 10 mm pathlength quartz cuvette.

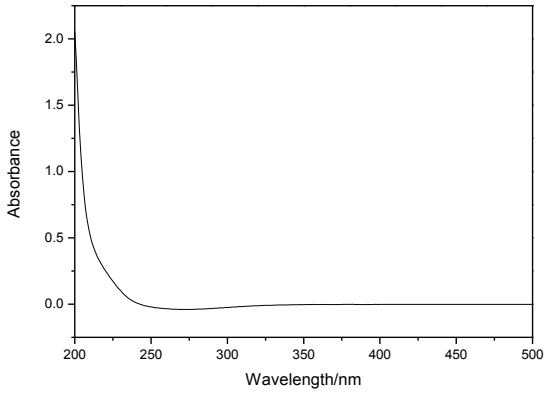

Figure 2.8: UV absorption spectrum of methanol measured in a 10 mm pathlength quartz cuvette.

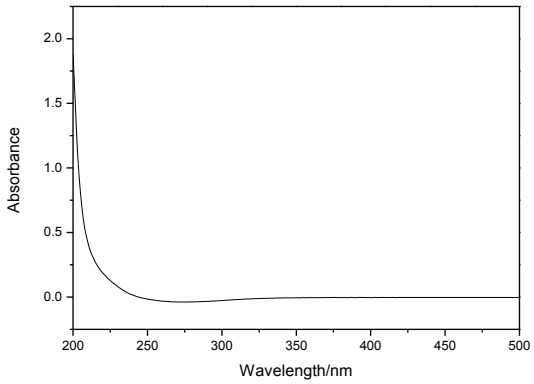

Figure 2.9: UV absorption spectrum of ethanol measured in a 10 mm pathlength quartz cuvette.

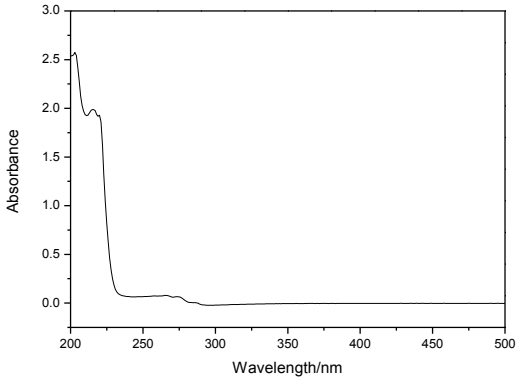

Figure 2.10: UV absorption spectrum of 2-propanol measured in a 10 mm pathlength quartz cuvette.

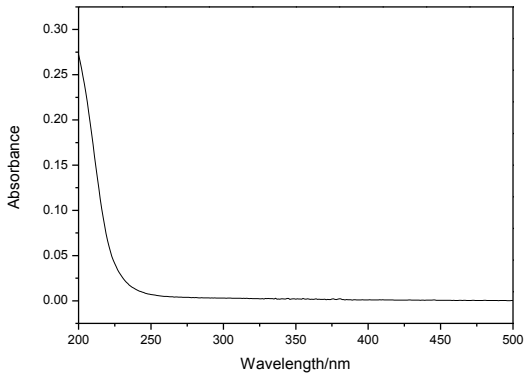

Figure 2.11: UV absorption spectrum of acetonitrile measured in a 10 mm pathlength quartz cuvette.

2.5.3. Solvent photostability

An investigation of the photostability of the solvent is essential in order to determine whether the solvent masks or influences the photostability of a chemical absorber since photo-unstable solvents can photodegrade to produce reactive chemical species that can react with the absorber [91]. In this work the photostability of the polar solvents, namely, water (**Fig. 2.12**), methanol (**Fig. 2.13**), ethanol (**Fig. 2.14**), 2-propanol (**Fig. 2.15**), and acetonitrile (**Fig. 2.16**) were investigated. All solvents were irradiated for 5 hours under UV light and were subsequently monitored with a PerkinElmer Lambda 35 double-beam UV/Vis spectrophotometer. All spectra were acquired in a 10 mm pathlength quartz cuvette against air in the reference beam. All solvents were photostable.

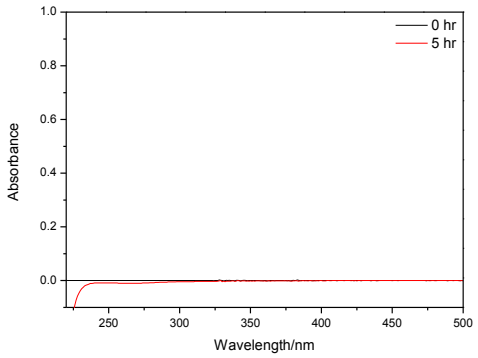

Figure 2.12: UV/Vis spectra of water before and after 5 hours of irradiation.

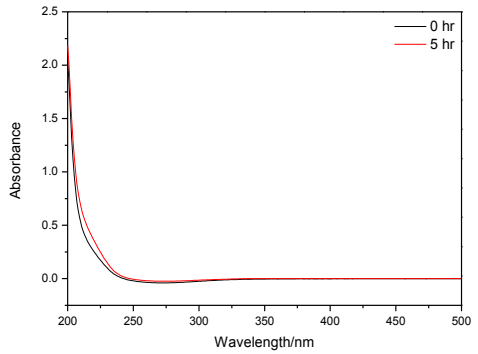

Figure 2.13: UV/Vis spectra of methanol before and after 5 hours of irradiation.

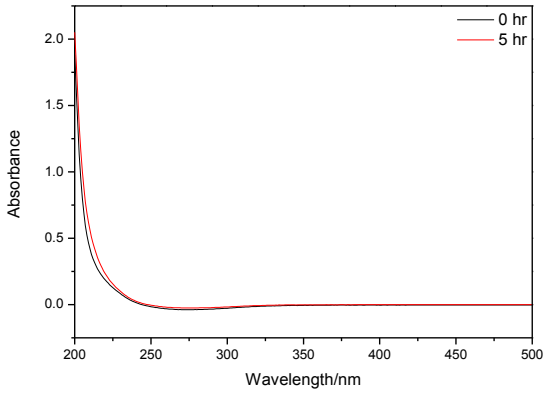

Figure 2.14: UV/Vis spectra of ethanol before and after 5 hours of irradiation.

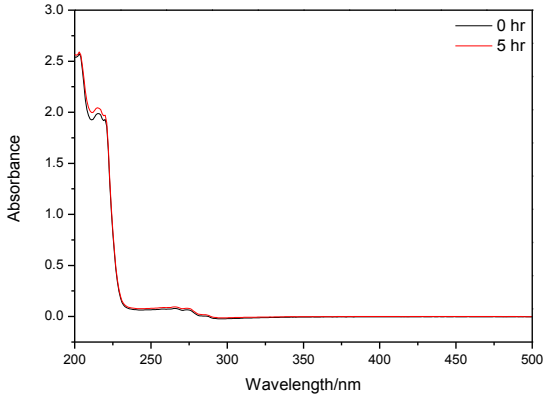

Figure 2.15: UV/Vis spectra of 2-propanol before and after 5 hours of irradiation.

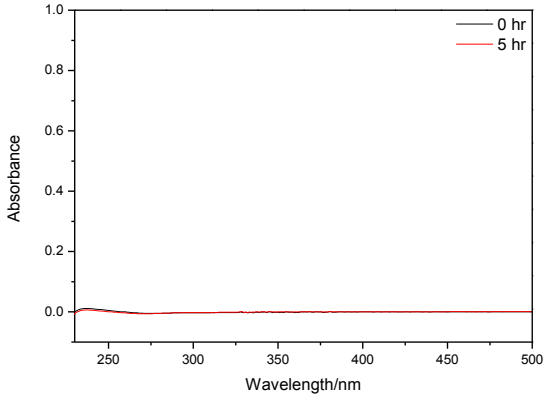

Figure 2.16: UV/Vis spectra of acetonitrile before and after 5 hours of irradiation.

2.5.4. Dark experiment

The dark controls were performed for each of the solvents, namely, water, methanol, ethanol, 2-propanol and acetonitrile. AZT (4.94×10^{-4} M) was kept in the dark for 5 hours and the samples were subsequently monitored with a PerkinElmer Lambda 35 double-beam UV/Vis spectrophotometer. For UV/Vis analysis, the samples were prepared by pipetting 800 µL of 4.94×10^{-4} M from a sample of AZT into a volumetric flask (10 mL) and all diluted to the mark with the specific solvent. All spectra were acquired in a 10 mm pathlength quartz cuvette against air in the reference beam. AZT did not degrade in the dark as shown in **Fig. 2.17 to 2.21**.

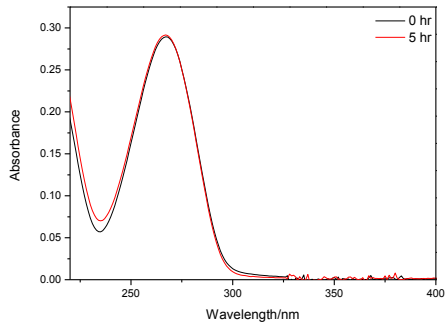

Figure 2.17: UV spectra of AZT (4.94×10^{-4} M) in water before and after 5 hours in the dark.

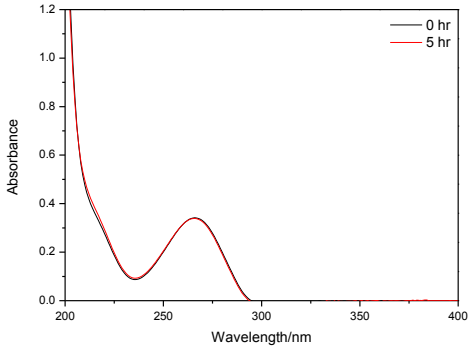

Figure 2.18: UV spectra of AZT (4.94×10^{-4} M) in methanol before and after 5 hours in the dark.

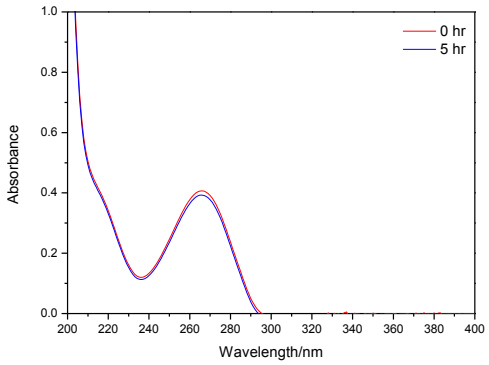

Figure 2.19: UV spectra of AZT (4.94 $\times 10^{-4}$ M) in ethanol before and after 5 hours in the dark.

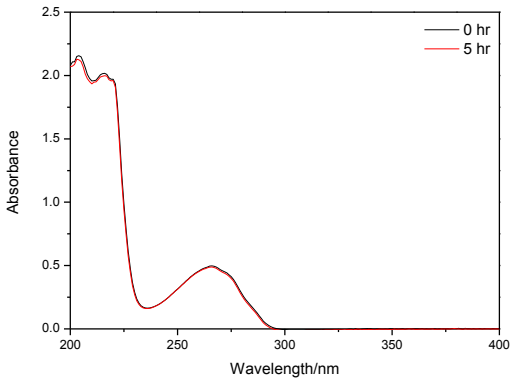

Figure 2.20: UV spectra of AZT (4.94 $\times 10^{-4}$ M) in 2-propanol before and after 5 hours in the dark.

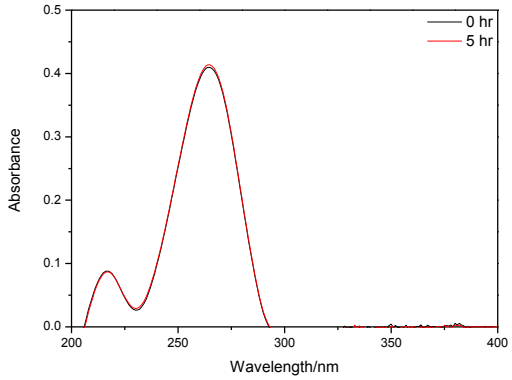

Figure 2.21: UV spectra of AZT (4.94 $\times 10^{-4}$ M) in acetonitrile before and after 5 hours in the dark.

2.5.5. Sample preparation for UV assessment

The samples for UV spectroscopy were prepared by pipetting 8 μL of 5.01 $\times 10^{-2}$ M, 800 μL of 4.94 $\times 10^{-4}$ M and 1600 μL of 2.39 $\times 10^{-4}$ M from an irradiated sample of AZT into a volumetric flask (10 mL) and diluted to the mark with the appropriate solvent or with water for the reactions in different pH. All UV/Vis spectra were recorded with a double-beam PerkinElmer Lambda 35 UV/Vis spectrophotometer (**Fig. 2.21**) with the samples contained in sealed 10 mm quartz cells under the following conditions: scan speed: 480 nm/min, scan wavelength range: 200-500 nm, smooth: 2 nm, slit width: 1.00 nm, lamp change: 326 nm, ordinate mode and the number of cycles: 1. The spectra acquired are presented and discussed in **Section 3.1**.

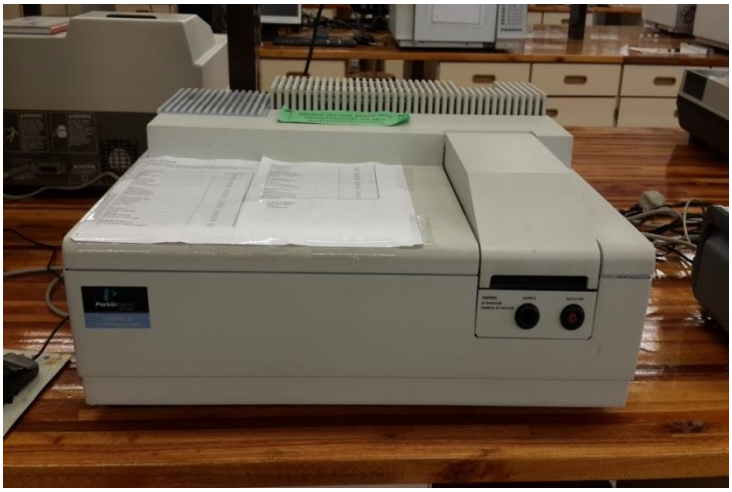

Figure 2.21: PerkinElmer Lambda 35 double-beam UV/Vis spectrophotometer used for photostability assessment.

2.5.6. Determination of linear response and molar absorptivity of AZT in different solvents

The Beer-Lambert law (described in **Section 2.5.1**) gives a linear relationship. However, under certain circumstances it can also give a non-linear relationship. In this work the determination of the linear response and the molar absorptivity of AZT was performed in

different solvents. For each curve, five solutions of AZT in the particular solvent were prepared in the concentration range of 9.35×10^{-6} to 7.48×10^{-5} M. The absorbance of each of these solutions was then recorded at the wavelength of maximum absorption, λ_{max} (266 nm), with, the respective solvent as the blank. The resulting data were plotted to obtain the curves shown in **Fig 2.22** to **2.26**. These curves were all linear in the concentration range tested. The slopes of those curves provide the molar absorptivity of AZT in each solvent. These values are provided and discussed in **Section 3.1.1**. All curves passed through zero as expected for adherence of the Beer-Lambert law (zero intercept) expect for that of 2-propanol. Again, this may be due to the low-grade of 2-propanol used.

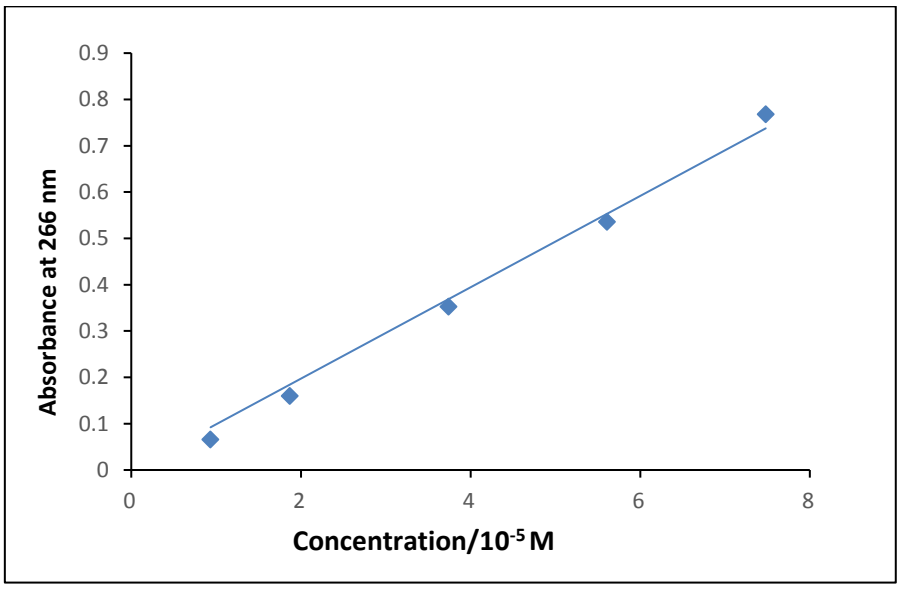

Figure 2.22: The linear response of absorbance and determination of the molar absorptivity coefficient of AZT in water.

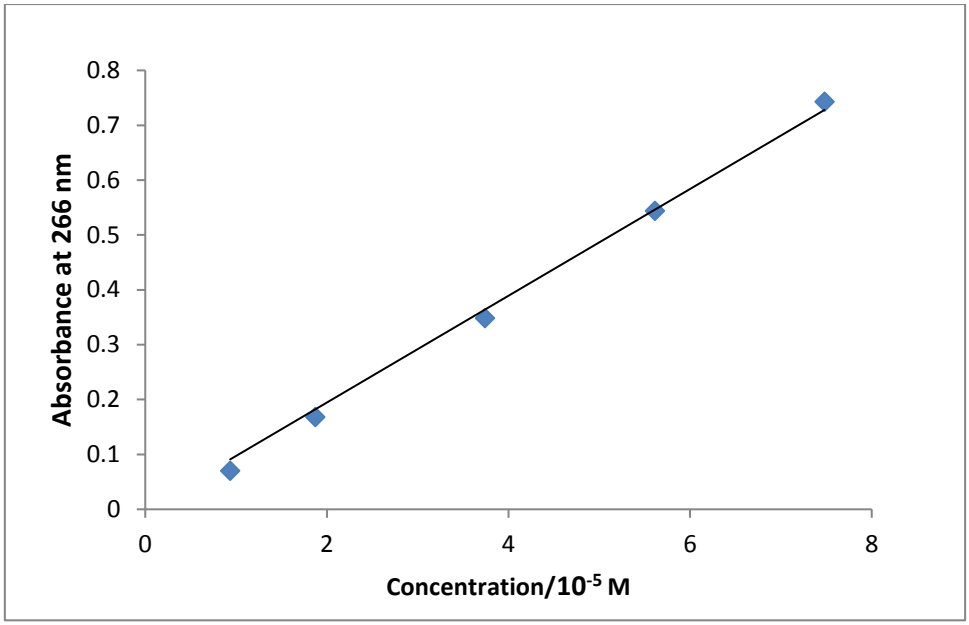

Figure 2.23: The linear response of absorbance and determination of the molar absorptivity coefficient of AZT in methanol.

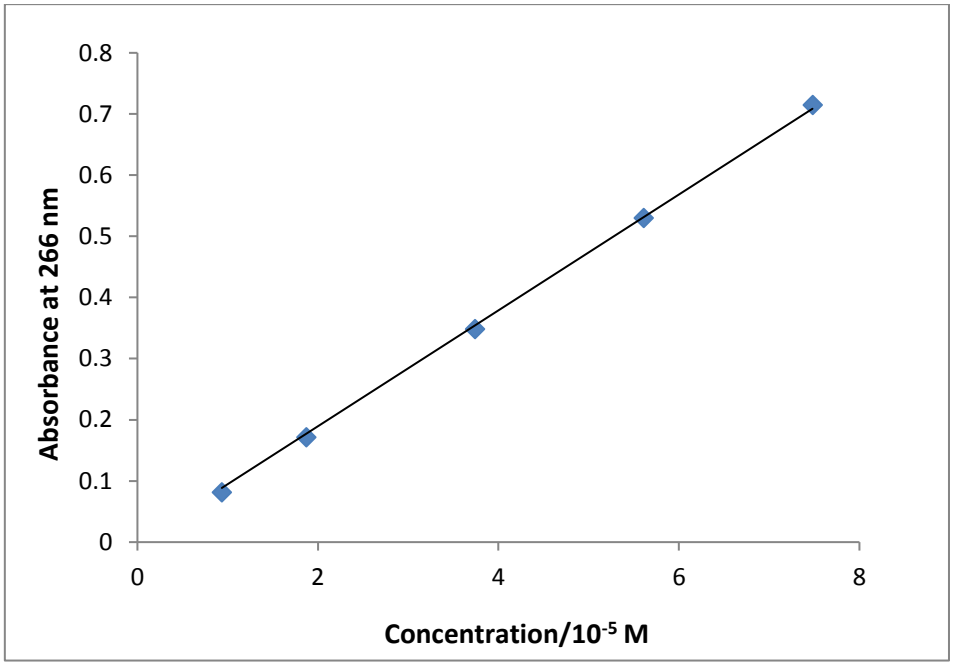

Figure 2.24: The linear response of absorbance and determination of the molar absorptivity coefficient of AZT in ethanol.

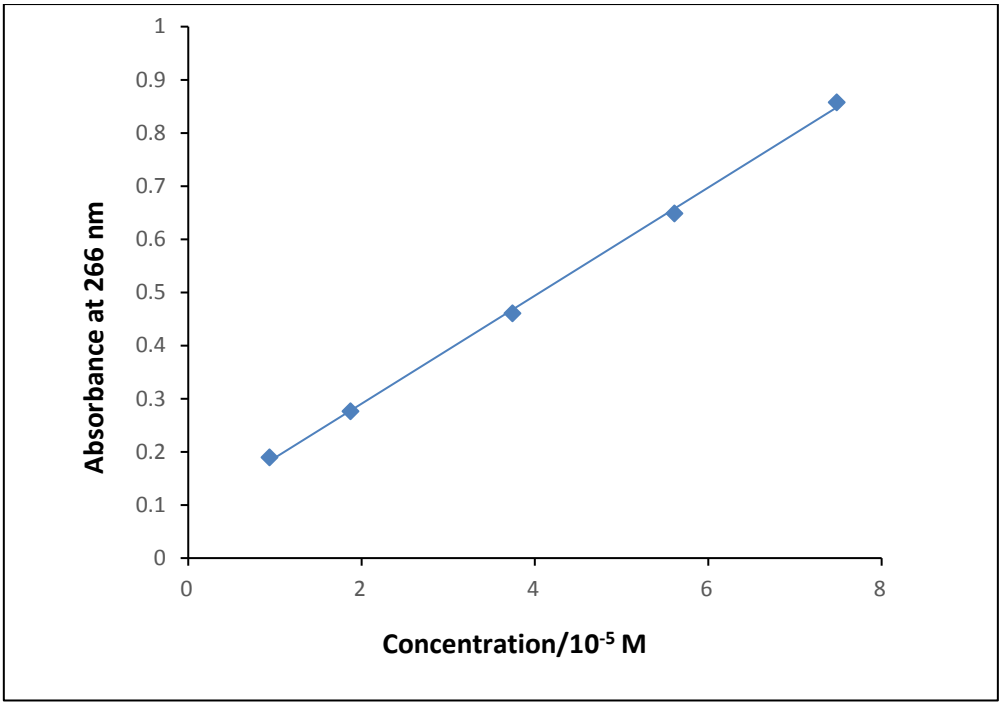

Figure 2.25: The linear response of absorbance and determination of the molar absorptivity coefficient of AZT in 2-propanol.

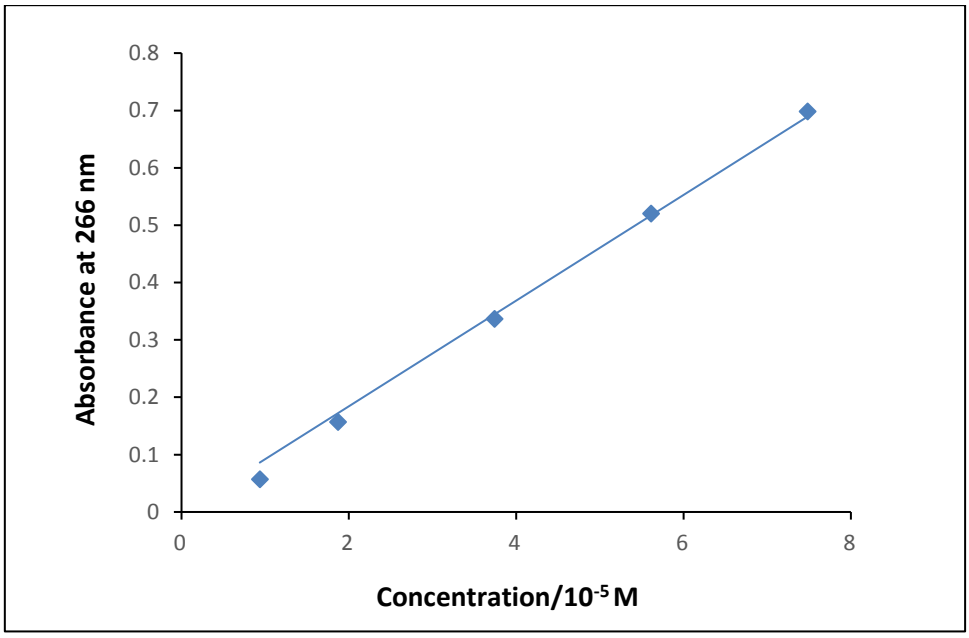

Figure 2.26: The linear response of absorbance and determination of the molar absorptivity coefficient of AZT in acetonitrile.

2.6. High performance liquid chromatography

High performance liquid chromatography (HPLC) was used for the separation and quantification of the photoproducts of AZT.

2.6.1. Theory and instrumentation

HPLC is an analytical technique used for separation of non-volatile compounds. It is widely employed in the pharmaceutical industry for drug discovery as well as in biochemistry and analytical chemistry laboratories for the identification, quantification and purification of components in a mixture [92]. There are many modes of HPLC, namely, normal phase mode, reversed phase (RP-HPLC), ion-exchange, etc. However, RP-HPLC is the most commonly used because of its simplicity, versatility and ability to handle compounds of diverse polarity and molecular mass [93].

RP-HPLC involves the separation of molecules on a hydrophobic surface [94]. The name "reversed phase" is derived from "normal phase" chromatography which involves the separation of molecules based upon their interaction with a polar matrix. Silica is one of the commonly used stationary phases in RP-HPLC in which its surface has been modified with RMe_2SiCl, where R is a straight chain alkyl group such as $C_{18}H_{37}$ and C_8H_{17} [95, 96].

Practical application of HPLC consists of the basic concepts of chromatographic theory such as retention time and resolution. Retention time is defined as the time duration of a component retained in the column [93]. The retention time is best described as a column capacity ratio (k') in equation (1).

$$k' = \frac{t_R - t_0}{t_0} \qquad (1)$$

where, t_R is the retention time of the peak and t_0 is the dead time of the column. The longer a component is retained by the column, the greater is the capacity factor.

Resolution (R_s) is expressed as the ratio of the distance between two peak maxima to the mean value of the peak width at the base line sensitivity. Resolution is best described as in equation (2) [97].

$$R_s = \frac{2[T_{R2} - T_{R1}]}{W_1 + W_2} \qquad (2)$$

where T_{R1} and T_{R2} are the retention times of a pair of peaks, and W_1 and W_2 are their corresponding baseline peak widths.

An HPLC system includes the mobile phase, pump, injection system, column, detector and the display system (**Fig. 2.27**). The process begins by the injection of the sample at the end of the column, followed by mobile phase pumped through the column to help in the separation of the components. Then, the eluting components pass through the detector and the property monitored is displayed in the form of a chromatogram. To collect, store and analyze the chromatographic data, integrators and other data-processing equipment are frequently used.

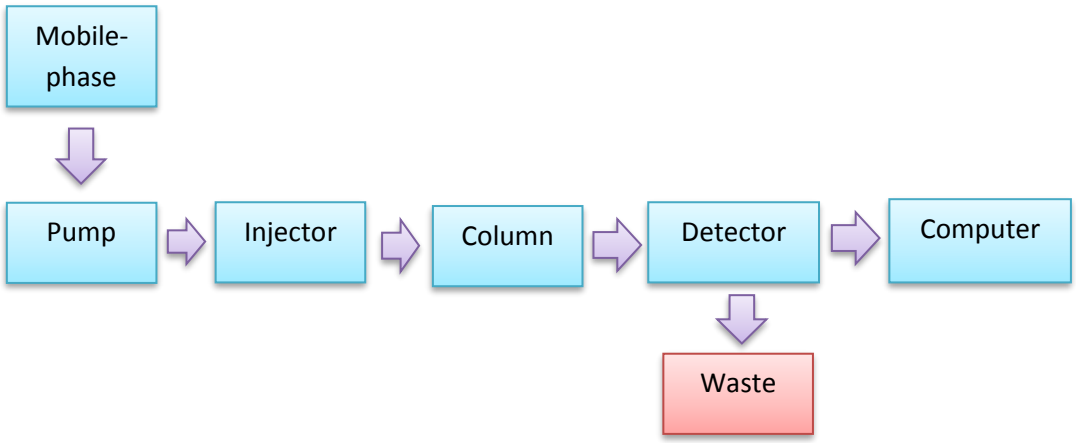

Figure 2.27: Schematic of the components of a typical HPLC.

2.6.1.1. Mobile phase

The separation of the components depends on the type and composition of the mobile phase. Different solvents are used for different types of HPLC. For example, normal phase HPLC uses non-polar solvents, whereas RP-HPLC uses polar solvents. The most common solvent reservoirs are as simple as glass bottles with tubing connecting them to the pump inlet. The mobile phase must be filtered (in this work HVLP 0.45 μm Millipore filters were used) and degassed with helium gas prior to chromatographic runs. This is done to ensure the absence of any particulate matter that could block the column and to degas the solvent.

2.6.1.2. Pump

HPLC pumps are used to force the solvent (mobile phase) through the stationary phase at a constant flow rate. The pump pressure should always be kept constant to produce accurate and consistent results.

2.6.1.3. Sample injector

The sample injection can be performed manually or automatically depending on the type of HPLC. The injector is positioned just after the pump and is used to transport the sample into the column. The HPLC injector should be able to provide injection of the liquid sample within the range of 0.1-100 mL with high reproducibility and under high pressure (up to 4000 psi) [98].

2.6.1.4. Column

The column is known as the heart of the chromatography system. It is used to separate the components which are placed in it by the injector. The columns differ in their lengths, bore sizes and packing materials. The components of the sample separate based on their differing interactions with the column packing. The species that strongly interact with the stationery

phase in the column tend to have longer retention times due to the time spent to adsorb to the column's adsorbent. In RP-HPLC functional groups are bonded to the silanol groups of silica to produce a hydrophobic packing. In the case of C18 column packing material, octadecyl groups are bonded to the silanol groups as shown in **Fig. 2.28** [99].

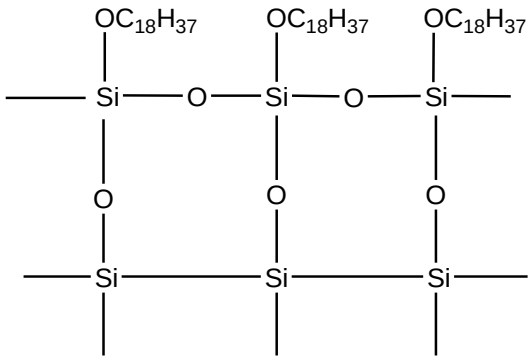

Figure 2.28: C18 groups attached to silica particles.

2.6.1.5. Detectors

HPLC detectors are used to examine and identify the eluted components from the column. Different kinds of detectors are used in HPLC such as refractive index (RI), ultraviolet (UV/Vis), fluorescence, mass spectrometric, electrochemical and conductivity detectors. However, the UV/Vis detector is the most common one used because many organic compounds absorb UV light of various wavelengths [100]. Each detector has its assets, limitations and sample types for which it is most effective. In this work use was made of a UV/Vis detector in the form of a photodiode-array detector. In addition, a mass spectrometric detector was also used in order to identify the photoproducts of AZT.

2.6.1.5.1. UV detector

UV detectors use light as a sensor and they are most commonly employed in biology and pharmaceutical laboratories for the analysis of nucleic acids and drugs. There are three types of UV detectors, namely, fixed wavelength, variable wavelength and the photodiode-array

[100]. However, the photodiode-array (PDA) detector is the most commonly used because it provides the UV/Vis spectrum for each component which can be used for identification purposes, it gives sufficiently different spectra for two closely eluting peaks, and can also give a chromatogram with and without subtraction of a reference wavelength as well as the peak purity [101, 102]. A PDA detector uses a deuterium or xenon lamp which emits light over the UV spectral range. The light passes through an achromatic lens system which focuses the light through the sample cell and onto a halographic grating (**Fig. 2.29**).

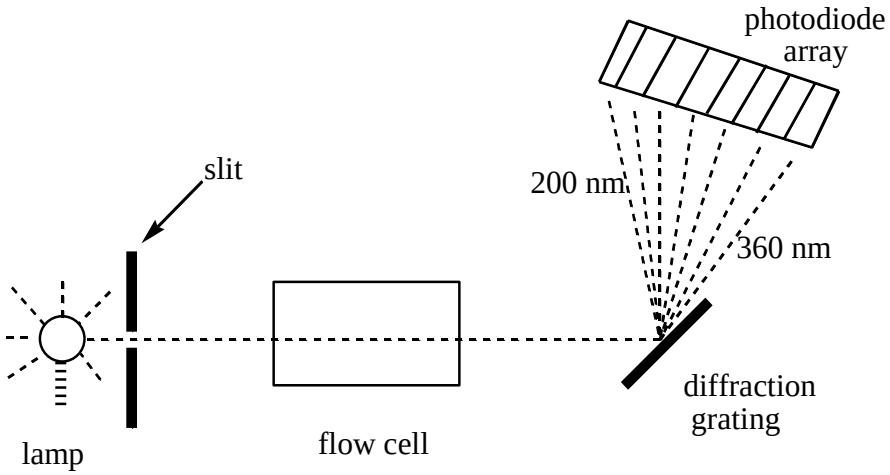

Figure 2.29: Schematic of a photodiode-array UV detector [101].

2.6.1.5.2. Mass spectrometric detector

HPLC equipped with tandem mass spectrometric (MS) detection has been used as a powerful technique for the quantitative determination of drugs and metabolites in biological fluids [103]. The technique combines physical separation with mass analysis. The MS functions by ionizing the chemical compounds, to generate molecular fragments and measuring their mass-to-charge ratio. The ions are separated in the analyzer by electromagnetic fields and processed into mass spectra.

MS instruments consist of three modules (**Fig. 2.30**):

1. An ion source, which creates gas-phase ions in a sample.

2. A mass analyzer, which separates the ions based on their mass-to-charge ratio by using electromagnetic fields.
3. A detector, which detects the ions and provides data for calculating the abundances of each ion present.

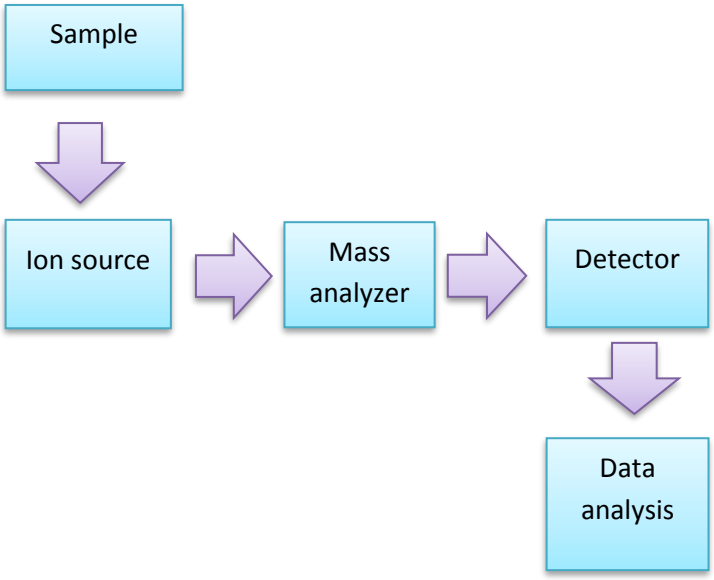

Figure 2.30: Mass spectroscopy process.

2.6.2. Separation techniques

There are two types of separation method in HPLC, namely, the isocratic and gradient method. Isocratic elution involves a constant composition of mobile phase through the separation process, whereas in the gradient method the composition changes with time. The isocratic method is the simplest technique and should always be the first choice for method development. Gradient methods are normally performed by combining the pressurized flows from two pumps and changing their individual flow rates with an electronic controller while maintaining the overall flow rate constant. In this work, an isocratic elution method was used to separate the photoproducts from AZT.

2.6.3. Sample preparation for HPLC analysis

The samples were prepared by pipetting 8 µL of 5.01 $\times 10^{-2}$ M, 800 µL of 4.94 $\times 10^{-4}$ M and 1600 µL of 2.39 $\times 10^{-4}$ M from an irradiated sample of AZT into a volumetric flask (10 mL) and all diluted to the mark with water (see **Section 3.2**). All samples were filtered through a Sartorius Ministart 0.45 µm syringe filter prior to HPLC analysis.

2.6.4. Quantitative analysis

The quantitation theory involves the measurement of peak height or peak area. There are three different calibration methods that can be utilized in quantitative analysis: external standard, internal standard and the standard addition method [104]. An internal standard is a most effective method as compared with the other two methods [105]. In this work this was the method used for quantification of the degradation of AZT.

2.6.4.1. Internal standard

The internal standard is a compound with a similar chemical structure but not identical to the analyte, which is used to assist the quantification process [106]. In this method, an equal amount of an internal standard (IS) is added to both the sample and calibration solutions. The method uses the response factor, r, given by equation (3) to determine the concentration of the unknown [106, 107].

$$r = \frac{C/A}{C_S/A_S} \qquad (3)$$

where C is the concentration of the unknown, A is the peak area/height of the unknown, C_S is the concentration of the IS and A_S is the peak area of the IS. In this work acetophenone was used as the internal standard.

2.6.4.2. Calibration curve and sample preparation

Stock solutions of AZT and thymine were prepared by weighing AZT (0.025 g) and thymine (0.025 g) separately, dissolving the reagents with water and making up to volume in a volumetric flask (25 mL). These stock solutions were diluted to obtain standards with concentrations of 5, 10, 15, 20, 25 and 30 μg/mL. Acetophenone was used as the internal standard (IS) and was added to these six solutions. A stock solution of IS was prepared by weighing acetophenone (0.025 g) into a volumetric flask (25 mL) and diluted to the mark with water. An aliquot of 25 μL of this solution was added to each of the calibration solutions before making up to volume. A calibration line was obtained by plotting the peak area ratio against the concentration ratio, that is, the peak area of the analyte/peak area of acetophenone against the concentration of the analyte/concentration of acetophenone. The slope of this line provided the required response factor, r, from which concentrations could be calculated. This calibration line is shown in **Section 3.3**.

An aliquot of 25 μL of the 2.081×10^{-5} M acetophenone solution was also added to each of the irradiated sample solutions (prepared as described in **Section 2.6.3**.) prior to making up to volume.

2.6.4.3. HPLC separation conditions

The separations were carried out on an Agilent Technologies 1200 series HPLC system (**Fig. 2.31**). The column was a Phenomenex Kinetex C18 (150 × 4.6 mm i.d., 2.6 μm particle size) column. The mobile phase composition was methanol:water (60:40 v/v) with a flow rate of 0.25 ml/min. The chromatograms were collected at a detection wavelength of 266 nm. The injection volume was 10 μL. The mobile phase was degassed with helium prior to each run. The PDA detector was used to obtain the UV spectra of each analyte present over the wavelength range of 190 to 400 nm.

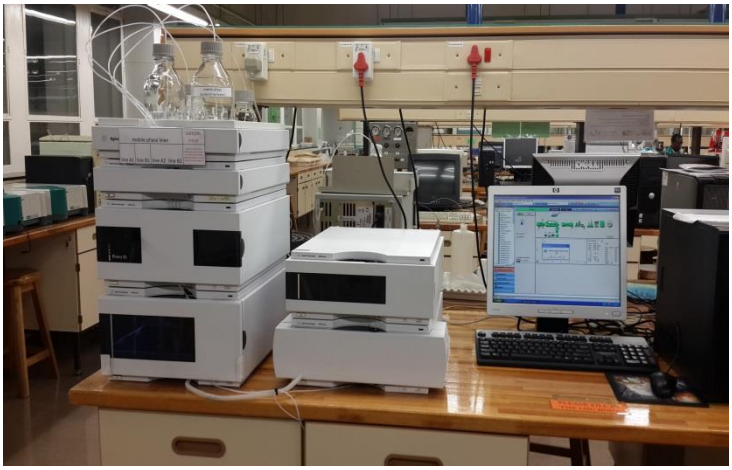

Figure 2.31: Agilent 1200 series HPLC system used for all chromatographic separations.

2.6.4.4. Liquid chromatography-mass spectrometry separation conditions

Photodegradation products were identified on a Shimadzu Prominence-i-LC-2030C 3D HPLC connected to a Shimadzu LC-MS 2020 Quadrupole MS as well as on a Waters Synapt G2 instrument. The column used for the Shimadzu LC-MS 2020 was a Shimadzu Shim-pack GIST C18-HP (150 × 4.6 mm i.d., 3 μm particle size) column at 22 ^{o}C. The mobile phase composition was methanol:water (60:40 v/v) with a flow rate of 0.35 ml/min. The chromatograms were collected at a detection wavelength of 266 nm and the injection volume was 10 μL. The mass spectrometer was operated in both positive and negative electrospray ionization (ESI) modes and the mass-to-charge ratio (*m/z*) range scanned was from 16-400 u.

In the Waters Synapt G2 system, separation was achieved on a Waters BEH C18, 2.1 × 50 mm column with 1.7 μm particles. A gradient was applied by using 0.1% formic acid (solvent A) and acetonitrile containing 0.1% formic acid (solvent B). The gradient started at 100% solvent A for 1 minute and was changed to 28% B over 22 minutes in a linear way. It then went to 40% B over 50 seconds and was followed by a wash step of 1.5 minutes at 100% B, followed by re-equilibration to the initial conditions for 4 minutes. The flow rate was 0.3

ml/min and the column was kept at 55 ºC. The injection volume was 2 µL and the detection wavelength was 266 nm.

Data was acquired in MSE mode which consisted of a low collision energy scan (6 V) from *m/z* 150 to 1500 and a high collision energy scan from *m/z* 40 to 1500. The high collision energy scan was done by using a collision energy ramp of 30-60 V. The photodiode-array detector was set to scan from 220-600 nm.

The mass spectrometer was optimized for best sensitivity, a cone voltage of 15 V, desolvation gas was nitrogen at 650 L/hr and desolvation temperature 275 ºC. The instrument was operated with an electrospray ionization probe in the negative mode. Sodium formate was used for calibration and leucine encephalin was infused in the background as lock mass for accurate mass determinations.

The results of these experiments are presented and discussed in Chapter 3.

CHAPTER 3

RESULTS AND DISCUSSION

In this chapter the results obtained from the investigation of the photostability of AZT in different solvent media, pH and concentration conditions are presented and discussed. Dark controls were performed for each of the experiments and no photoproducts were detected (see **Section 2.5.4**), in agreement with the reports of Dunge and Santos [85, 87].

3.1. Photostability of AZT assessed by UV spectroscopy

The photostability of AZT (4.94×10^{-4} M) was investigated in different polar solvents, namely, water, methanol, ethanol, 2-propanol and acetonitrile, as its solubility is limited in non-polar media [108]. In order to meet the required concentration for UV/Vis analysis, each sample was diluted with the specific solvent after every UV-exposure to make up a concentration of approximately 4×10^{-5} M. The dilution factors were as stated in **Section 2.5.5**. The UV/Vis spectra shown in this Section are all for these diluted solutions that fall within the linear range of the Beer-Lambert law.

3.1.1. UV spectra of AZT in different solvents prior to irradiation

The UV/Vis absorbance spectra of AZT recorded in different solvents prior to irradiation are shown in **Fig. 3.1**. The spectra are characterised by one absorption peak at approximately 265 nm (λ_2) and another peak at a shorter wavelength of approximately 213 nm (λ_1). The wavelength of maximum absorption (λ_{max}) of the longer wavelength band shows a red shift (bathochromic effect) as the polarity of the solvent increases. The results can be seen in **Table 3.1**. This absorption band ($S_0 \rightarrow S_1$) corresponds to a $\pi \rightarrow \pi^*$ transition [109]. It was observed that the greater the proton donation ability of the solvent the greater is the shift. The proton donating ability of the solvents decreases in the order: water > methanol > ethanol

> 2-propanol > acetonitrile, as does the relative polarity. Our results agree with those of Gustavsson *et al.*, who showed that thymine exhibits a red shift in λ_{max} as the polarity of the solvent increases [109]. A blue shift was observed for the band with an absorption wavelength of approximately 213 nm as the polarity of the solvent decreases (see **Table 3.1**). except for 2-propanol. The solvent polarity and proton donating ability characteristics of the solvents are summarised in **Table 3.2**.

The molar absorption coefficient of the longer wavelength band of AZT prepared in five different solvents (see **Table 3.1**) was determined from the slopes of calibration curves as described in **Section 2.5.5**. The results show that the molar absorption coefficient of AZT decreases as the polarity of the solvent decreases. Thus, for the same concentration of AZT the peak absorption is less intense as the solvent polarity decreases again with the exception of 2-propanol.

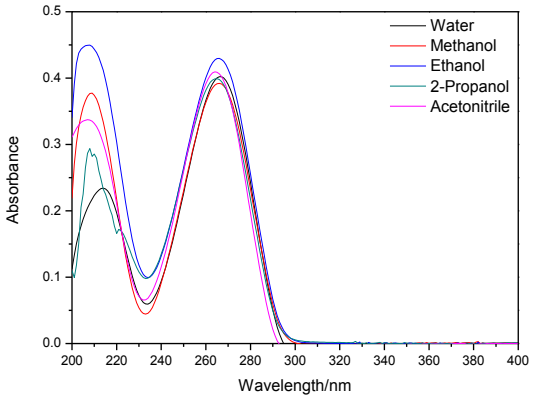

Figure 3.1: UV absorption spectrum of AZT (4.94×10^{-4} M) in different solvents before irradiation recorded on a PerkinElmer Lambda 35 double beam UV/Vis spectrophotometer in a 10 mm pathlength quartz cuvette against air.

Table 3.1: The wavelengths of maximum absorption and the molar absorption coefficient of AZT in different solvents.

Solvent	Maximum Wavelength of λ_1/nm	Maximum Wavelength of λ_2/nm	Molar absorption coefficient of λ_2/L mol^{-1} cm^{-1}
Water	213	266.60	9859.6
Methanol	207	265.50	9731.4
Ethanol	205	265.43	9472.8
2-propanol	208	264.44	10169
Acetonitrile	203	264.15	9211.6

Table 3.2: Characteristics of the solvents used to investigate the photostability of AZT.

Solvent	μ/D [110]	Relative polarity [111]	ε (25 °C) [112]	α [113]	β [113]	π* [114]	E_T(30)/kJ mol^{-1} [114]	$\lambda_{cut-off}$/nm [115]
Water	1.77	1.00	80	1.17	0.18	1.90	224.7	190
Methanol	1.70	0.762	32	0.93	0.62	0.60	231.8	205
Ethanol	1.74	0.654	24	0.83	0.77	0.54	210.9	205
2-propanol	1.65	0.546	18	0.76	0.95	0.48	203.3	205
Acetonitrile	3.54	0.460	38	0.19	0.31	0.75	190.8	190

μ dipole moment
ε dielectric constant
α parameter related to the hydrogen-donating ability of the solvent
β parameter related to the solvent's ability to accept a proton in a solute-solvent hydrogen bond
π^* index of solvent polarity-polarizability
E_T(30) empirical parameter that incorporates both solvent polarity and hydrogen bonding effects

3.1.2. Effect of solvent

AZT was irradiated for a total duration of 5 hours under UVB-light in different solvents, namely, water, methanol, ethanol, 2-propanol and acetonitrile. The solutions changed from clear to yellow after each irradiation in water, methanol, ethanol and 2-propanol (as shown in **Fig. 3.2**) whereas in acetonitrile a yellow precipitate was formed. This change in colour is associated with the azido group [116]. It was also observed that the colour became darker with increase in the irradiation time.

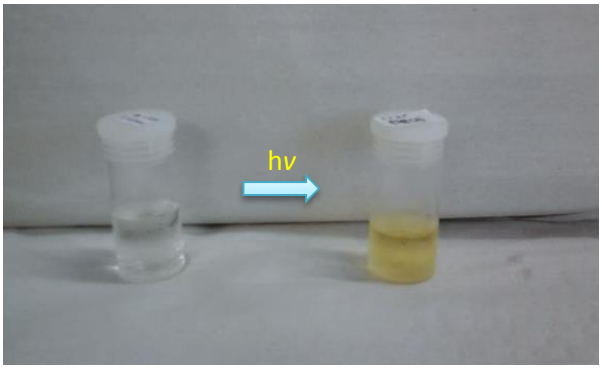

Figure 3.2: Photolysis of AZT in water after 5 hours of irradiation.

For each solvent, the UV spectra were monitored at hourly intervals. The spectra prior to irradiation and after 5 hours of irradiation are shown in **Fig. 3.3**. For all solvents an increase in absorbance (hyperchromic effect) and a hypsochromic effect in λ_{max} at the absorption wavelength of 213 nm was observed with increasing irradiation time. However, in acetonitrile a new band forms at 355 nm. We propose that this arises from elimination of nitrogen to generate a nitrene as a reactive intermediate, which may further undergo intermolecular interaction with the solvent to form a new photoproduct. The increment in absorbance observed with all solvents after five hours of irradiation is possibly due to the formation of photoproducts of AZT that absorb almost in the same region as AZT. This was confirmed by HPLC with a PDA detector and will be described in **Section 3.2**.

(a)

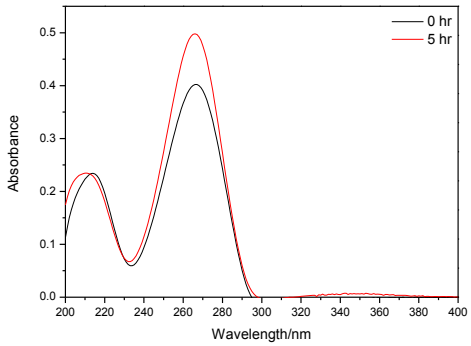

(d)

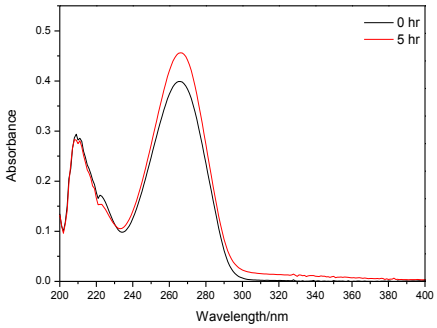

(b)

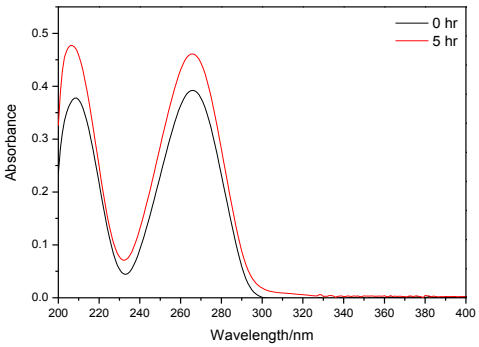

(e)

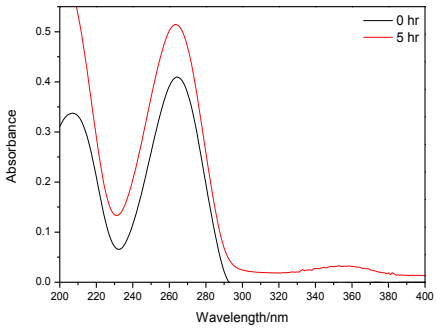

(c)

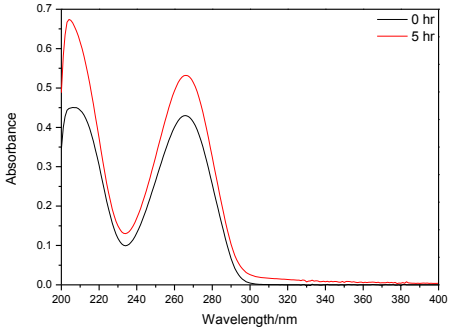

Figure 3.3: UV absorption spectrum of AZT (4.94×10^{-4} M) in (a) water, (b) methanol, (c) ethanol, (d) 2-propanol and (e) acetonitrile before and after 5 hours of irradiation.

3.1.3. Effect of concentration

The photolysis of AZT was investigated at three different concentrations, namely, 2.39×10^{-4} 4.94×10^{-4} and 5.01×10^{-2} M, in five different solvents: water, methanol, ethanol, 2-propanol and acetonitrile.

The UV/Vis spectra of AZT in water monitored at hourly irradiation intervals for the three different starting concentrations (2.39×10^{-4}, 4.94×10^{-4} and 5.01×10^{-2} M) are shown in **Fig. 3.4**. For the highest concentration (5.01×10^{-2} M) no significant change in absorbance was observed as the irradiation time increased. However, for the intermediate concentration (4.94×10^{-4} M) the absorbance generally increased with irradiation time. In the case of the lowest concentration (2.39×10^{-4} M), the absorbance increased between 0 and 3 hours and then decreased during the subsequent two hours. A blue shift at the absorption wavelength of 213 nm was observed for all the three different concentrations and was in the order: highest < intermediate < lowest concentration (see **Fig. 3.4**).

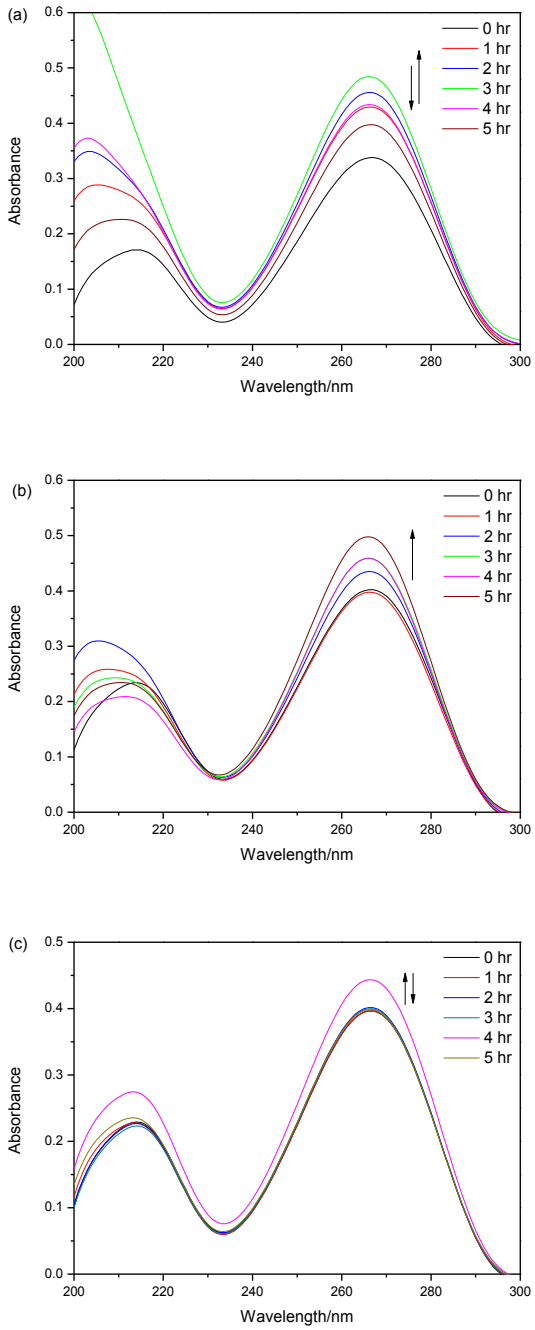

Figure 3.4: UV absorption spectra monitored at hourly intervals for the photolysis of AZT at three different concentrations: (a) 2.39×10^{-4} M, (b) 4.94×10^{-4} M, and (c) 5.01×10^{-2} M, in aqueous solution.

The UV/Vis spectra of AZT in methanol showed a hyperchromic effect for all three concentrations. However, the change in absorbance was not consistent (**Fig. 3.5**) indicating different photoproducts were formed at different UV exposure times. Unlike in water, there

was no observed hypsochromic shift at 213 nm and therefore no significant modification of the chromophores was expected in the photoproducts.

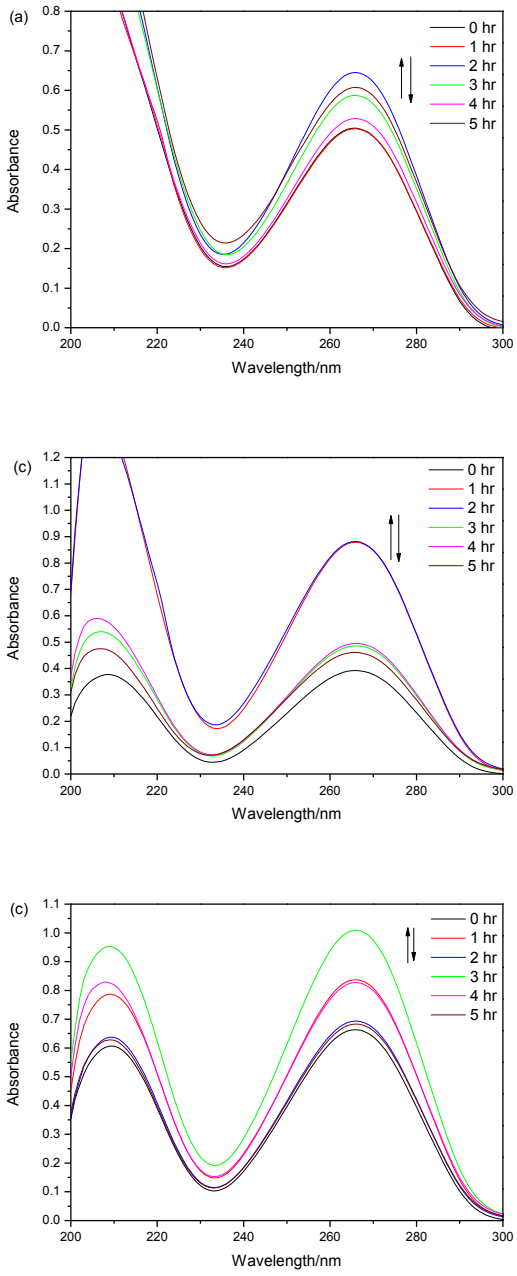

Figure 3.5: UV absorption spectra monitored at hourly intervals for the photolysis of AZT at three different concentrations: (a) 2.39×10^{-4} M, (b) 4.94×10^{-4} M, and (c) 5.01×10^{-2} M in methanol.

The UV/Vis spectra for AZT irradiated in ethanol at three different starting concentrations: 2.39×10^{-4}, 4.94×10^{-4} and 5.01×10^{-2} M, are shown in **Fig. 3.6**. The hyperchromic effect in λ_{max} was observed for all three concentrations. However, there was no hypsochromic effect for all concentrations.

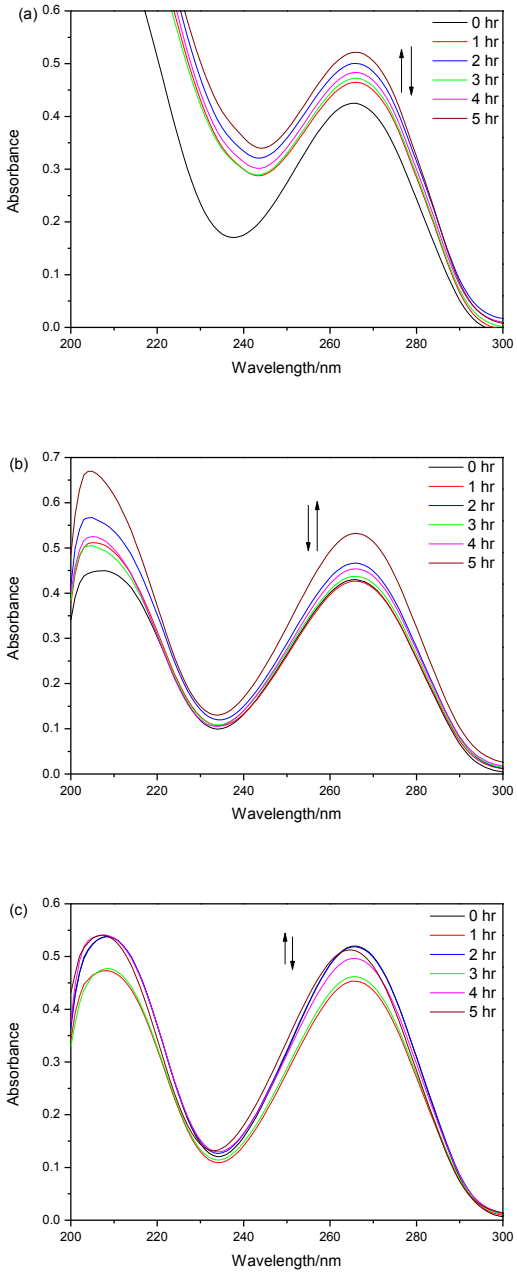

Figure 3.6: UV absorption spectra monitored at hourly intervals for the photolysis of AZT at three different concentrations: (a) 2.39×10^{-4} M, (b) 4.94×10^{-4} M, and (c) 5.01×10^{-2} M in ethanol.

The photolysis of AZT in 2-propanol also showed a hyperchromic effect at λ_1 and at λ_2 for all three concentrations (**Fig. 3.7**) although the change in absorbance was not consistent. A comparison of the absorbance at 213 nm with that in water, methanol or ethanol, shows that it is less intense at all exposure times. This would imply the photoproducts absorbing at this wavelength were few or less efficient absorbers.

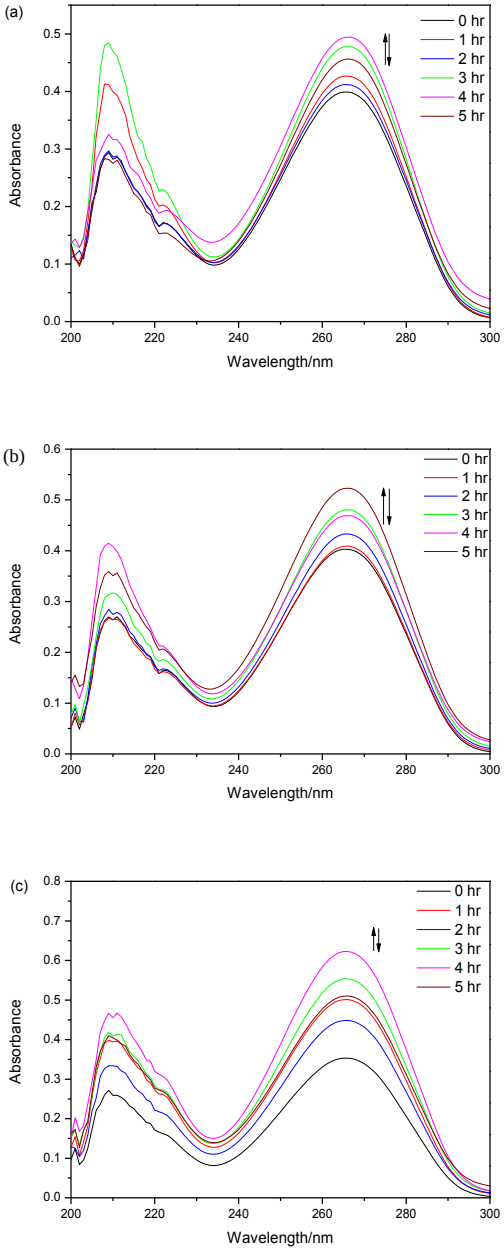

Figure 3.7: UV absorption spectra monitored at hourly intervals for the photolysis of AZT at three different concentrations: (a) 2.39×10^{-4} M, (b) 4.94×10^{-4} M, and (c) 5.01×10^{-2} M in 2-propanol.

The UV/Vis spectra of AZT dissolved in acetonitrile and irradiated at three different concentrations (2.39×10^{-4}, 4.94×10^{-4} and 5.01×10^{-2} M) are shown in **Fig. 3.8**. The results showed three absorption maxima at 213, 266 and 355 nm with hyperchromic effects. The new absorption wavelength at 355 nm was not observed at the highest concentration tested (5.01×10^{-2} M) but was more visible at the lowest concentration (2.39×10^{-4} M). In the case of the two more dilute solutions (2.39×10^{-4} and 4.94×10^{-4} M) the hyperchromic effect was more pronounced. This indicates that AZT is more easily photodegraded at low concentrations. However, the magnitudes of the absorbances observed did not show a specific trend with time, as well as with concentration.

To determine that this irregular change in absorbance with irradiation time was not an artefact of dilution error, the whole experiment was repeated with fresh solutions. The results of one of the repeat experiments are shown in **Fig. 3.9**. As can be seen the same trend was observed and hence this variation could be solely attributed to the nature of the absorptive characteristics of the photoproducts formed.

The changes in absorbance with increasing irradiation time for the three concentrations of AZT in each of the five solvents investigated are summarised in **Tables 3.3 to 3.7**. In addition, the tables show what would have been the absorbance value of AZT in the actual solution irradiated. It must be borne in mind that all the solutions irradiated were diluted to approximately 4×10^{-5} M for analysis of the resulting changes.

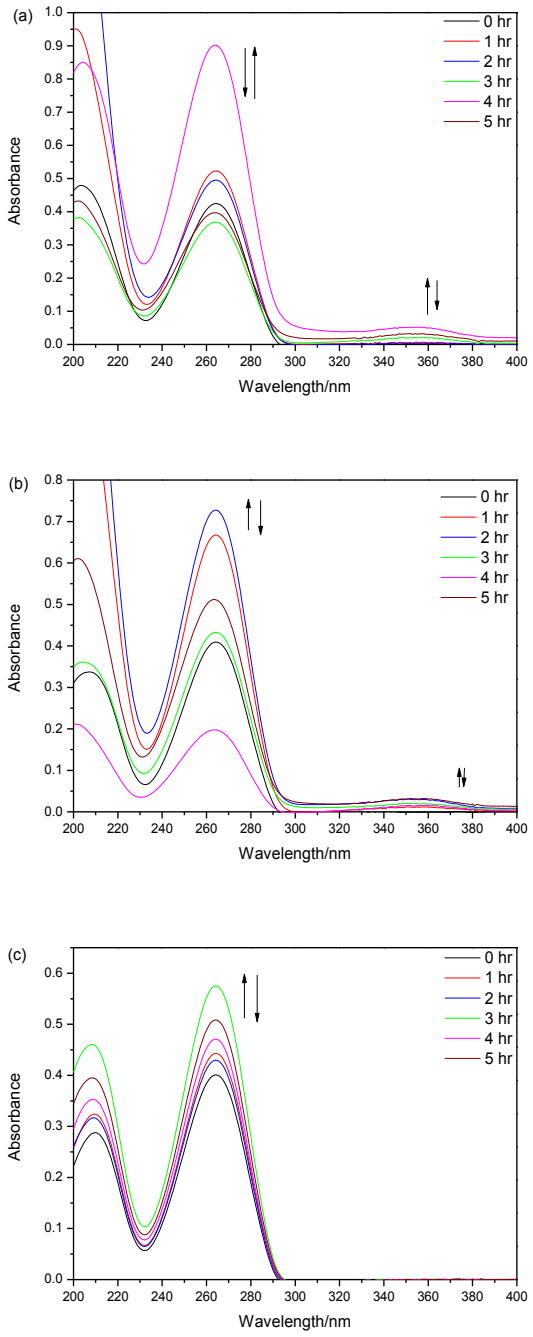

Figure 3.8: UV absorption spectra monitored at hourly intervals for the photolysis of AZT in acetonitrile at three different concentrations: (a) 2.39×10^{-4} M, (b) 4.94×10^{-4} M, and (c) 5.01×10^{-2} M.

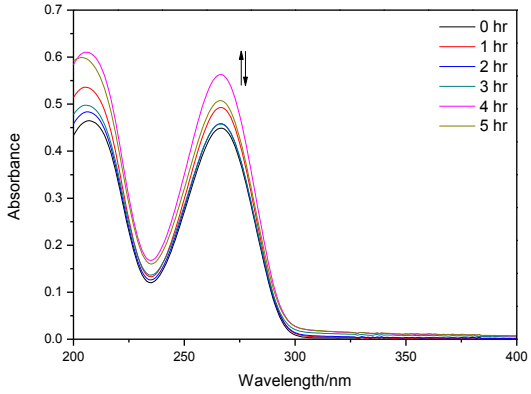

Figure 3.9: Repeated UV absorption spectra for the photolysis of AZT (5.01×10^{-2} M) in water.

Table 3.3: Change in absorbance of AZT when dissolved in water at different concentrations.

Irradiation time/hours	λ_{max}/nm	Absorbance	Change in absorbance	Absorbance	Change in absorbance
		As observed in the 4.01×10^{-5} M solution		As expected in the original 5.01×10^{-2} M solution	
0	266.71	0.3967	0	495.9	0
1	266.50	0.3967	0	495.9	0
2	265.52	0.4017	0.0050	502.1	6.250
3	265.57	0.3999	0.0032	499.9	4.000
4	266.36	0.4437	0.0470	554.6	58.75
5	266.62	0.3996	0.0029	499.5	3.625
		As observed in the 3.94×10^{-5} M solution		As expected in the original 4.94×10^{-4} M solution	
0	266.52	0.4024	0	5.030	0
1	266.41	0.3977	-0.0047	4.971	0
2	266.27	0.4351	0.0327	5.439	0.409
3	266.05	0.4590	0.0566	5.738	0.708
4	266.00	0.4591	0.0567	5.739	0.709
5	265.89	0.4981	0.0957	6.226	1.200
		As observed in the 3.82×10^{-5} M solution		As expected in the original 2.39×10^{-4} M solution	
0	266.84	0.3381	0	2.113	0
1	266.48	0.4294	0.0913	2.684	0.571
2	266.25	0.4558	0.1177	2.849	0.736
3	266.18	0.4842	0.1461	3.026	0.913
4	266.23	0.4338	0.0957	2.711	0.598
5	266.60	0.3954	0.0594	2.471	0.371

Table 3.4: Change in absorbance of AZT when dissolved in methanol at different concentrations.

Irradiation time/hours	λ_{max}/nm	Absorbance	Change in absorbance	Absorbance	Change in absorbance
		As observed in the 4.01×10^{-5} M solution		As expected in the original 5.01×10^{-2} M solution	
0	265.80	0.6633	0	829.1	0
1	265.89	0.8375	0.1742	1046	217.8
2	265.98	0.6934	0.0301	866.8	37.62
3	265.91	1.009	0.3457	1261	432.1
4	265.84	0.8274	0.1641	1034	205.1
5	266.08	0.6331	-0.0302	791.4	-37.75
		As observed in the 3.94×10^{-5} M solution		As expected in the original 4.94×10^{-4} M solution	
0	265.93	0.3922	0	4.903	0
1	265.90	0.8787	0.4865	10.98	6.077
2	265.65	0.8819	0.4897	11.02	6.117
3	266.12	0.4859	0.0937	6.070	1.167
4	266.11	0.4949	0.1027	6.190	1.287
5	265.67	0.4611	0.0689	5.760	0.857
		As observed in the 3.82×10^{-5} M solution		As expected in the original 2.39×10^{-4} M solution	
0	265.60	0.5046	0	3.154	0
1	265.78	0.5030	-0.0016	3.144	-0.010
2	265.81	0.6452	0.1406	4.033	0.879
3	265.81	0.5874	0.0828	3.671	0.517
4	265.85	0.5288	0.0242	3.305	0.151
5	265.96	0.6076	0.1030	3.798	0.644

Table 3.5: Change in absorbance of AZT when dissolved in ethanol at different concentrations.

Irradiation time/hours	λ_{max}/nm	Absorbance	Change in absorbance	Absorbance	Change in absorbance
		As observed in the 4.01×10^{-5} M solution		As expected in the original 5.01×10^{-2} M solution	
0	265.70	0.5199	0	649.9	0
1	265.50	0.4534	-0.0665	566.8	-83.13
2	265.56	0.5186	-0.0013	648.2	-1.700
3	265.49	0.4621	-0.0578	577.6	-72.25
4	265.41	0.4967	-0.0232	620.9	-29.00
5	264.63	0.5127	-0.0072	640.9	-9.000
		As observed in the 3.94×10^{-5} M solution		As expected in the original 4.94×10^{-4} M solution	
0	265.59	0.4299	0	5.374	0
1	265.73	0.4265	-0.0034	5.331	-0.043
2	265.69	0.4664	0.0365	5.830	0.456
3	265.75	0.4373	0.0074	5.466	0.092
4	265.94	0.4537	0.0238	5.671	0.297
5	265.88	0.5321	0.1022	6.651	1.277
		As observed in the 3.82×10^{-5} M solution		As expected in the original 2.39×10^{-4} M solution	
0	265.32	0.4248	0	2.655	0
1	265.32	0.4252	0.0004	2.658	0.003
2	265.85	0.5007	0.0759	3.129	0.474
3	265.92	0.4725	0.0477	2.953	0.298
4	265.97	0.4834	0.0586	3.021	0.366
5	265.97	0.5217	0.0969	3.260	0.605

Table 3.6: Change in absorbance of AZT when dissolved in 2-propanol at different concentrations.

Irradiation time/hours	λ_{max}/nm	Absorbance	Change in absorbance	Absorbance	Change in absorbance
		As observed in the 4.01×10^{-5} M solution		As expected in the original 5.01×10^{-2} M solution	
0	265.34	0.3533	0	441.6	0
1	265.63	0.3533	0	441.6	0
2	265.59	0.4485	0.0952	560.6	119.0
3	265.43	0.5539	0.2006	692.4	250.8
4	265.57	0.6229	0.2696	778.6	337.0
5	265.69	0.5102	0.1569	637.8	196.1
		As observed in the 3.94×10^{-5} M solution		As expected in the original 4.94×10^{-4} M soution	
0	265.36	0.4031	0	5.039	0
1	266.66	0.4090	0.0059	5.113	0.074
2	266.69	0.4330	0.0299	5.413	0.374
3	266.00	0.4807	0.0776	6.009	0.970
4	266.19	0.4691	0.0660	5.864	0.825
5	265.94	0.5231	0.1200	6.539	1.500
		As observed in the 3.82×10^{-5} M solution		As expected in the original 2.39×10^{-4} M solution	
0	265.51	0.3991	0	2.494	0
1	265.55	0.4268	0.0277	2.668	0.174
2	265.53	0.4120	0.0129	2.575	0.081
3	266.10	0.4781	0.0790	2.988	0.494
4	266.38	0.4945	0.0954	3.091	0.597
5	266.35	0.4563	0.0572	2.852	0.358

Table 3.7: Change in absorbance of AZT when dissolved in acetonitrile at different concentrations.

Irradiation time/hours	**λ_{max}/nm**	**Absorbance**	**Change in absorbance**	**Absorbance**	**Change in absorbance**
		As observed in the 4.01×10^{-5} M solution		As expected in the original 5.01×10^{-2} M solution	
0	264.26	0.4035	0	504.4	0
1	264.18	0.4457	0.0422	557.1	52.75
2	264.14	0.4322	0.0287	540.3	35.87
3	264.16	0.5776	0.1741	722.0	217.6
4	264.12	0.4737	0.0702	592.1	87.75
5	264.17	0.5112	0.1077	639.0	134.6
		As observed in the 3.94×10^{-5} M solution		As expected in the original 4.94×10^{-4} M solution	
0	264.20	0.4120	0	5.150	0
1	264.17	0.6704	0.2584	8.380	3.230
2	264.16	0.7302	0.3182	9.128	3.978
3	264.26	0.4357	0.0237	5.446	0.296
4	263.57	0.2001	-0.2119	2.501	-2.649
5	263.36	0.5145	0.1025	6.431	1.281
		As observed in the 3.82×10^{-5} M solution		As expected in the original 2.39×10^{-4} M solution	
0	264.27	0.4271	0	2.669	0
1	264.32	0.5255	0.0984	3.284	0.615
2	264.18	0.4980	0.0709	3.113	0.444
3	264.09	0.3711	-0.0560	2.319	-0.350
4	263.88	0.9023	0.4752	5.639	2.970
5	263.68	0.3997	-0.0274	2.498	-0.171

3.1.4. Effect of pH

The photostability of AZT (4.94×10^{-4} M) in aqueous solution was further investigated under different conditions of pH (3, 5 and 7). The pH was adjusted by the addition of either HCl (0.1 M) or NaOH (0.1 M). AZT is known as a weak acid compound and has a pK_a value of 9.55 [117, 118]. Its deprotonation occurs at the imide nitrogen of the pyrimidine ring (thymine) [118].

The UV/Vis spectra of AZT (4.94×10^{-4} M) in aqueous solution at pH 3, 5 and 7 are shown in **Fig. 3.10**. A blue shift (hypsochromic effect) in the wavelength of maximum absorption, λ_{max}, was observed with increasing irradiation time and this effect was more marked at pH 3. We propose that this could be due to the protonation of AZT that arises after the loss of N_2 from the azide group forming a nitrene anion radical which further reacts with water to give the hydroxylamine derivative, RNHOH [119]. As regards the change in absorbance as the irradiation time increased, no significant change was observed for pH 3 but a marked change was observed at pH 5 and pH 7. These changes are summarized in **Table 3.8**. For pH 3 there was no observable relationship in absorbance with irradiation time. However, for both pH 5 and 7 the absorbance increased with irradiation time. No observable hypsochromic effects were observed at 213 nm.

Table 3.8: Change in absorbance of AZT when dissolved in aqueous solution at pH 3, pH 5 and pH 7.

Irradiation time/hours	λ_{max}/nm	Absorbance	Change in absorbance	Absorbance	Change in absorbance
		As observed in the 3.94×10^{-5} M solution		As expected in the original 4.94×10^{-4} M solution	
		pH 3			
0	266.72	0.3970	0	496.25	0
1	266.16	0.3670	-0.0300	458.75	-37.50
2	265.90	0.3841	-0.0129	480.13	-16.12
3	265.69	0.3956	-0.0014	494.50	-1.75
4	265.01	0.4147	0.0177	518.38	22.13
5	264.99	0.4012	0.0042	501.50	5.25
		pH 5			
0	266.72	0.3898	0	4.87	0
1	266.60	0.4218	0.0320	5.27	0.40
2	266.30	0.4619	0.0721	5.77	0.90
3	266.17	0.5095	0.1197	6.37	1.50
4	266.20	0.5101	0.1203	6.38	1.51
5	265.96	0.5258	0.1360	6.57	1.70
		pH 7			
0	266.72	0.3890	0	2.67	0
1	266.57	0.4288	0.0398	2.68	0.25
2	266.53	0.4472	0.0582	2.80	0.37
3	266.23	0.5001	0.1111	3.13	0.70
4	266.19	0.5409	0.1519	3.38	0.95
5	266.11	0.5460	0.1570	3.41	0.98

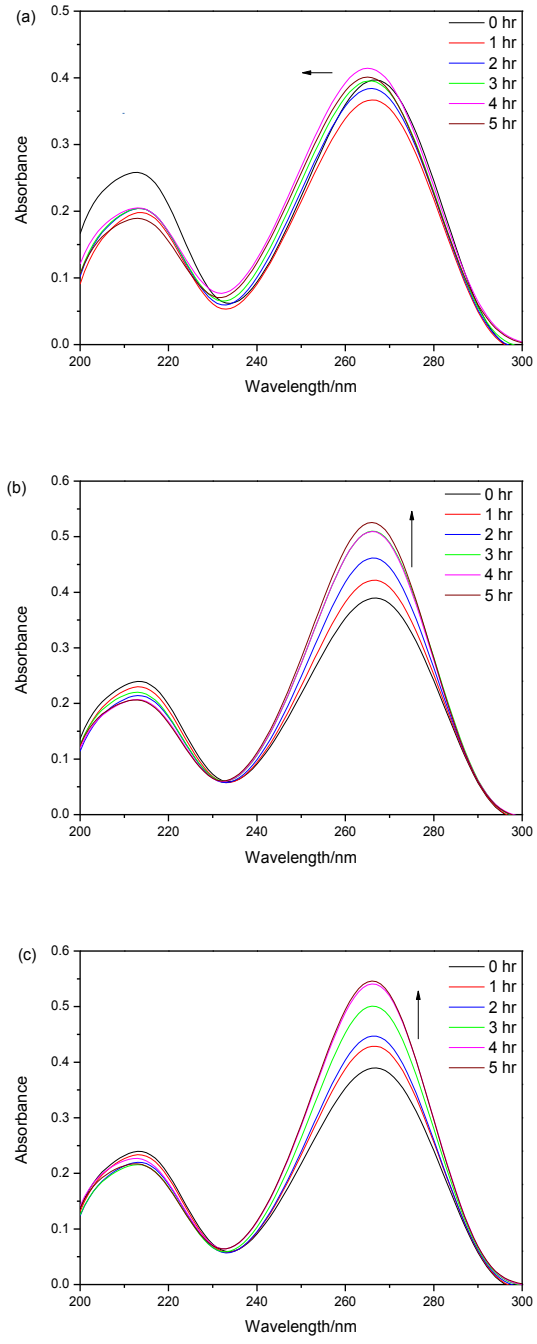

Figure 3.10: UV absorption spectra monitored at hourly intervals for the photolysis of AZT (4.94×10^{-4} M) at (a) pH 3, (b) pH 5, and (c) pH 7 in aqueous solution.

3.2. Photostability of AZT assessed by HPLC

High performance liquid chromatography was used for the separation, quantification and identification of the photoproducts of AZT. The separation was carried out on a Phenomenex Kinetex C18 (150 × 4.6 mm i.d., 2.6 μm particle size) column with methanol:water (60:40 v/v) as the mobile phase at a flow rate of 0.25 mL/min, in the isocratic mode. The detection wavelength was 266 nm. In order to meet the required concentration for HPLC analysis, each sample was diluted with water after every UV-exposure to make up a concentration of approximately 4×10^{-5} M. The dilution factors were as stated in **Section 2.6.3**. All the chromatograms and peak areas discussed in this section are for these diluted solutions.

3.2.1. HPLC analysis of AZT prior to irradiation

The HPLC chromatogram of AZT before irradiation was the same under all conditions of solvents, pH and concentration (**Fig. 3.11**) excluding AZT (2.39×10^{-4} M) in 2-propanol which gave a broad peak as shown in **Fig. 3.12**. This behaviour could be due to the smaller dielectric constant of 2-propanol in comparison with water (see **Table 3.2**). Only one peak (AZT) was detected although the retention time was not constant and ranged between 6.600-6.810 min. The peak at a retention time of 5.554 min is the peak from the blank (**Fig. 3.13**) and was constant throughout all samples. All attempts to clean the column, injector, tubing and detector failed to remove this impurity. Hence, all the chromatograms show this peak.

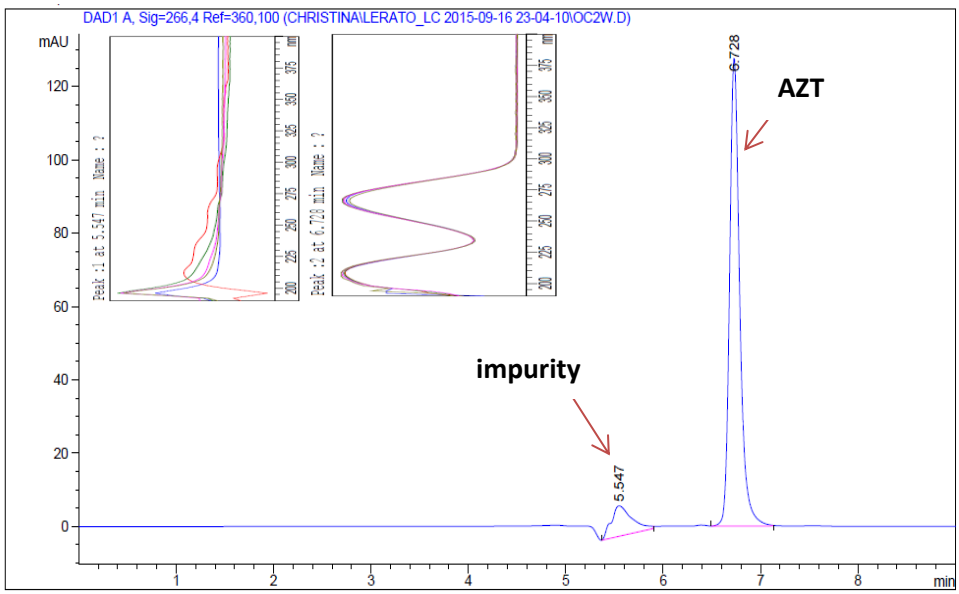

Figure 3.11: HPLC chromatogram of AZT (4.94×10^{-4} M) dissolved in water before irradiation eluted on a Phenomenex Kinetex C18 (150 × 4.6 mm i.d., 2.6 µm particle size) column with methanol:water (60:40 v/v) as the mobile phase at a flow rate of 0.25 mL/min. The detection wavelength was 266 nm.

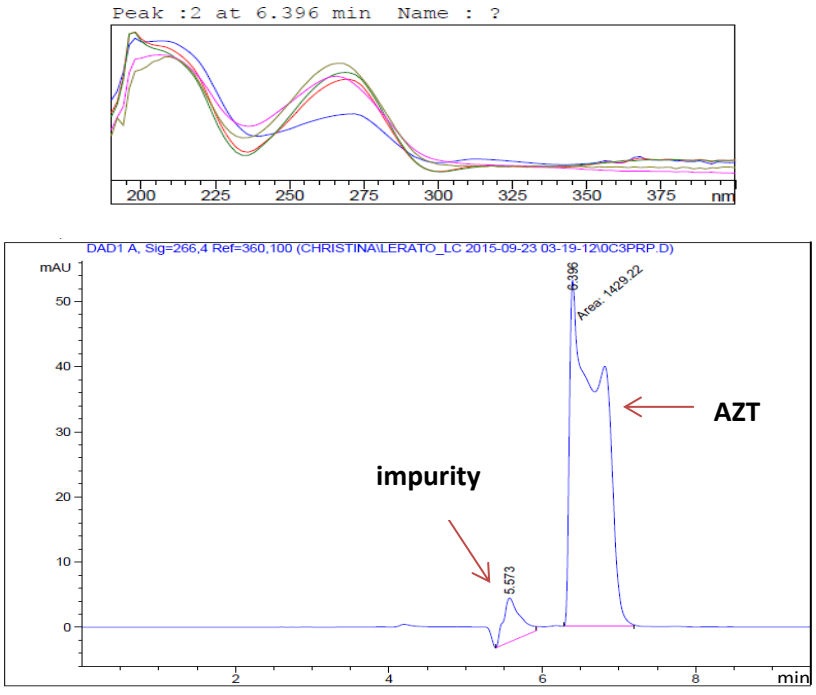

Figure 3.12: HPLC chromatogram of AZT (2.39×10^{-4} M) dissolved in 2-propanol before irradiation eluted on a Phenomenex Kinetex C18 (150 × 4.6 mm i.d., 2.6 µm particle size) column with methanol:water (60:40 v/v) as the mobile phase at a flow rate of 0.25 mL/min. The detection wavelength was 266 nm.

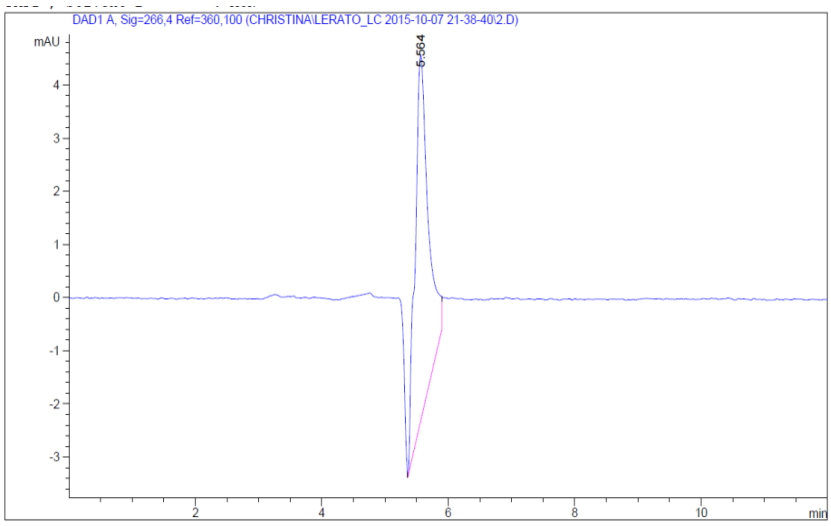

Figure 3.13: HPLC chromatogram of a blank eluted on a Phenomenex Kinetex C18 (150 × 4.6 mm i.d., 2.6 µm particle size) column with methanol:water (60:40 v/v) as the mobile phase at a flow rate of 0.25 mL/min. The detection wavelength was 266 nm.

3.2.2. Effect of concentration

The photolysis of AZT was investigated at three different concentrations, 2.39×10^{-4}, 4.94×10^{-4} and 5.01×10^{-2} M, in different solvents, namely, water, methanol, ethanol, 2-propanol and acetonitrile.

3.2.2.1. Photolysis of AZT in water

The HPLC chromatogram of AZT (5.01×10^{-2} M) in aqueous solution acquired at 266 nm showed the formation of one photoproduct at a retention time of 5.689 minutes (**Fig. 3.14**) whereas for the lower concentrations of 4.94×10^{-4} (**Fig. 3.16**) and 2.39×10^{-4} M (**Fig. 3.18**) three photoproducts were formed. A gradual increase in the peak area of the photoproducts is observed as the irradiation time increases whereas the peak area of AZT decreases with the irradiation time as shown in **Fig. 3.15**, **3.17** and **3.19**. The relative decrease at high concentration is less than that at low concentration as observed by UV spectroscopy (see **Fig. 3.4**).

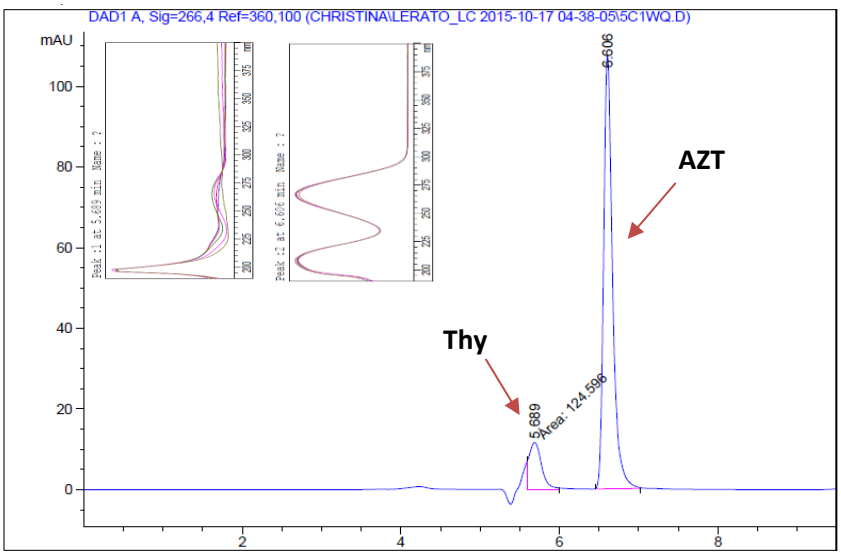

Figure 3.14: HPLC chromatogram of AZT (5.01×10^{-2} M) irradiated for 5 hours in water eluted on a Phenomenex Kinetex C18 (150 × 4.6 mm i.d., 2.6 µm particle size) column with methanol:water (60:40 v/v) as the mobile phase at a flow rate of 0.25 mL/min. The detection wavelength was 266 nm.

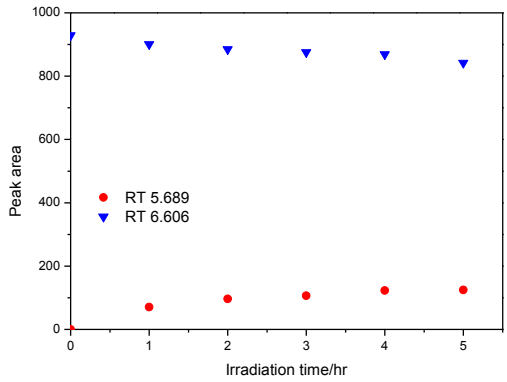

Figure 3.15: Variation of the HPLC peak areas of AZT (5.01×10^{-2} M) and its photoproducts in water with increasing irradiation time.

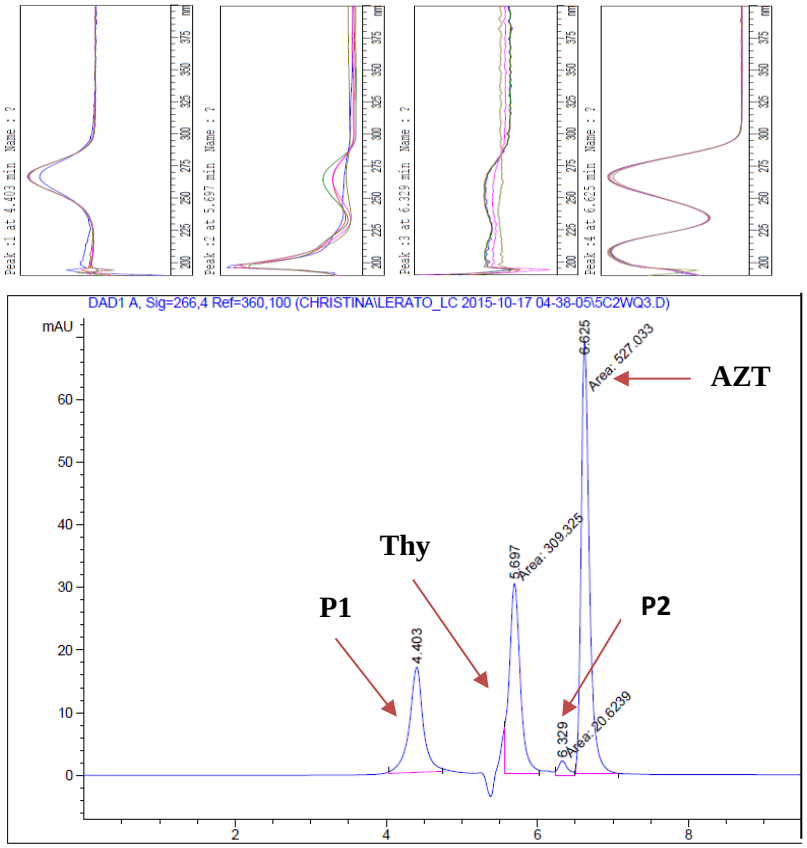

Figure 3.16: HPLC chromatograph of AZT (4.94×10^{-4} M) irradiated for 5 hours in water eluted on a Phenomenex Kinetex C18 (150 × 4.6 mm i.d., 2.6µm particle size) column with methanol:water (60:40 v/v) as the mobile phase at a flow rate of 0.25 mL/min. The detection wavelength was 266 nm.

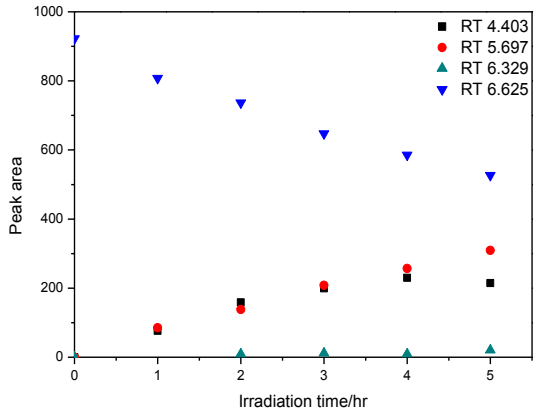

Figure 3.17: Variation of the HPLC peak areas of AZT (4.94×10^{-4} M) and its photoproducts in water with increasing irradiation time.

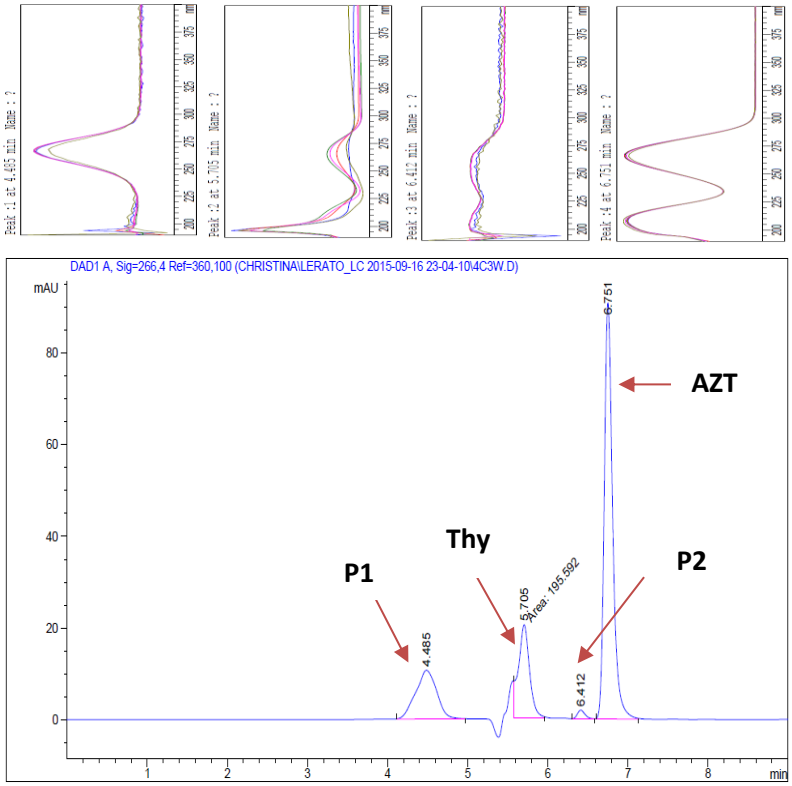

Figure 3.18: HPLC chromatogram of AZT (2.39×10^{-4} M) irradiated for 5 hours in water eluted on a Phenomenex Kinetex C18 (150 × 4.6 mm i.d., 2.6 µm particle size) column with methanol:water (60:40 v/v) as the mobile phase at a flow rate of 0.25 mL/min. The detection wavelength was 266 nm.

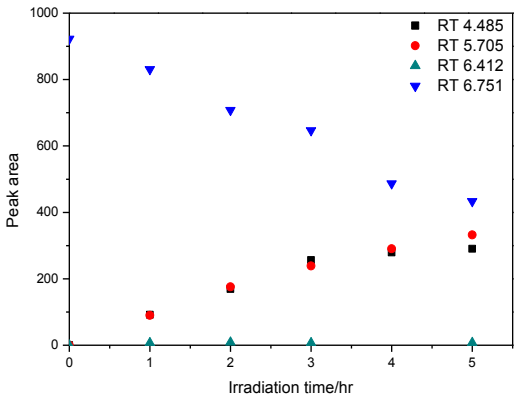

Figure 3.19: Variation of the HPLC peak areas of AZT (2.39×10^{-4} M) and its photoproducts in water with increasing irradiation time.

3.2.2.2. Photolysis of AZT in methanol

The HPLC chromatogram of AZT at 5.01×10^{-2} M (**Fig. 3.20**) in methanol, acquired at 266 nm, showed the formation of two photoproducts at a retention time of 5.698 and 6.400 min whereas the chromatograms of AZT at 4.94×10^{-4} M (**Fig. 3.22**) and 2.39×10^{-4} M (**Fig. 3.24**) showed the formation of three photoproducts. The graph in **Fig. 3.21** shows a slight decrease in the peak area of AZT at a retention time of 6.742 min while there is a slight increment in the peak areas of the photoproducts. **Fig. 3.23** shows a significant decrease in the peak area of AZT at a retention time of 6.737 min as the irradiation time increases. The peak areas of the photoproducts at retention times of 4.495 and 6.396 min were almost constant whereas that of the photoproduct at 5.692 min increases substantially with increasing irradiation time. The graph in **Fig. 3.25** also showed a decrease in the peak area of AZT at 6.766 min as the irradiation time increased.

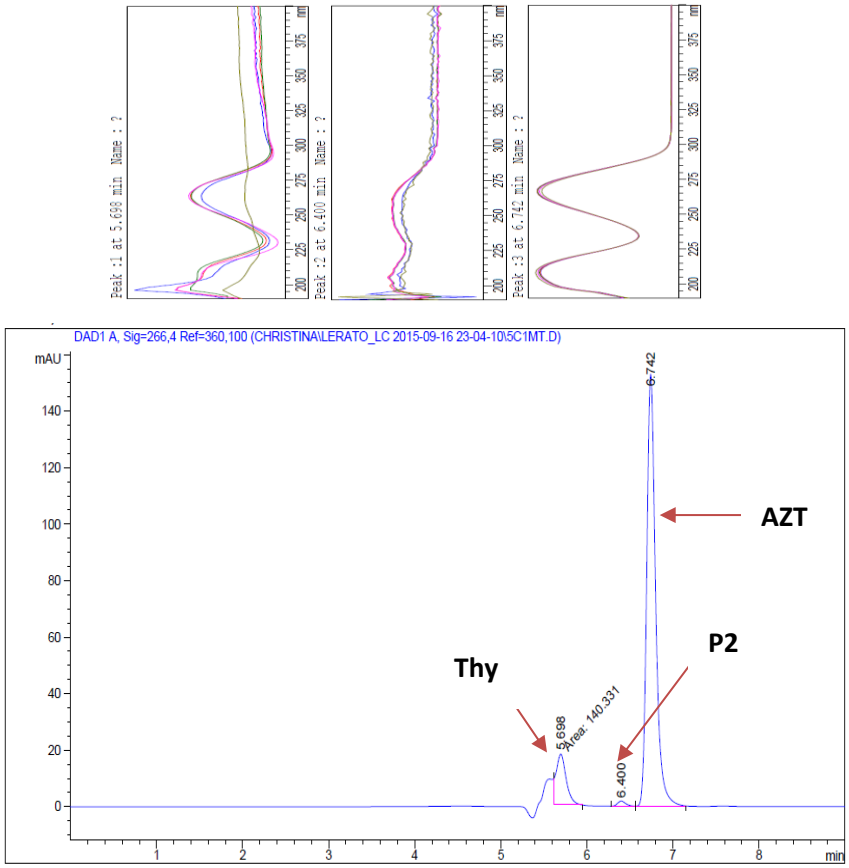

Figure 3.20: HPLC chromatogram of AZT (5.01×10^{-2} M) irradiated for 5 hours in methanol eluted on a Phenomenex Kinetex C18 (150 × 4.6 mm i.d., 2.6 µm particle size) column with methanol:water (60:40 v/v) as the mobile phase at a flow rate of 0.25 mL/min. The detection wavelength was 266 nm.

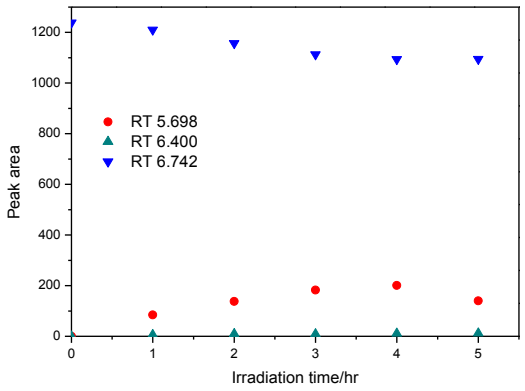

Figure 3.21: Variation of the HPLC peak areas of AZT (5.01×10^{-2} M) and its photoproducts in methanol with increasing irradiation time.

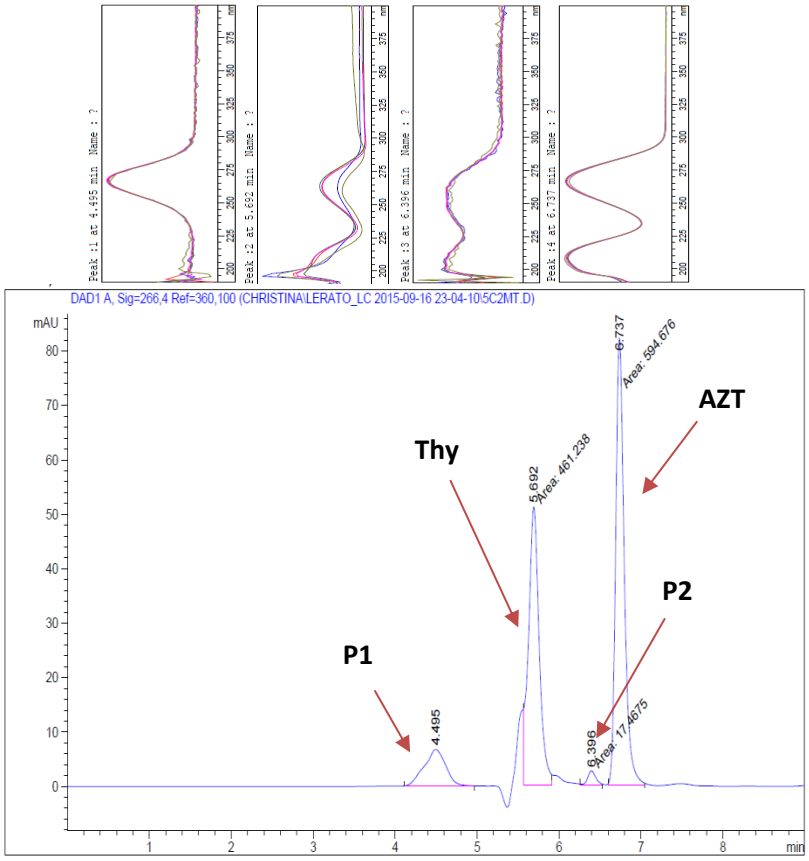

Figure 3.22: HPLC chromatogram of AZT (4.94×10^{-4} M) irradiated for 5 hours in methanol eluted on a Phenomenex Kinetex C18 (150 × 4.6 mm i.d., 2.6 µm particle size) column with methanol:water (60:40 v/v) as the mobile phase at a flow rate of 0.25 mL/min. The detection wavelength was 266 nm.

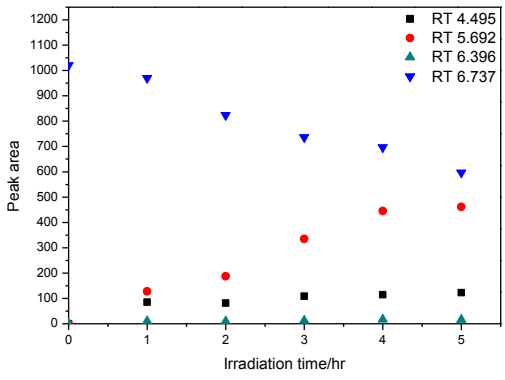

Figure 3.23: Variation of the HPLC peak areas of AZT (4.94×10^{-4} M) and its photoproducts in methanol with increasing irradiation time.

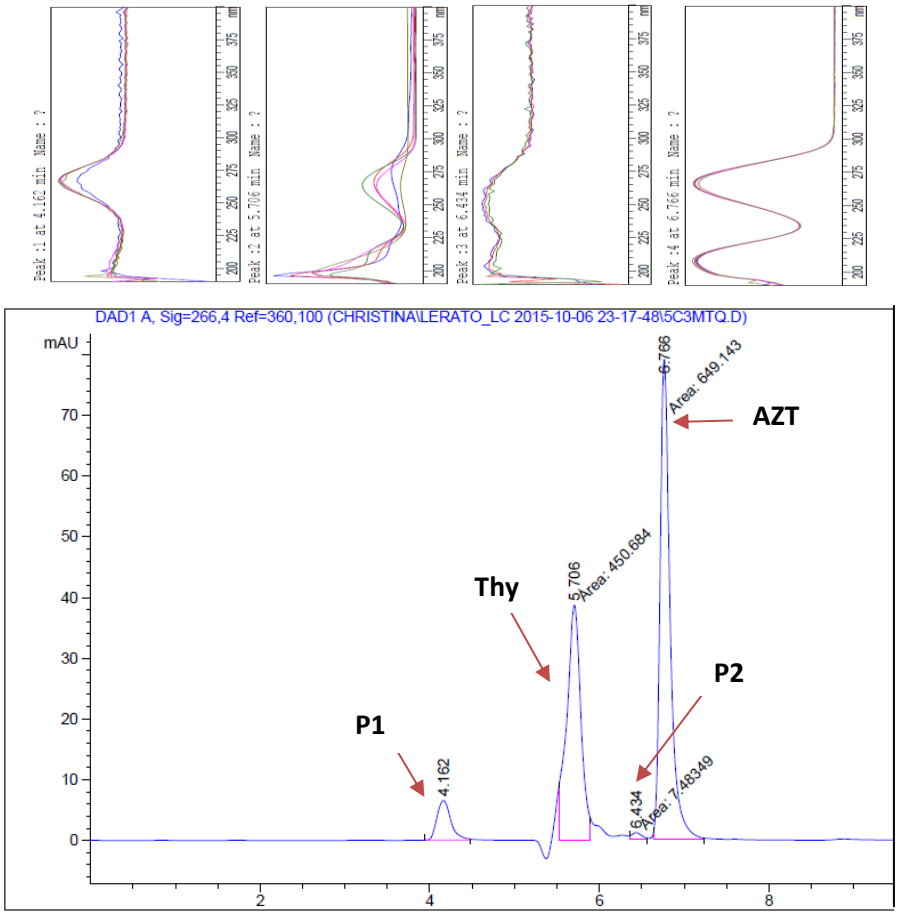

Figure 3.24: HPLC chromatogram of AZT (2.39×10^{-4} M) irradiated for 5 hours in methanol eluted on a Phenomenex Kinetex C18 (150 × 4.6 mm i.d., 2.6 µm particle size) column with methanol:water (60:40 v/v) as the mobile phase at a flow rate of 0.25 mL/min. The detection wavelength was 266 nm.

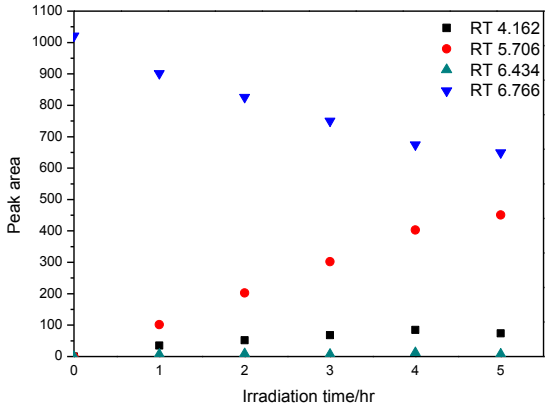

Figure 3.25: Variation of the HPLC peak areas of AZT (2.39×10^{-4} M) and its photoproducts in methanol with increasing irradiation time.

3.2.2.3. Photolysis of AZT in ethanol

The HPLC chromatogram of AZT (5.01×10^{-2} M) in ethanol, acquired at 266 nm, showed the formation of two photoproducts at a retention time of of 5.701 and 6.404 min as shown in **Fig. 3.26**. The graph in **Fig. 3.27** showed a slight decrease in the peak area of AZT, at a retention time of 6.749 min, as the irradiation time increases whereas a slight increase was observed for the peak with a retention time of 5.701 min whilst that with a retention time of 6.404 min was almost constant.

Three photoproducts were formed in the intermediate concentration of AZT (4.94×10^{-4} M) dissolved in ethanol at retention times of 4.500, 5.696 and 6.394 min as shown in **Fig. 3.28**. The graph in **Fig. 3.29** shows a slight decrease in the peak area of AZT, at a retention time of 6.737 min, as the irradiation time increases, whereas a slight increase in the peak area of the peak with a retention time of 5.696 min is observed and that of the peak with a retention time of 6.394 min is almost constant.

Two photoproducts were formed in the lowest concentration of AZT (2.39×10^{-4} M) in ethanol at retention times of 4.378, 5.689 and 6.610 min as shown in **Fig. 3.30** and the peak area graph (**Fig. 3.31**) shows a gradual decrease in the peak area of AZT as the irradiation times increases, while the peak areas of the photoproducts increase as the irradiation time increases.

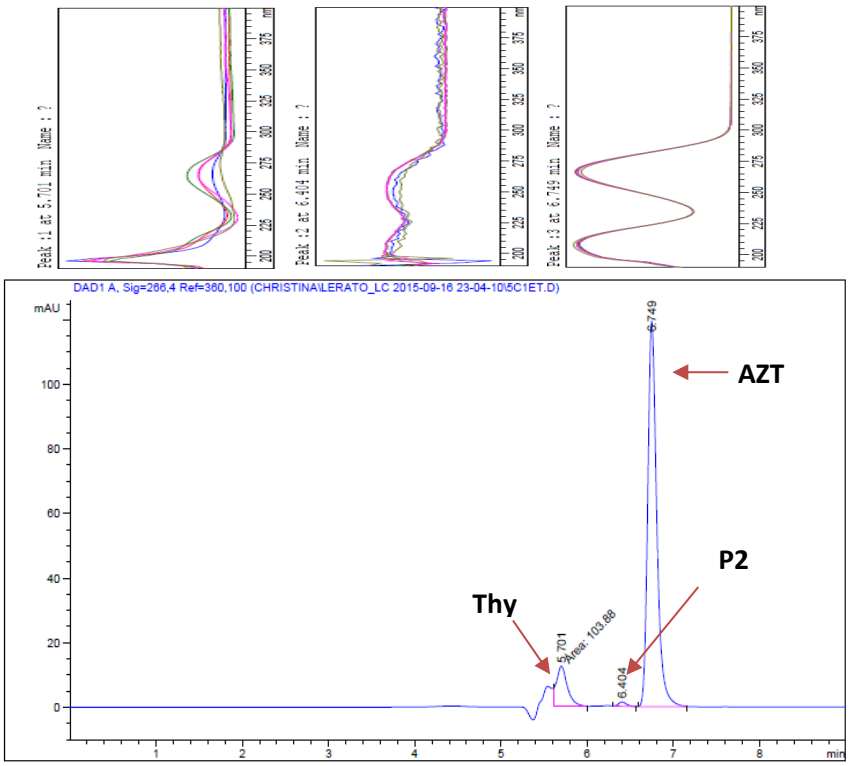

Figure 3.26: HPLC chromatogram of AZT (5.01×10^{-2} M) irradiated for 5 hours in ethanol eluted on a Phenomenex Kinetex C18 (150 × 4.6 mm i.d., 2.6 µm particle size) column with methanol:water (60:40 v/v) as the mobile phase at a flow rate of 0.25 mL/min. The detection wavelength was 266 nm.

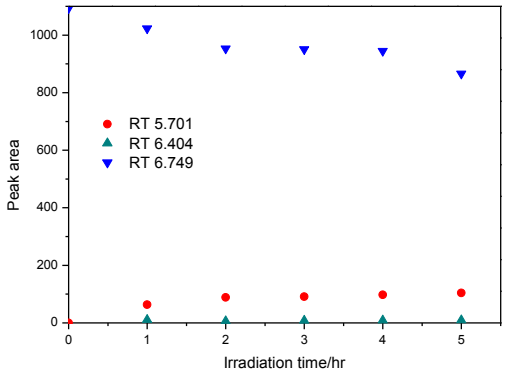

Figure 3.27: Variation of the HPLC peak areas of AZT (5.01×10^{-2} M) and its photoproducts in ethanol with increasing irradiation time.

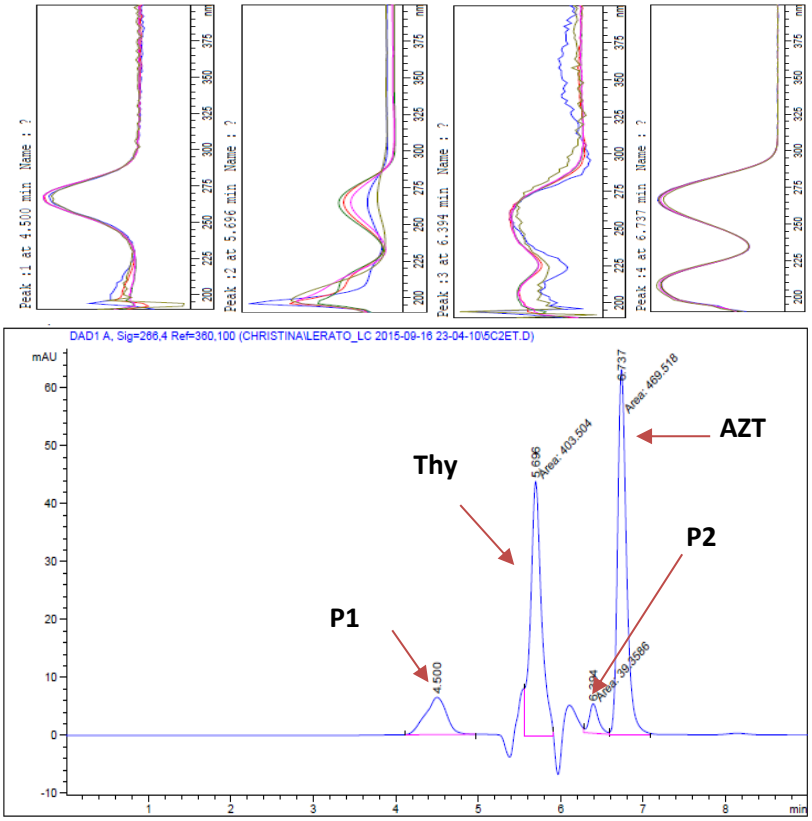

Figure 3.28: HPLC chromatogram of AZT (4.94×10^{-4} M) irradiated for 5 hours in ethanol eluted on a Phenomenex Kinetex C18 (150 × 4.6 mm i.d., 2.6 µm particle size) column with methanol:water (60:40 v/v) as the mobile phase at a flow rate of 0.25 mL/min. The detection wavelength was 266 nm.

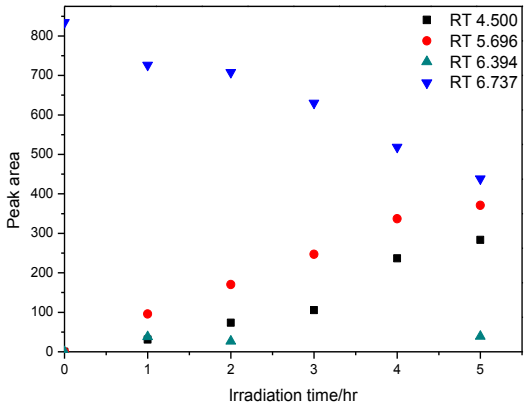

Figure 3.29: Variation of the HPLC peak areas of AZT (4.94×10^{-4} M) and its photoproducts in ethanol with increasing irradiation time.

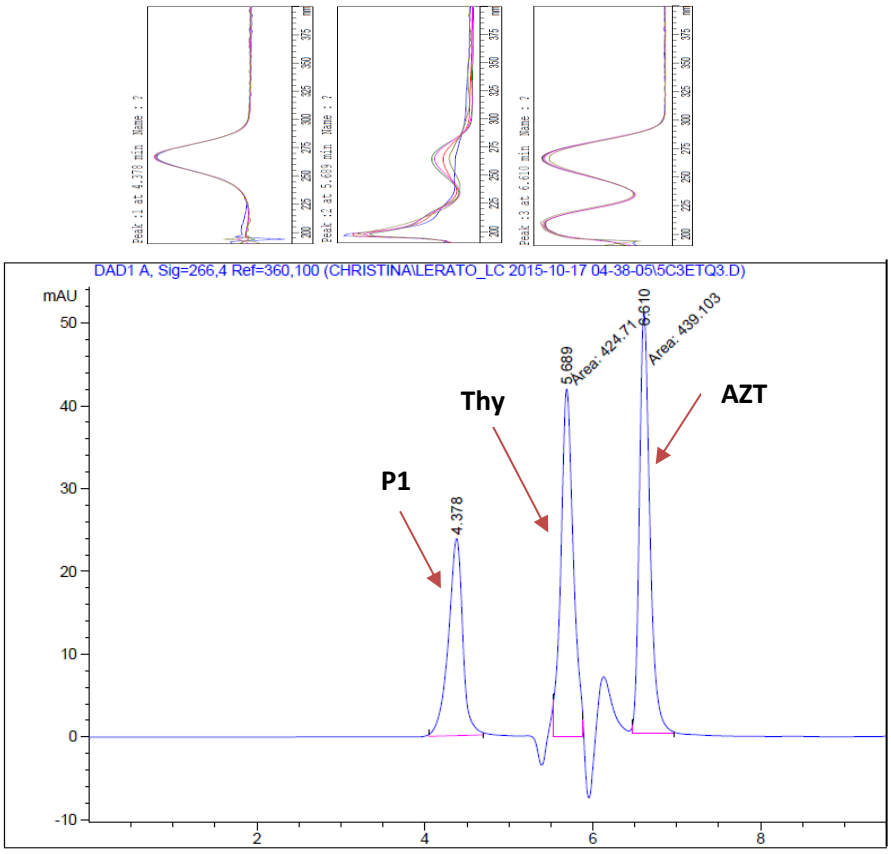

Figure 3.30: HPLC chromatogram of AZT (2.39×10^{-4} M) irradiated for 5 hours in ethanol eluted on a Phenomenex Kinetex C18 (150 × 4.6 mm i.d., 2.6 µm particle size) column with methanol:water (60:40 v/v) as the mobile phase at a flow rate of 0.25 mL/min. The detection wavelength was 266 nm.

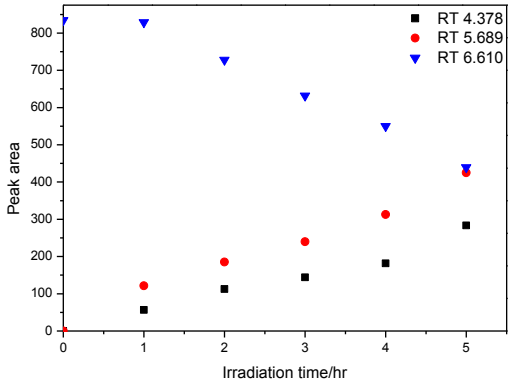

Figure 3.31: Variation of the HPLC peak areas of AZT (2.39×10^{-4} M) and its photoproducts in ethanol with increasing irradiation time.

3.2.2.4. Photolysis of AZT in 2-propanol

The HPLC chromatogram of AZT (5.01×10^{-2} M) in 2-propanol, acquired at 266 nm, showed the formation of two photoproducts at a retention time of 5.737 and 6.306 min as shown in **Fig. 3.32**. Three photoproducts were formed in the 4.94×10^{-4} M (**Fig. 3.34**) and 2.39×10^{-4} M (**Fig. 3.36**) solutions. A slight change in the peak area of the photoproduct at a retention time of 5.737 min is observed as the irradiation time increases (**Fig. 3.33**).

It can be observed from **Fig. 3.35** that the peak area of AZT at a RT of 6.733 min decreases with the irradiation time while the peak area of the photoproduct at a retention time of 5.713 min increases with the irradiation time. However, there is no significant change in the peak areas for the photoproducts observed at retention times of 5.069 and 6.200 min. The same behaviour is also observed in **Fig. 3.37** for the lowest concentration of AZT.

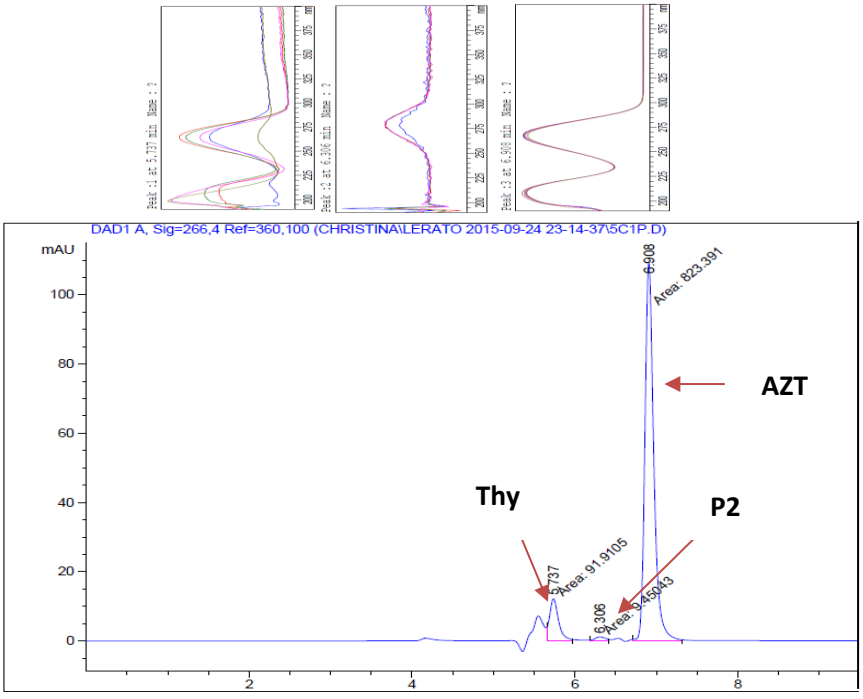

Figure 3.32: HPLC chromatogram of AZT (5.01×10^{-2} M) irradiated for 5 hours in 2-propanol eluted on a Phenomenex Kinetex C18 (150 × 4.6 mm i.d., 2.6 µm particle size) column with methanol:water (60:40 v/v) as the mobile phase at a flow rate of 0.25 mL/min. The detection wavelength was 266 nm.

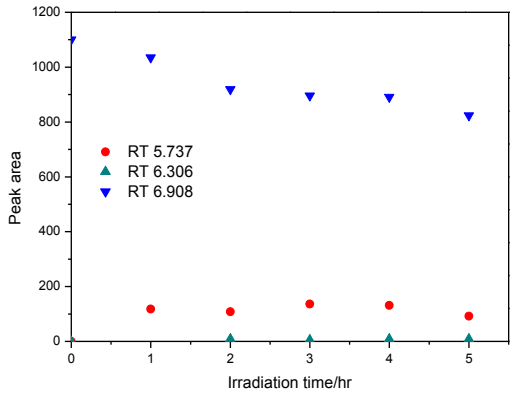

Figure 3.33: Variation of the HPLC peak areas of AZT (5.01×10^{-2} M) and its photoproducts in 2-propanol with increasing irradiation time.

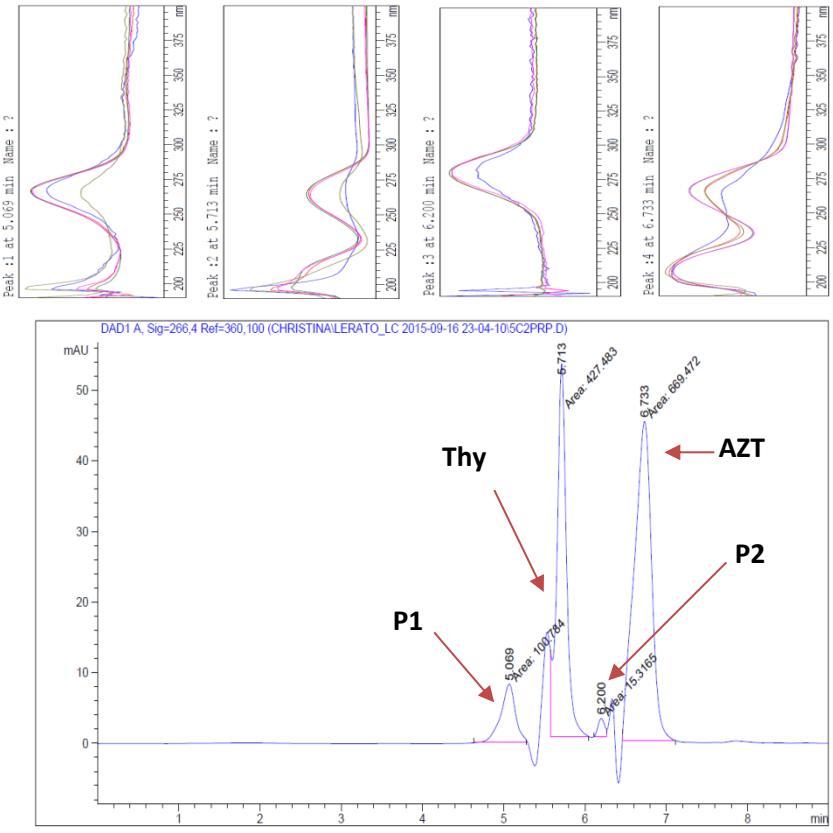

Figure 3.34: HPLC chromatogram of AZT (4.94×10^{-4} M) irradiated for 5 hours in 2-propanol eluted on a Phenomenex Kinetex C18 (150 × 4.6 mm i.d., 2.6 µm particle size) column with methanol:water (60:40 v/v) as the mobile phase at a flow rate of 0.25 mL/min. The detection wavelength was 266 nm.

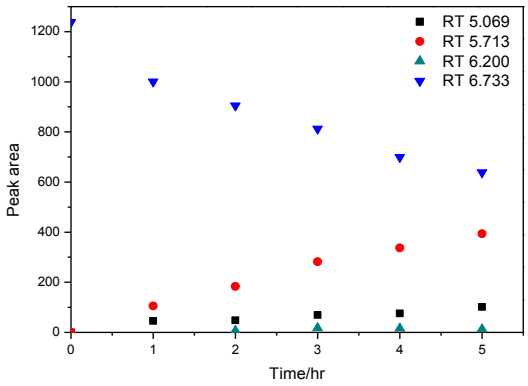

Figure 3.35: Variation of the HPLC peak areas of AZT (4.94×10^{-4} M) and its photoproducts in 2-propanol with increasing irradiation time.

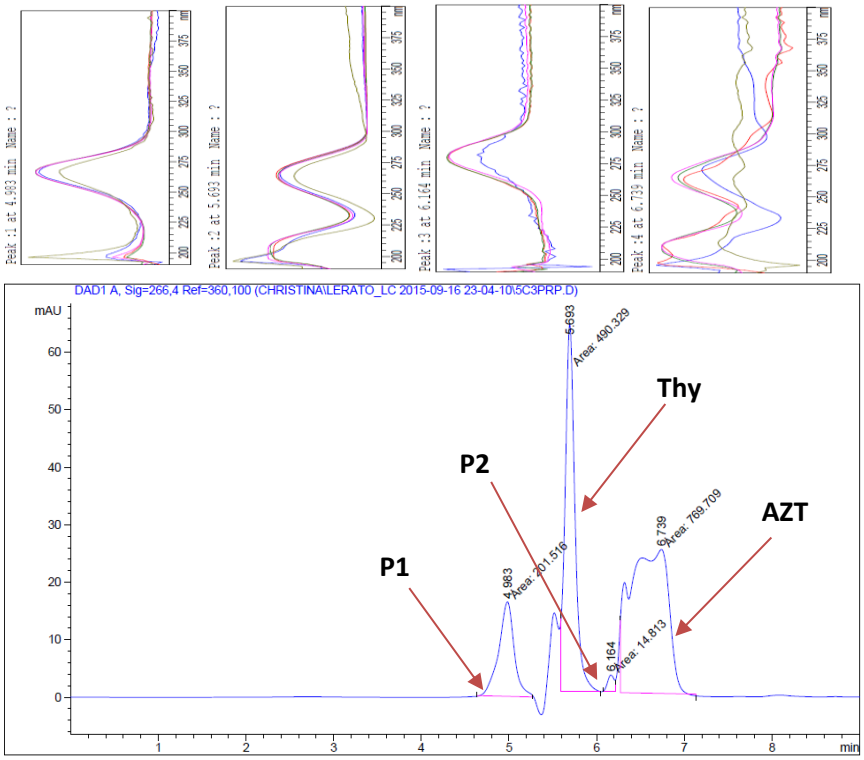

Figure 3.36: HPLC chromatogram of AZT (2.39×10^{-4} M) irradiated for 5 hours in 2-propanol eluted on a Phenomenex Kinetex C18 (150 × 4.6 mm i.d., 2.6 μm particle size) column with methanol:water (60:40 v/v) as the mobile phase at a flow rate of 0.25 mL/min. The detection wavelength was 266 nm.

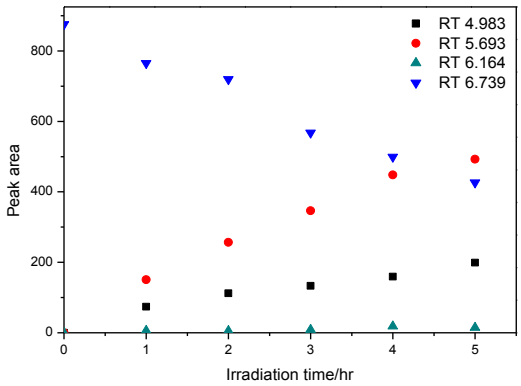

Figure 3.37: Variation of the HPLC peak areas of AZT (2.39×10^{-4} M) and its photoproducts in 2-propanol with increasing irradiation time.

3.2.2.5. Photolysis of AZT in acetonitrile

Only one photoproduct with a retention time of 5.690 min was formed in the highest concentration of AZT (5.01×10^{-2} M) dissolved in acetonitrile (**Fig. 3.38**). Three photoproducts were formed in acetonitrile for both the 4.94×10^{-4} and 2.39×10^{-4} M concentrations as shown in **Fig. 3.40** and **Fig. 3.42** respectively. The peaks at retention times of 4.365 and 4.079 min had UV/Vis spectra with a new absorption band formed at 355 nm and correspond with the UV/Vis spectra seen in **Fig. 3.8 (a) and (b)**. As can be seen from **Fig. 3.39**, **Fig. 3.41** and **Fig. 3.43** the peak areas of the photoproducts increase with irradiation time while that of AZT decreases with irradiation time.

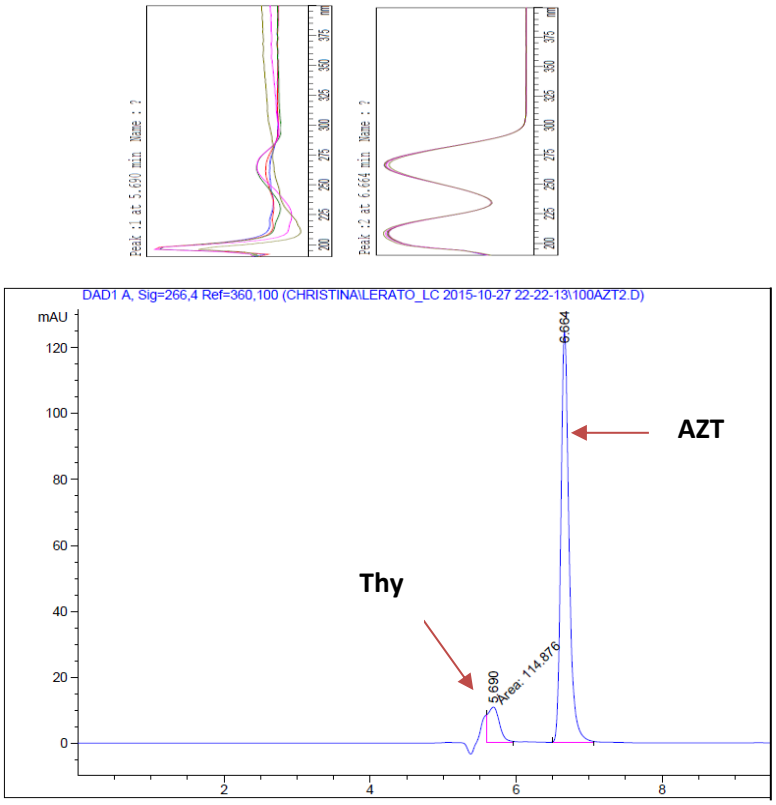

Figure 3.38: HPLC chromatogram of AZT (5.01×10^{-2} M) irradiated for 5 hours in acetonitrile eluted on a Phenomenex Kinetex C18 (150 × 4.6 mm i.d., 2.6 µm particle size) column with methanol:water (60:40 v/v) as the mobile phase at a flow rate of 0.25 mL/min. The detection wavelength was 266 nm.

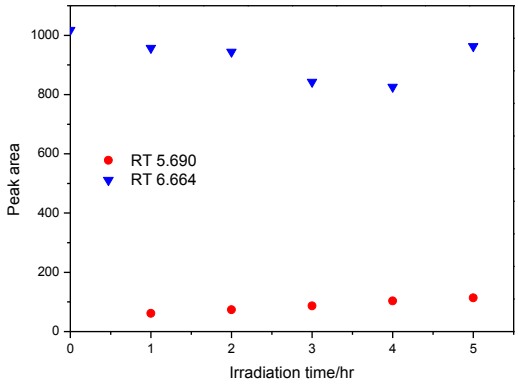

Figure 3.39: Variation of the HPLC peak areas of AZT (5.01×10^{-2} M) and its photoproducts in acetonitrile with increasing irradiation time.

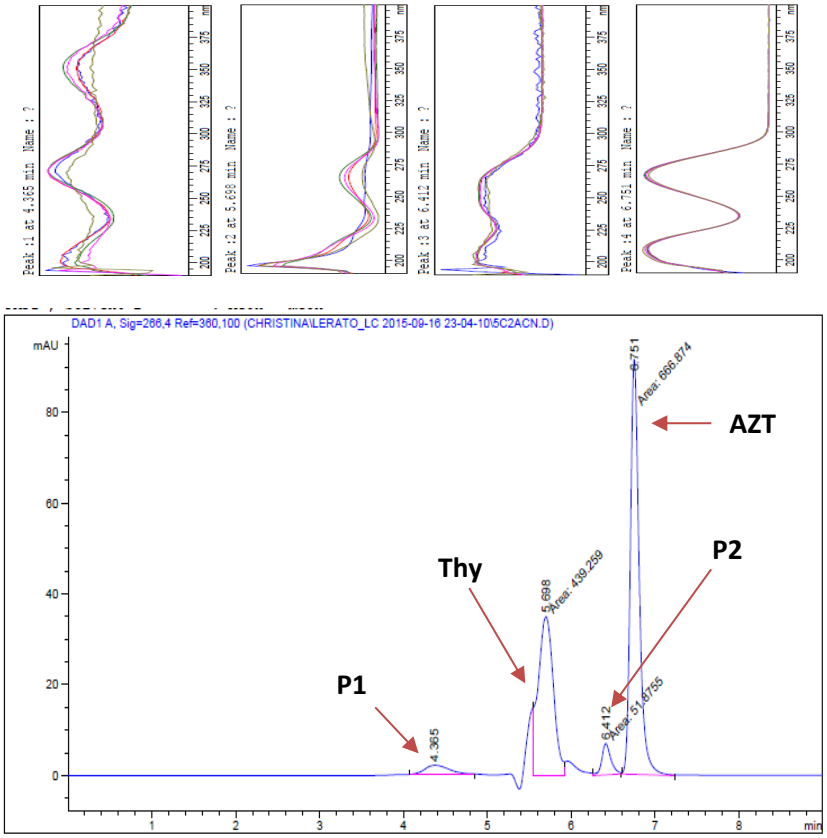

Figure 3.40: HPLC chromatogram of AZT (4.94×10^{-4} M) irradiated for 5 hours in acetonitrile eluted on a Phenomenex Kinetex C18 (150 × 4.6 mm i.d., 2.6 µm particle size) column with methanol:water (60:40 v/v) as the mobile phase at a flow rate of 0.25 mL/min. The detection wavelength was 266 nm.

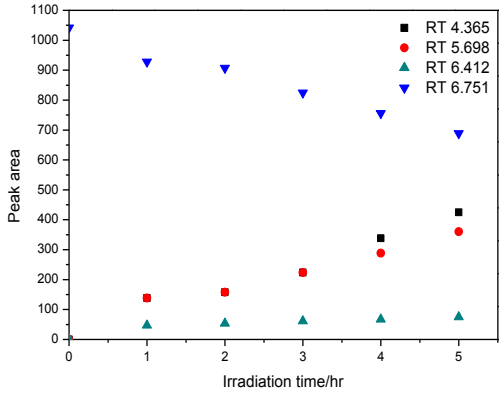

Figure 3.41: Variation of the HPLC peak areas of AZT (4.94×10^{-4} M) and its photoproducts in acetonitrile with increasing irradiation time.

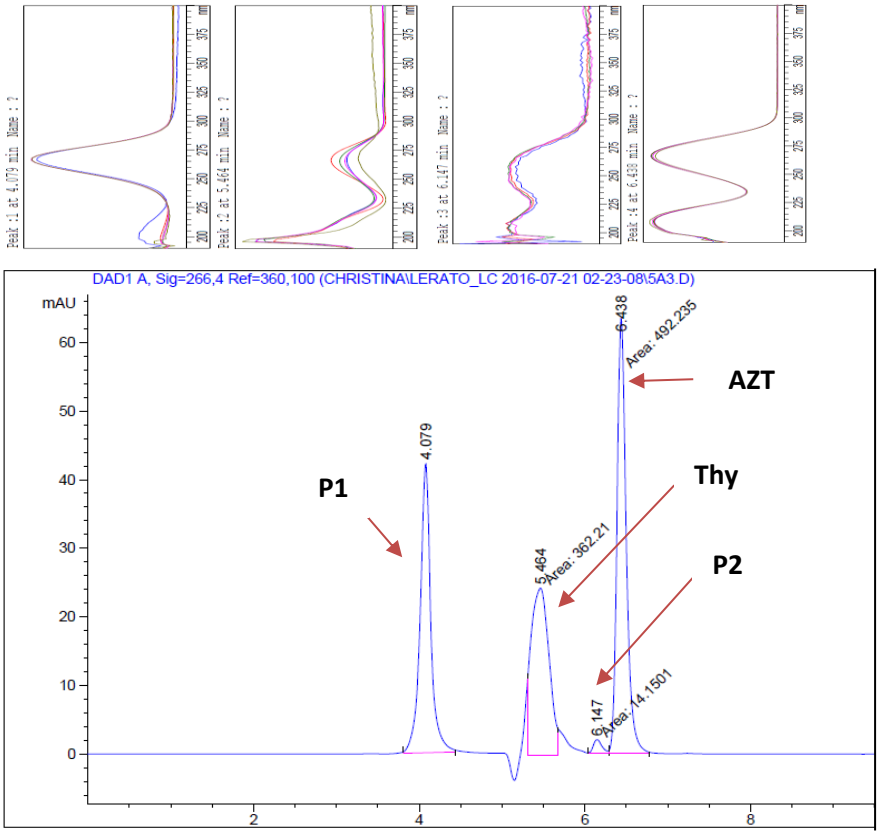

Figure 3.42: HPLC chromatogram of AZT (2.39×10^{-4} M) irradiated for 5 hours in acetonitrile eluted on a Phenomenex Kinetex C18 (150 × 4.6 mm i.d., 2.6 µm particle size) column with methanol:water (60:40 v/v) as the mobile phase at a flow rate of 0.25 mL/min. The detection wavelength was 266 nm.

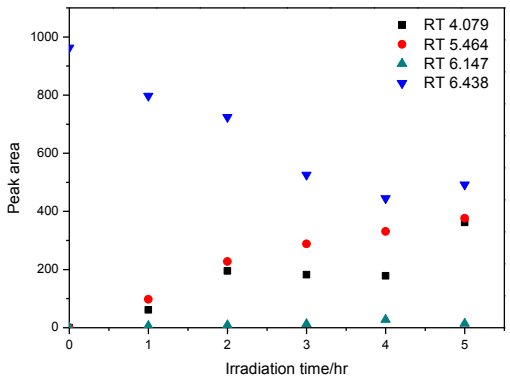

Figure 3.43: Variation of the HPLC peak areas of AZT (2.39×10^{-4} M) and its photoproducts in acetonitrile with increasing irradiation time.

3.2.3. Effect of pH

The separation of the photoproducts of AZT in water was achieved by reversed-phase HPLC under isocratic elution. The HPLC chromatograms, acquired at 266 nm, showed the formation of more hydrophilic photoproducts than AZT at all conditions of pH, namely, 3, 5 and 7. Two photoproducts were formed at pH 3 as seen in **Fig. 3.44** and three photoproducts were formed at pH 5 and 7 (**Fig. 3.46** and **Fig. 3.48** respectively). The photoproducts formed at retention times of 4.406 and 5.710 min were considered as the main products whereas the photoproduct formed at a retention time of 6.332 min was a minor product. Dunge *et al.* reported only one main photoproduct formed after UVB-exposure of AZT in aqueous solution both in acidic and basic media and identified this photoproduct as thymine [86]. Santos *et al*. showed three photoproducts formed after UV-exposure of AZT in aqueous solution under acidic media and two photoproducts formed under basic media [87]. But the products were not identified.

It was observed that the decrease in the pH of the solution affects the resolution of the peak of the first photoproduct at a retention time of 4.406 min. This tells us that this photoproduct is sensitive to acid. We also observed that the peak areas of the two photoproducts at retention times of 4.406 and 5.710 minutes increase with irradiation time in the acidic medium of pH 3 as shown **Fig 3.45**. However, the peak area of AZT at a retention time of 6.678 minutes decreases with increase in irradiation time. The graph in **Fig. 3.47** for the intermediate pH showed the same behaviour as the graph in **Fig. 3.45**.

Just as was observed for pH 5, three photoproducts were also formed at pH 7 as shown in **Fig. 3.48**. It can be observed in **Fig. 3.49** that the peak areas of the first two photoproducts at retention times of 4.175 and 5.704 min increase with irradiation time whereas the peak area

of the photoproduct formed at a retention time of 6.379 min is almost constant. The peak area of AZT at a retention time of 6.680 min decreases with increase in irradiation time.

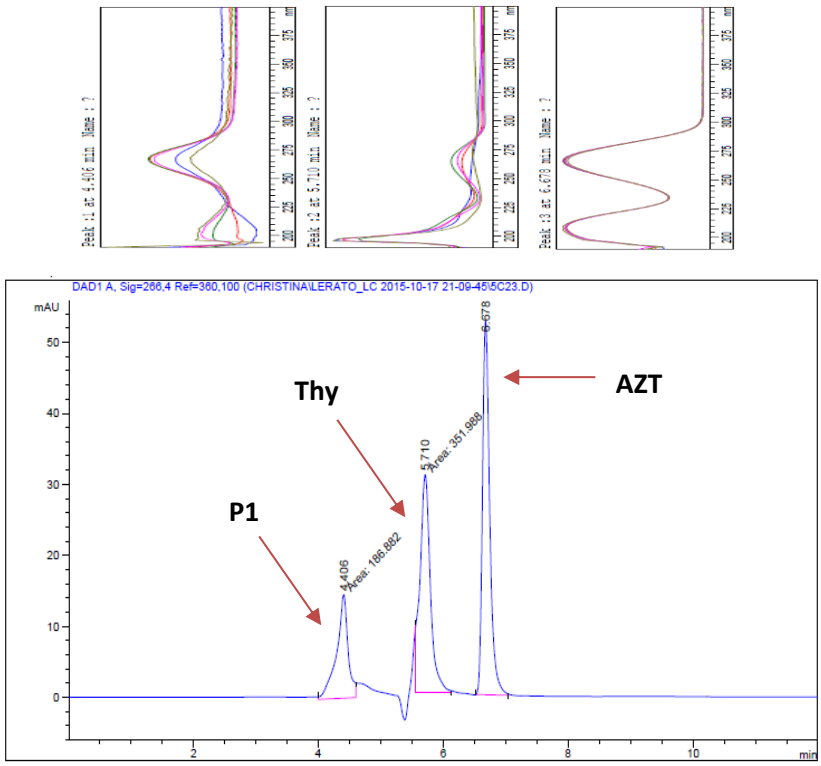

Figure 3.44: HPLC chromatogram of AZT (4.94×10^{-4} M) irradiated for 5 hours in water at pH 3 eluted on a Phenomenex Kinetex C18 (150 × 4.6 mm i.d., 2.6 µm particle size) column with methanol:water (60:40 v/v) as the mobile phase at a flow rate of 0.25 mL/min. The detection wavelength was 266 nm.

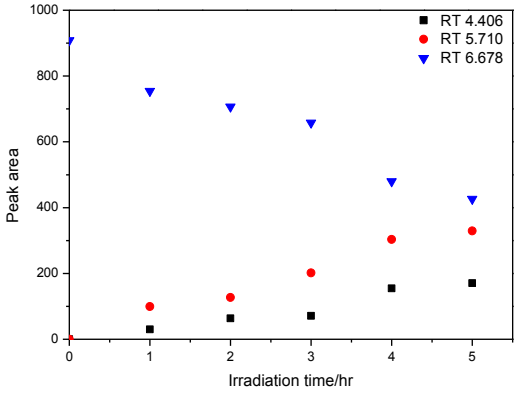

Figure 3.45: Variation of the HPLC peak areas of AZT (4.94×10^{-4} M) and its photoproducts at pH 3 with increasing irradiation time.

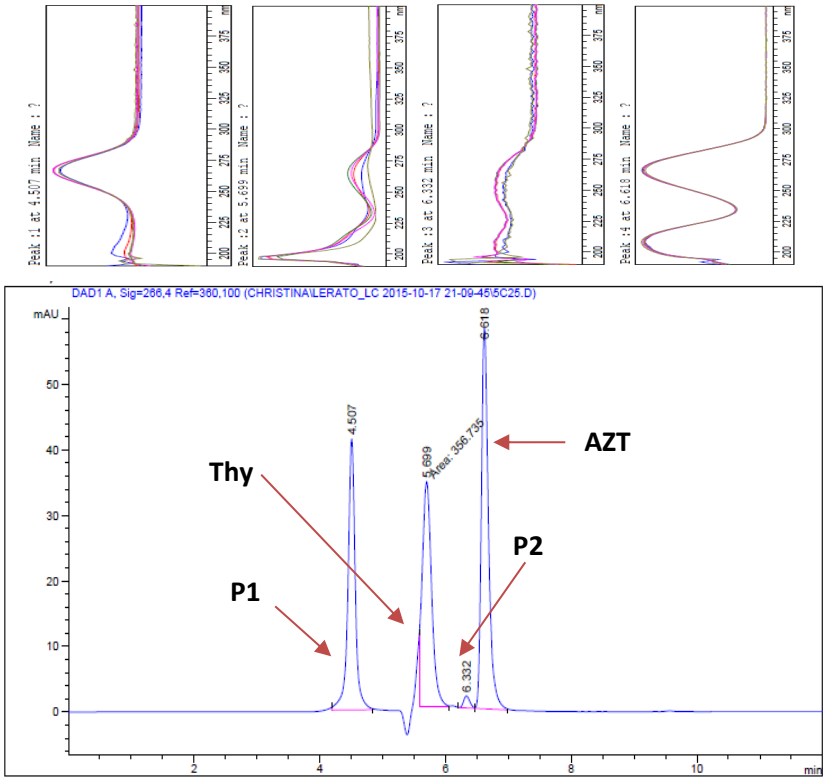

Figure 3.46: HPLC chromatogram of AZT (4.94×10^{-4} M) irradiated for 5 hours in water at pH 5 eluted on a Phenomenex Kinetex C18 (150 × 4.6 mm i.d., 2.6 µm particle size) column with methanol:water (60:40 v/v) as the mobile phase at a flow rate of 0.25 mL/min. The detection wavelength was 266 nm.

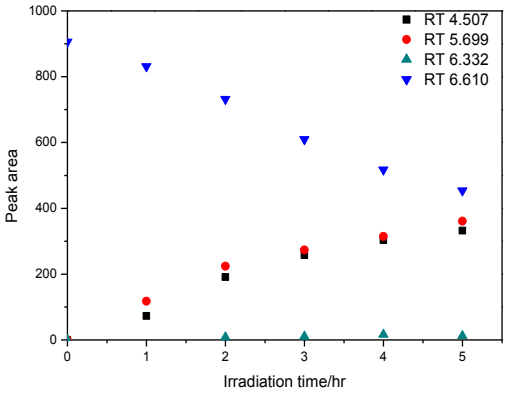

Figure 3.47: Variation of the HPLC peak areas of AZT (4.94×10^{-4} M) and its photoproducts at pH 5 in water with increasing irradiation time.

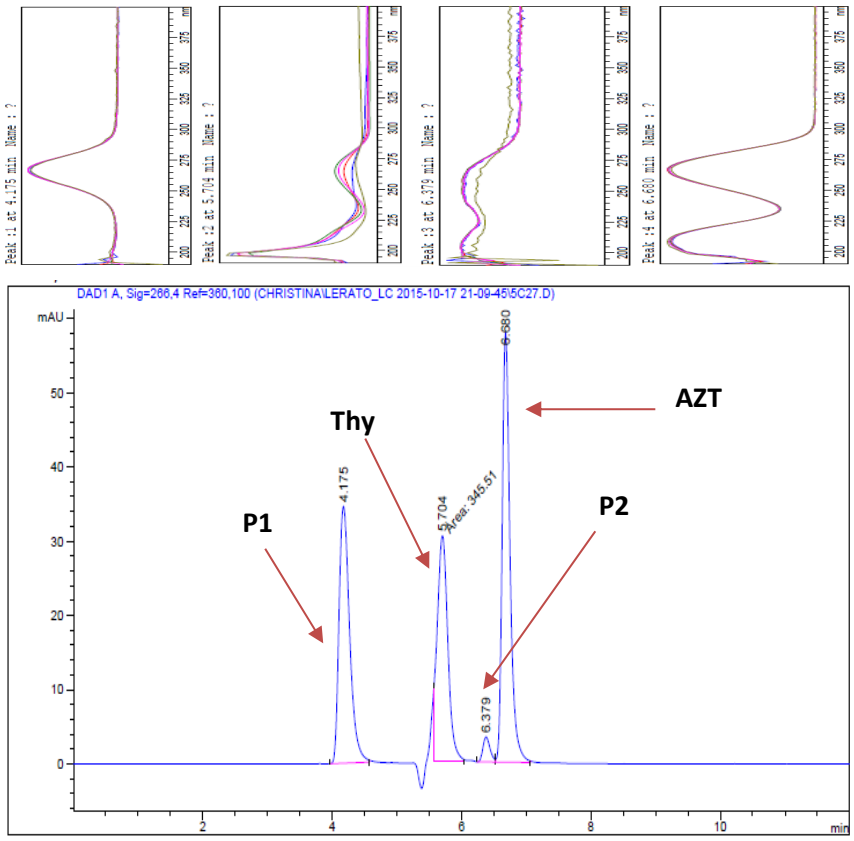

Figure 3.48: HPLC chromatogram of AZT (4.94×10^{-4} M) irradiated for 5 hours in water at pH 7 eluted on a Phenomenex Kinetex C18 (150 × 4.6 mm i.d., 2.6 µm particle size) column with methanol:water (60:40 v/v) as the mobile phase at a flow rate of 0.25 mL/min. The detection wavelength was 266 nm.

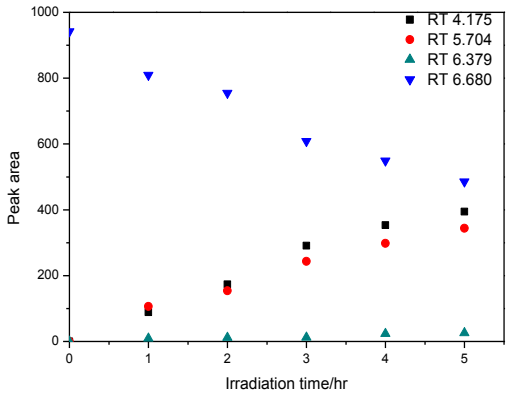

Figure 3.49: Variation of the HPLC peak areas of AZT (4.94×10^{-4} M) and its photoproducts at pH 7 in water with increasing irradiation time.

In summary, the photodegradation products of AZT retained almost the same retention time (see **Table 3.4**) and the same UV spectra in all different conditions of solvents, pH and concentration. This indicates that the photoproducts formed under all conditions are essentially the same and have the same chromophore as AZT, which we propose to be a thymine moiety. We also observed inconsistencies in the absorbance values of the spectra as described in **Section 3.1**, however, the peak areas of the photoproducts of AZT increased with time as the peak area of AZT dropped on the HPLC analysis. The inconsistency in absorbance could be attributed to the competition of photoproducts to UV-light.

A major photoproduct, thymine, at a retention time of 5.700 min was identified by spiking each sample with the standard, and comparison with the standard, as shown in **Fig. 3.50** and **Fig. 3.51**. A similar protocol was employed by Dunge *et al.* for the identification of thymine in the photolysis of AZT [86]. The other photoproducts were identified by LC-MS as described in **Section 3.4**. Since the UV spectra and retention times of P1 and P2 were essentially the same under all conditions only the aqueous samples were analysed by LC-MS. Thymine and AZT in all the samples were quantified as will be described in **Section 3.3**.

Table 3.4: Summary of the photolysis of AZT in different conditions of solvent and pH. The HPLC retention times of AZT and the photoproducts are given in minutes.

Conc./M	ID	H_2O	MeOH	EtOH	ProOH	ACN	pH3	pH 5	pH 7
5×10^{-2}	Thy	5.69	5.698	5.701	5.737	5.690			
	P2	-	6.400	6.404	-	-			
	AZT	6.61	6.742	6.749	6.903	6.664			
5×10^{-4}	P1	4.59	4.495	4.500	5.069	4.365	4.406	4.507	4.175
	Thy	5.69	5.692	5.696	5.713	5.698	5.710	5.699	5.704
	P2	6.38	6.396	6.394	6.200	6.412	-	6.332	6.379
	AZT	6.72	6.737	6.737	6.733	6.751	6.678	6.610	6.680
2.4×10^{-4}	P1	4.48	4.162	4.378	4.983	4.079			
	Thy	5.70	5.706	5.689	5.693	5.464			
	P2	6.41	6.436	-	6.164	6.147			
	AZT	6.75	6.766	6.610	6.739	6.438			

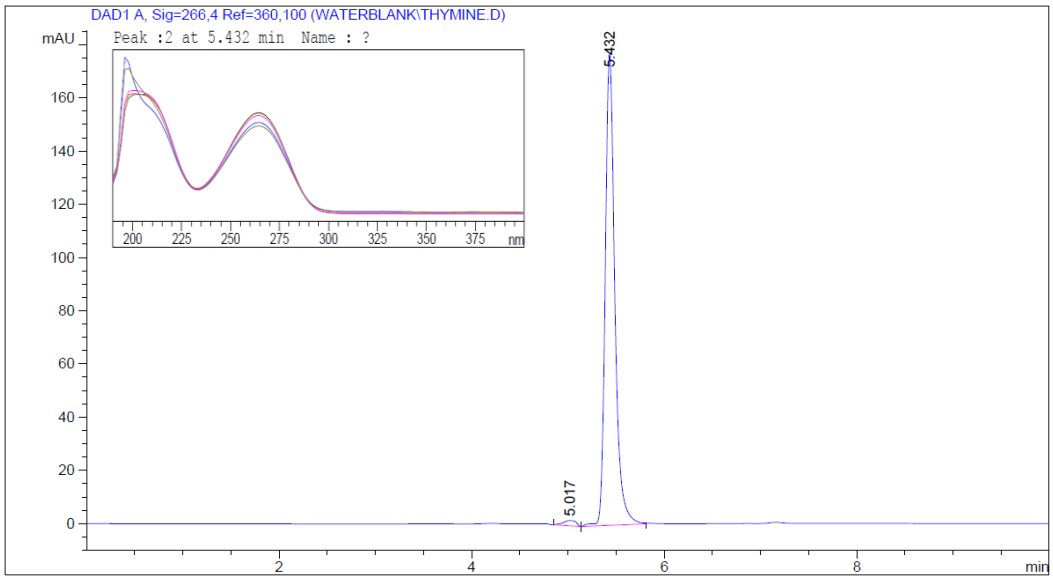

Figure 3.50: HPLC chromatogram of thymine dissolved in water eluted on a Phenomenex Kinetex C18 (150 × 4.6 mm i.d., 2.6 µm particle size) column with methanol:water (60:40 v/v) as the mobile phase at a flow rate of 0.25 mL/min. The detection wavelength was 266 nm.

(a)

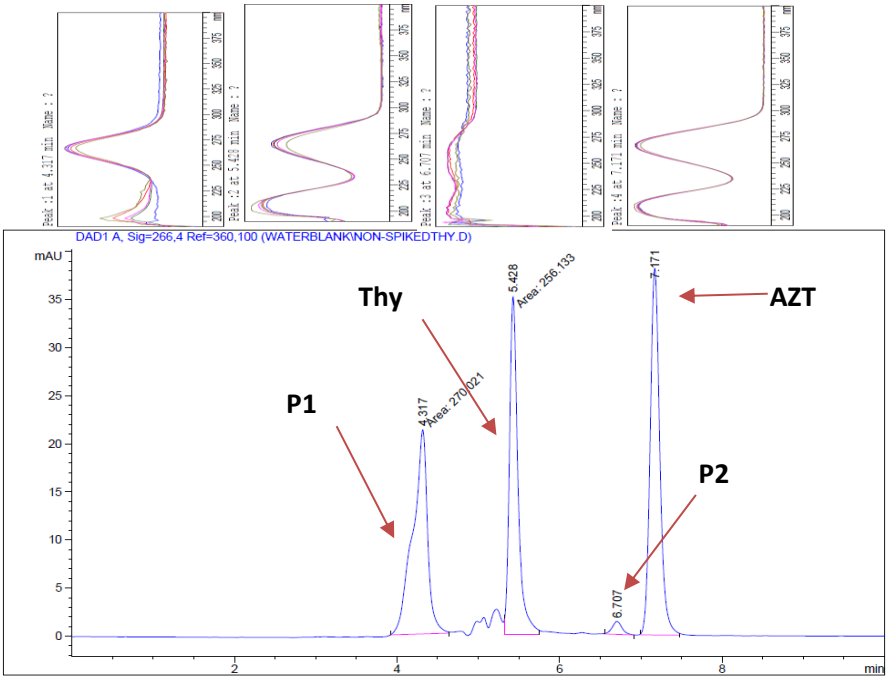

(b)

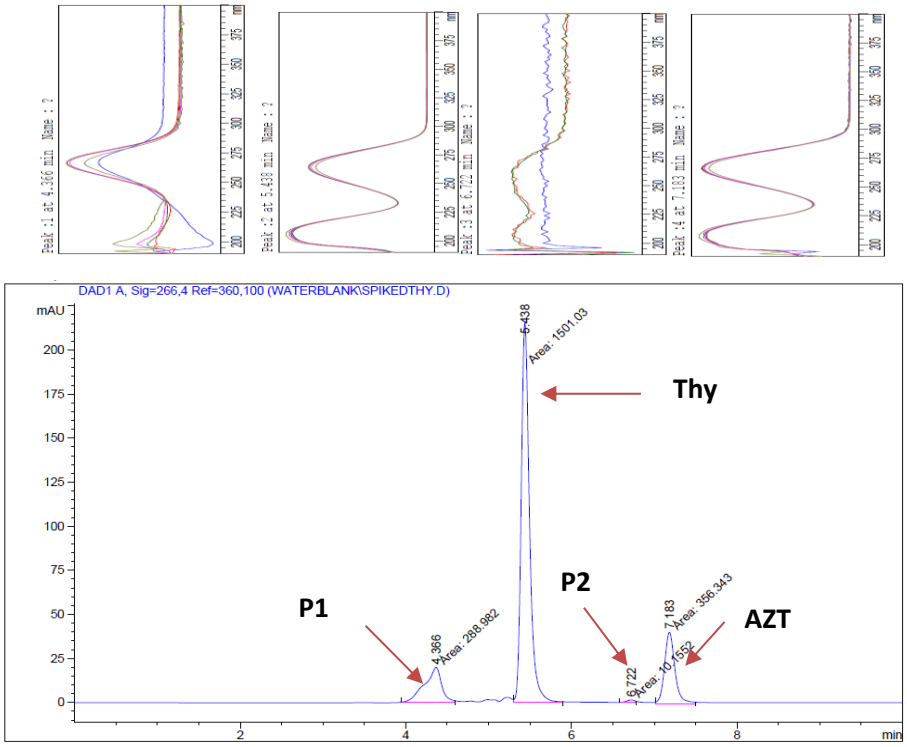

Figure 3.51: HPLC chromatogram of an irradiated sample of AZT (4.94 ×10^{-4} M) dissolved in water that was (a) not spiked, and (b) spiked with thymine dissolved in water eluted on a Phenomenex Kinetex C18 (150 × 4.6 mm i.d., 2.6 µm particle size) column with methanol:water (60:40 v/v) as the mobile phase at a flow rate of 0.25 mL/min. The detection wavelength was 266 nm.

3.3. Quantification analysis

AZT and thymine were quantified in all the samples by using acetophenone as the internal standard in the HPLC (see **Fig. 3.52**). The calibration curves for AZT (see **Fig. 3.53**) and thymine (see **Fig. 3.55**) were obtained by plotting the peak area ratio against the concentration ratio, that is, the peak area of the analyte/peak area of acetophenone against the concentration of the analyte/concentration of acetophenone and the associated residual plots are shown in **Fig. 3.54** for AZT and **Fig. 3.56** for thymine. Both calibration curves were linear with correlation coefficients of $R^2 = 1$ and their residual plots showed good distribution about the x-axis indicating no bias in the data.

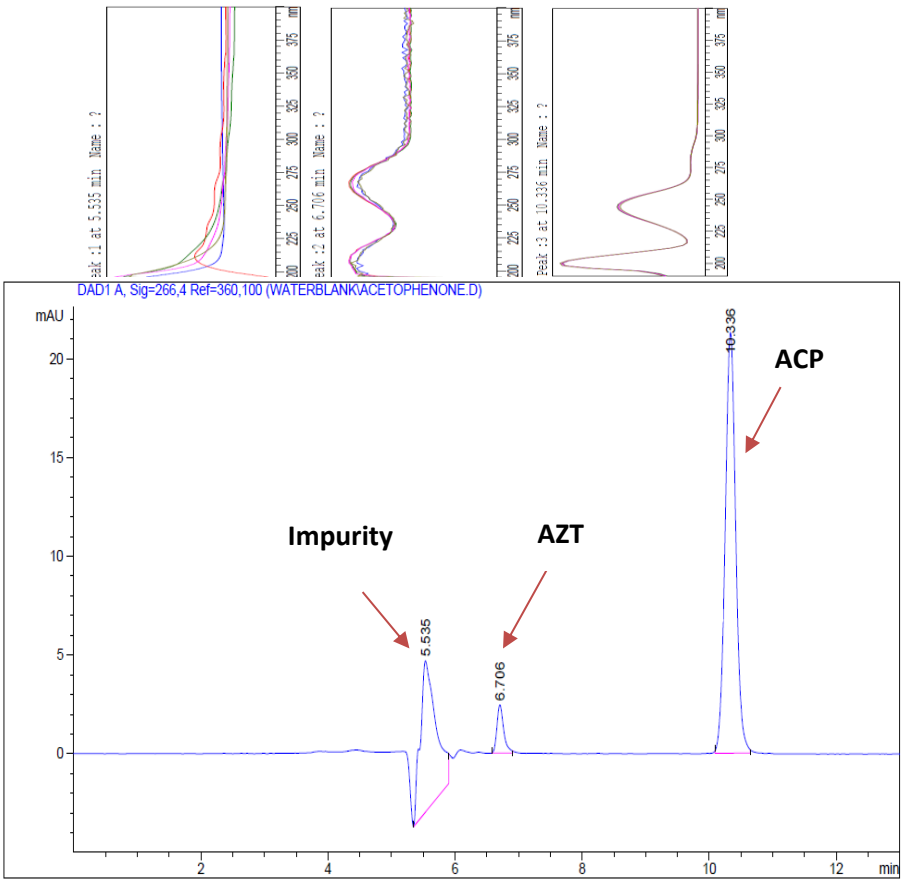

Figure 3.52: HPLC chromatogram of AZT and acetophenone (ACP) eluted on a Phenomenex Kinetex C18 (150 × 4.6 mm i.d., 2.6 µm particle size) column with methanol:water (60:40 v/v) as the mobile phase at a flow rate of 0.25 mL/min. The detection wavelength was 266 nm.

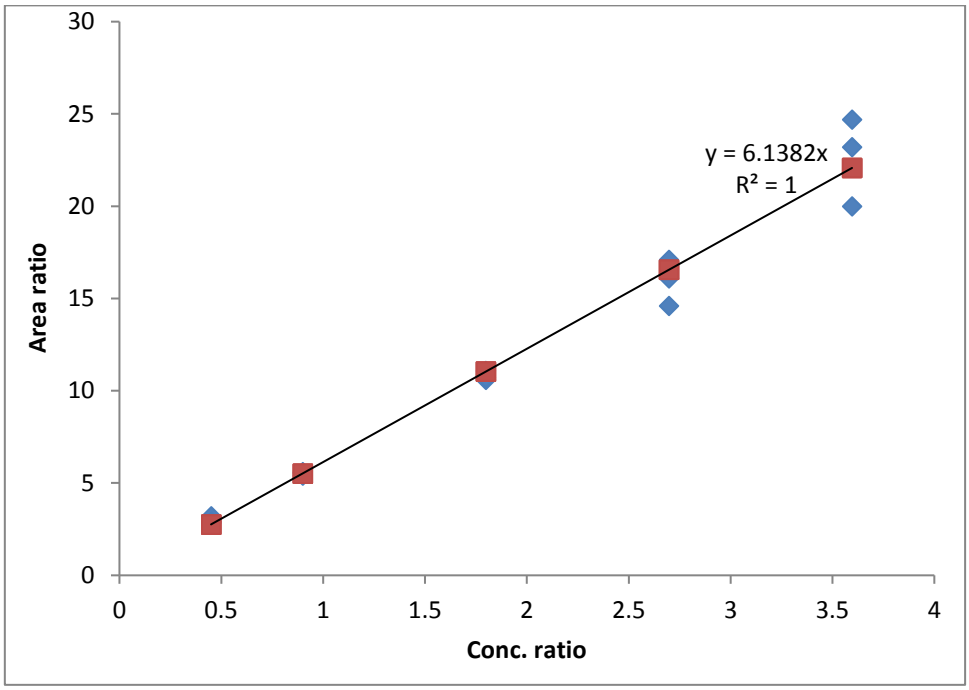

Figure 3.53: Calibration curve for AZT. The points depict the experimental data and the solid line shows the linear regression model fitted. Detection was at 266 nm.

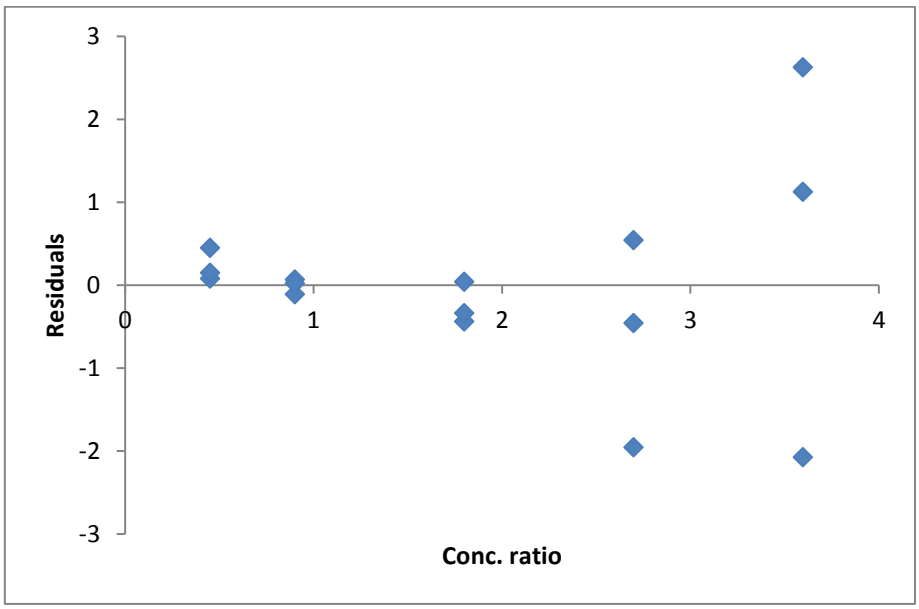

Figure 3.54: Residual plot for the HPLC calibration curve for AZT shown in Fig. 3.52.

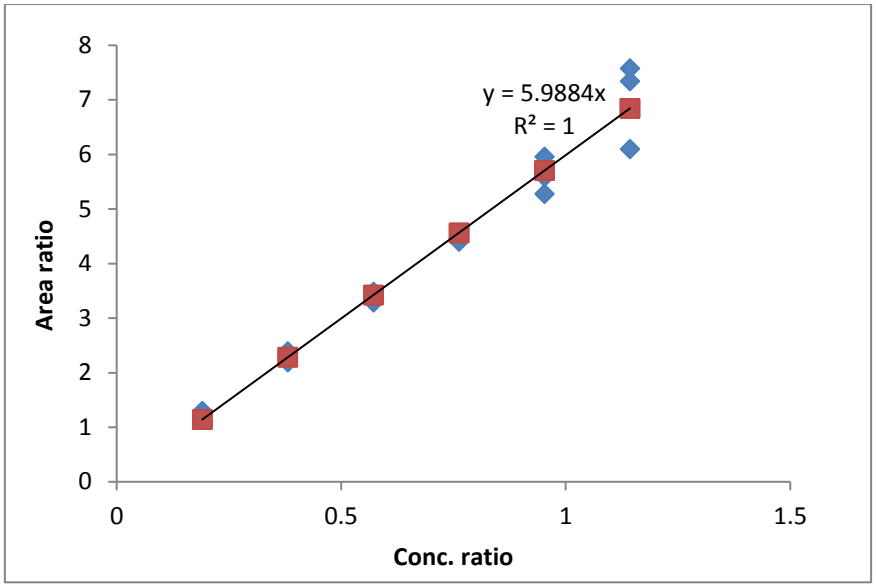

Figure 3.55: Calibration curve for thymine. The points depict the experimental data and the solid line shows the linear regression model fitted. Detection was at 266 nm.

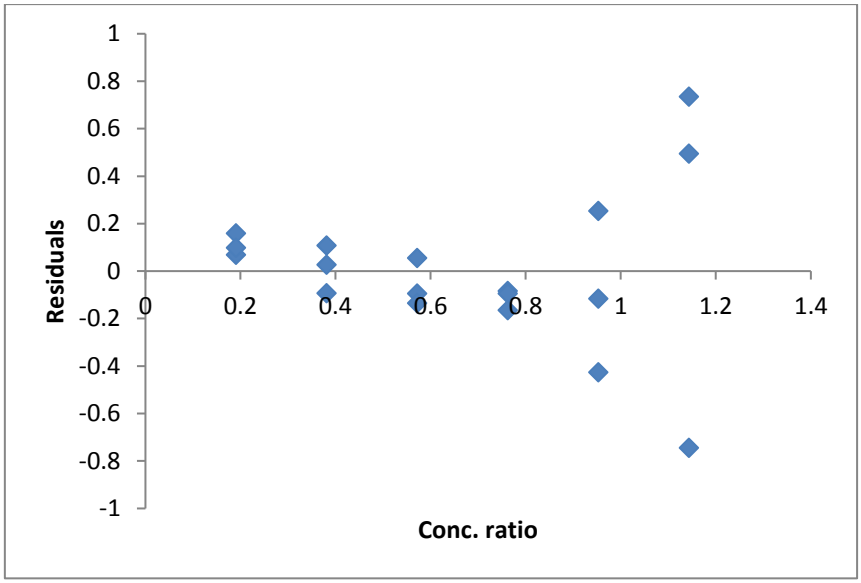

Figure 3.56: Residual plot for the HPLC calibration curve for thymine shown in Fig. 3.54.

3.3.1. Quantification analysis of AZT in different solvents

Fig. 3.57 shows the concentration of AZT remaining and the concentration of thymine formed at hourly intervals of UV-irradiation in the different solvents. After 5 hours of UV-irradiation, the amount of AZT photodegraded was observed to increase with the increase in

the dipole moment of the solvent (see **Section 3.1.1**). However, the amount of degradation in alcoholic solvents was almost the same. After 5 hours of UV-exposure, the photolysis of AZT resulted in a loss of about 0.393 mM, 0.254 mM, ±0.175 mM (as observed in the actual solutions irradiated) of the initial drug content in acetonitrile, water and alcoholic solutions, respectively. The rate of photodegradation of AZT occurred faster in the decreasing order: acetonitrile, water, 2-propanol, ethanol and methanol.

The formation of thymine was observed to be highest in methanol followed by ethanol, acetonitrile, 2-propanol and water. This indicates that thymine formation was independent of the dipole moment of the solvent.

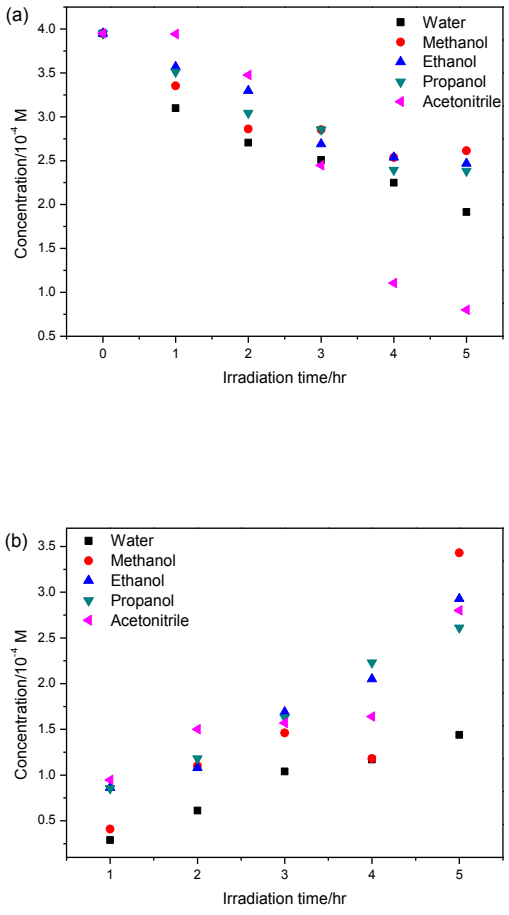

Figure 3.57: The concentration of (a) AZT remaining (4.94×10^{-4} M) and (b) thymine formed in different solvents at hourly intervals of UV-irradiation.

3.3.2. Quantification of AZT when irradiated at different concentrations in different solvents

The change in the concentration of AZT with irradiation time in water at different starting concentrations of 5.01×10^{-2}, 4.94×10^{-4} and 2.39×10^{-4} M is shown in **Fig. 3.58**. It was observed that AZT photodegradation increases with increase in irradiation time for all three concentrations.

For the highest concentration of AZT (5.01×10^{-2} M) in aqueous solution the change in the amount of AZT degraded per hour is small whereas at 4.94×10^{-4} M and 2.39×10^{-4} M the changes are larger for the diluted solutions of equivalent concentrations analysed (see **Fig. 3.58a**). This concurs with the UV spectroscopy results (see **Fig. 3.4c**) where very little change in absorbance was observed for the highest AZT concentration. However, this trend is still reflected in the relative amounts photodegraded (30, 52 and 58 % in the order from highest to lowest concentration respectively) (see Appendix B Table B1). Also, only one photoproduct could be detected at the highest concentration as opposed to the three observed for the other two concentrations.

The amount of thymine formed relative to the initial concentration of AZT in water is shown in **Fig. 3.59**. This showed an increase in thymine formed for all irradiation times at the three different starting concentrations. About 4.28 mM of thymine was formed after 5 hours of UV-irradiation at the higher concentration; 0.144 mM at the intermediate concentration and 0.0713 mM in the lowest concentration of the actual solutions irradiated.

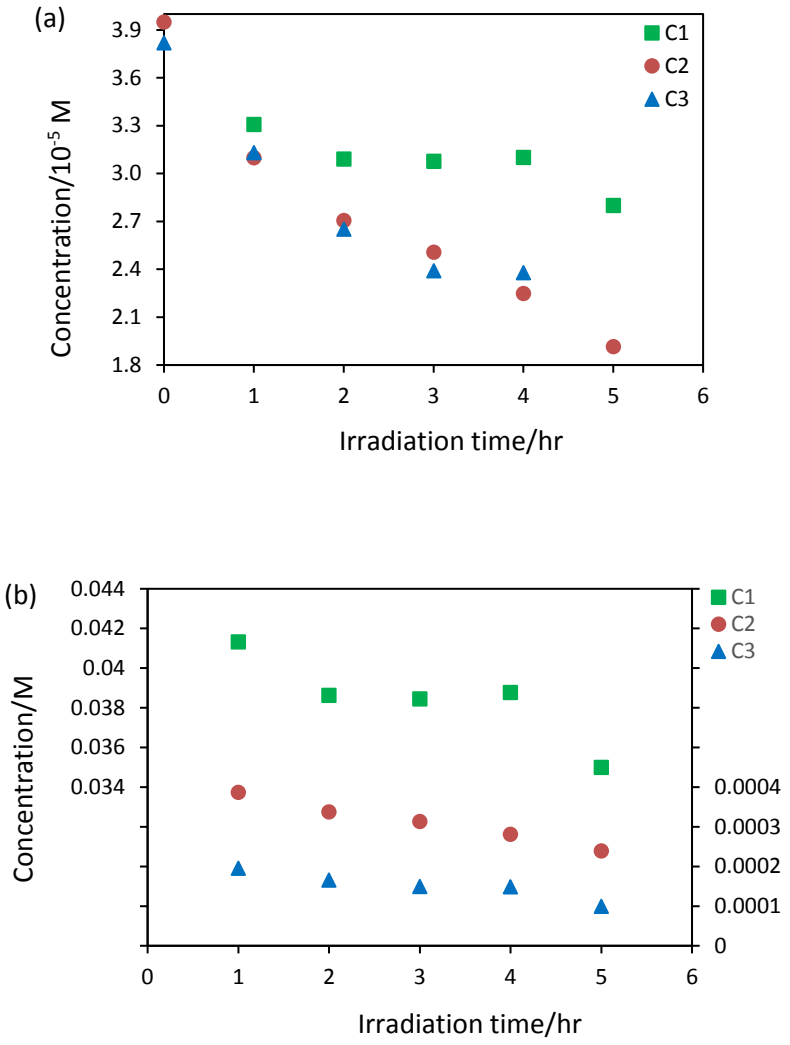

Figure 3.58: The change in the concentration of AZT with irradiation time in water at different starting concentrations of C1 = 5.01 × 10^{-2}, C2 = 4.94 × 10^{-4} and C3 = 2.39 × 10^{-4} M. (a) The concentrations shown are for the diluted solutions analyzed, namely, C1 = 4.01 × 10^{-5} M, C2 = 3.95 × 10^{-5} M and C3 = 3.82 × 10^{-5} M. (b) The concentration of AZT remaining at different irradiation times as would have been present in the actual solutions irradiated.

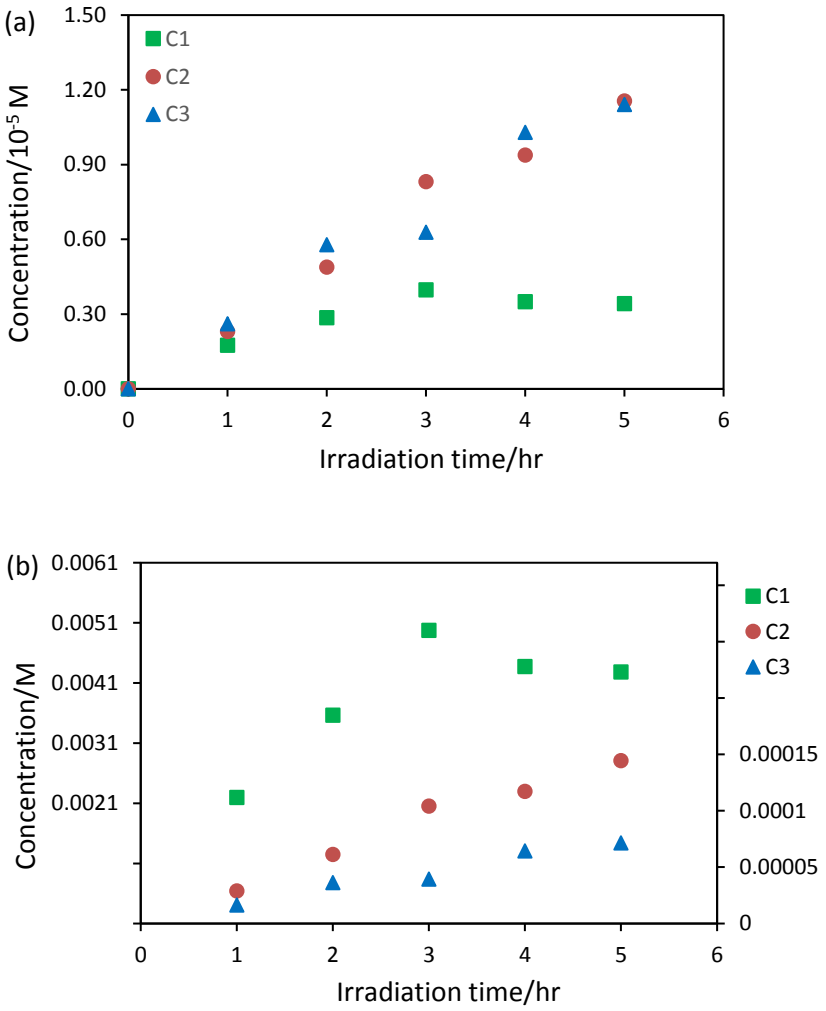

Figure 3.59: The concentration of thymine formed at different starting concentrations of AZT in water of C1 = 5.01×10^{-2}, C2 = 4.94×10^{-4} and C3 = 2.39×10^{-4} M. (a) The concentrations shown are for the diluted solutions analyzed, namely, C1 = 4.01×10^{-5} M, C2 = 3.95×10^{-5} M and C3 = 3.82×10^{-5} M. (b) The concentration of AZT remaining at different irradiation times as would have been present in the actual solutions irradiated.

The concentration of AZT remaining in methanol at the three different starting concentrations of 5.01×10^{-2}, 4.94×10^{-4} and 2.39×10^{-4} M is shown in **Fig. 3.60**. The photolysis of AZT (5.01×10^{-2} M) in methanolic solution resulted in a loss of about 7.03 mM of the AZT after 1 hour of irradiation. Between 3 and 4 hours ~ 26% of AZT was destroyed and about 14.4 mM of AZT was lost after 5 hours of irradiation. From these results we observed that the

photolysis of AZT in methanol occurs faster in the highest concentration than the lowest concentrations.

The amount of thymine formed for the three different concentrations of AZT in methanol (5.01×10^{-2}, 4.94×10^{-4} and 2.39×10^{-4} M) is shown in **Fig. 3.61**. It was observed that the formation of thymine increases with irradiation time for all the different starting concentrations. However, in the 3rd and 4th hour of UV-irradiation the amount of thymine formed in the highest concentration was almost the same. A significant increase was observed after 5 hours of UV-irradiation in the intermediate concentration. About 0.090 mM of thymine was formed in the lowest concentration; 0.343 mM in the intermediate concentration and 4.69 mM in highest concentration. We also observed that the formation of thymine in methanol was greater than that of water for all the different starting concentrations.

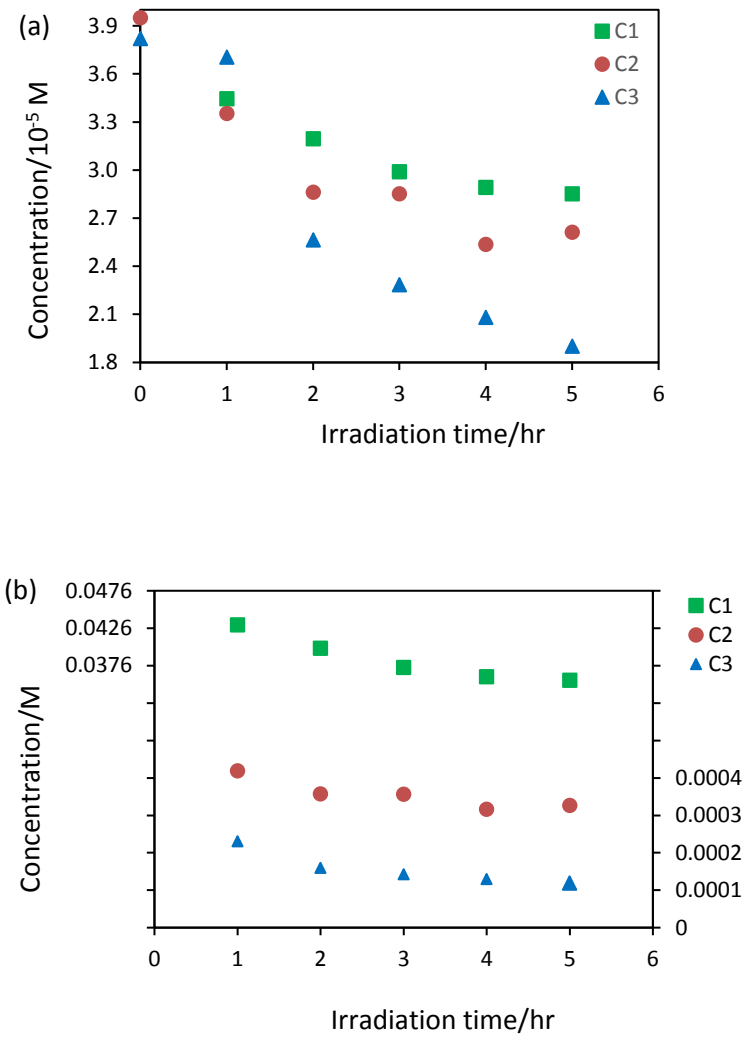

Figure 3.60: The change in the concentration of AZT with irradiation time in methanol at different starting concentrations of C1 = 5.01×10^{-2}, C2 = 4.94×10^{-4} and C3 = 2.39×10^{-4} M. (a) The concentrations shown are for the diluted solutions analyzed, namely, C1 = 4.01×10^{-5} M, C2 = 3.95×10^{-5} M and C3 = 3.82×10^{-5} M. (b) The concentration of AZT remaining at different irradiation times as would have been present in the actual solutions irradiated.

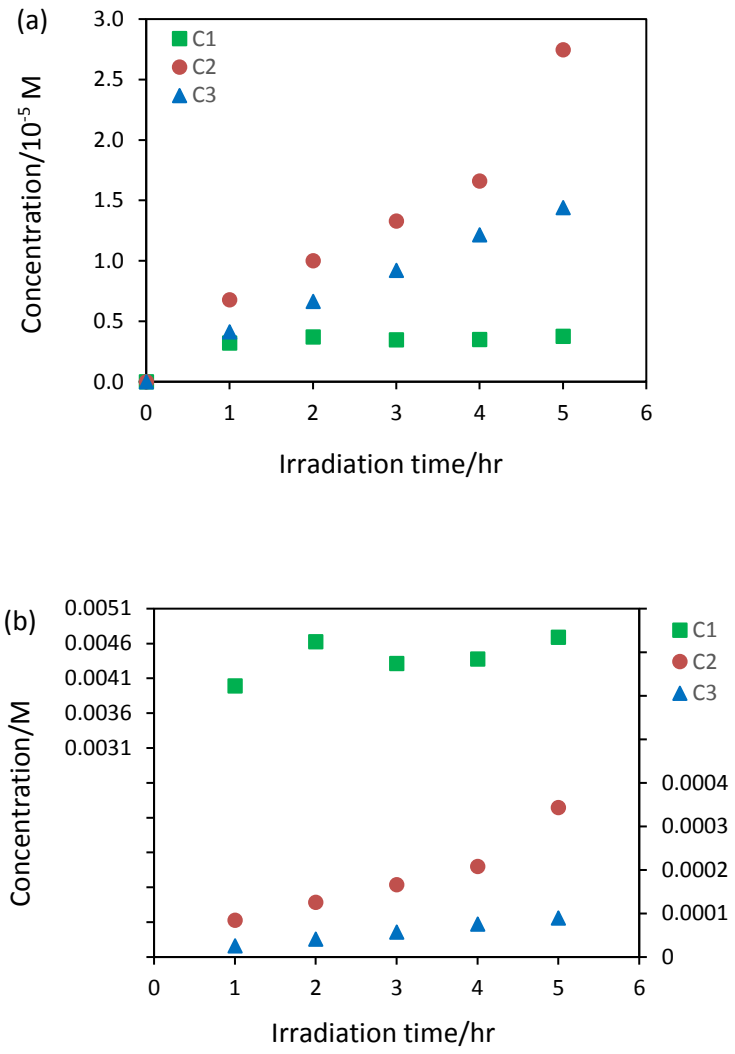

Figure 3.61: The concentration of thymine formed at different starting concentrations of AZT in methanol of C1 = 5.01×10^{-2}, C2 = 4.94×10^{-4} and C3 = 2.39×10^{-4} M. (a) The concentrations shown are for the diluted solutions analyzed, namely, C1 = 4.01×10^{-5} M, C2 = 3.95×10^{-5} M and C3 = 3.82×10^{-5} M. (b) The concentration of AZT remaining at different irradiation times as would have been present in the actual solutions irradiated.

The amount of AZT remaining after irradiation in ethanol at different concentrations of 5.01 × 10^{-2}, 4.94 × 10^{-4} and 2.39 × 10^{-4} M is shown in **Fig. 3.62**. It was observed that the rate of photodegradation of AZT before 2 hours of irradiation was faster at the highest concentration than at the lower concentrations. However, after 3 hours of irradiation the rate of photodegradation of AZT became faster in the lowest concentrations than at the highest concentration.

The concentration of thymine formed relative to the initial amount of AZT in ethanol at different concentrations of 5.01 × 10^{-2}, 4.94 × 10^{-4} and 2.39 × 10^{-4} M is shown in **Fig. 3.63**. An increase in the formation of thymine was observed as the irradiation time increased for all the different starting concentrations. However, after 2 and 4 hours of UV-irradiation the thymine formed at the lowest and intermediate concentration was almost the same. About 4.725 mM of thymine was formerd at the highest concentration; 0.2925 mM in the intermediate concentration and 0.1125 mM at lowest concentration after 5 hours of irradiation time.

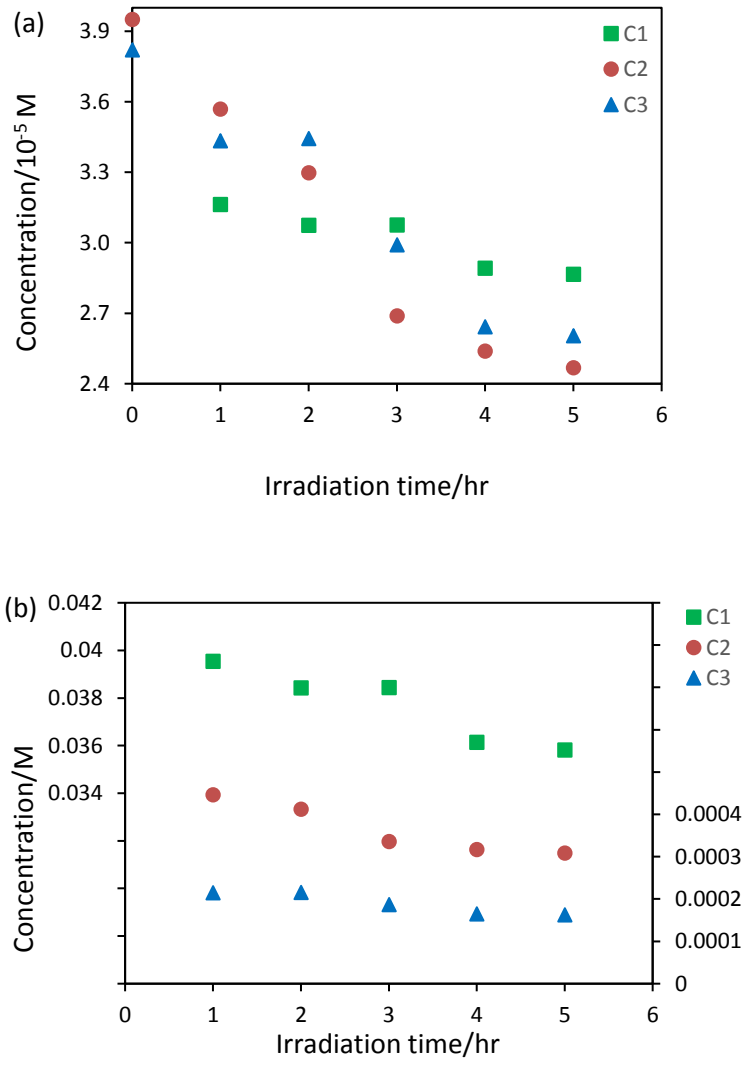

Figure 3.62: The change in the concentration of AZT with irradiation time in ethanol at different starting concentrations of C1 = 5.01×10^{-2}, C2 = 4.94×10^{-4} and C3 = 2.39×10^{-4} M. (a) The concentrations shown are for the diluted solutions analyzed, namely, C1 = 4.01×10^{-5} M, C2 = 3.95×10^{-5} M and C3 = 3.82×10^{-5} M. (b) The concentration of AZT remaining at different irradiation times as would have been present in the actual solutions irradiated.

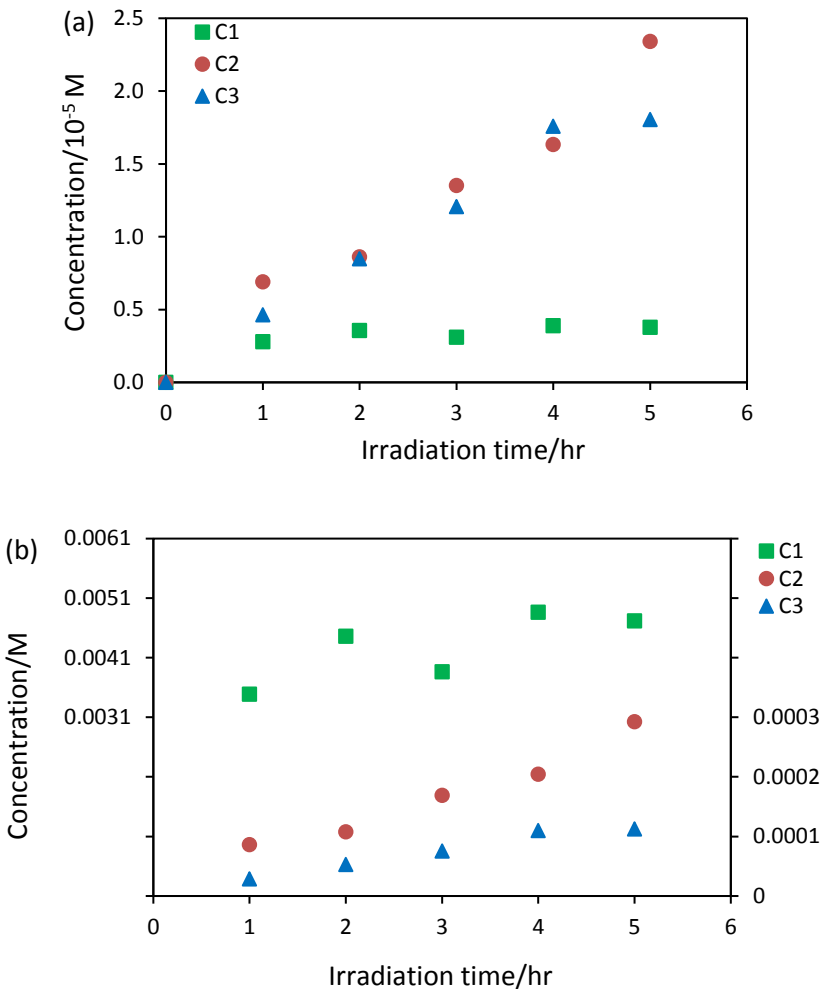

Figure 3.63: The concentration of thymine formed at different starting concentrations of AZT in ethanol of C1 = 5.01 × 10^{-2}, C2 = 4.94 × 10^{-4} and C3 = 2.39 × 10^{-4} M. (a) The concentrations shown are for the diluted solutions analyzed, namely, C1 = 4.01 × 10^{-5} M, C2 = 3.95 × 10^{-5} M and C3 = 3.82 × 10^{-5} M. (b) The concentration of AZT remaining at different irradiation times as would have been present in the actual solutions irradiated.

The amount of AZT remaining in 2-propanol at the three different starting concentrations of 5.01 × 10^{-2}, 4.94 × 10^{-4} and 2.39 × 10^{-4} M is shown in **Fig. 3.64**. About 13.2 mM of AZT was destroyed after 5 hours of irradiation for the 5.01 × 10^{-2} M solution, 0.196 mM for the 4.94 × 10^{-4} M solution and 0.117 mM was lost for the 2.39 × 10^{-4} M solution.

The concentration of thymine formed in 2-propanol for the different AZT starting concentrations of 5.01 × 10^{-2}, 4.94 × 10^{-4} and 2.39 × 10^{-4} M is shown in **Fig. 3.65**. An increase in the formation of thymine was observed here as the irradiation time increased for

the intermediate and the lowest concentrations. However, for the highest concentration formation of thymine did not show a linear trend. The highest rate of formation of thymine was observed at the intermediate concentration followed by the lowest concentration, while the highest concentration showed the least formation of photoproducts.

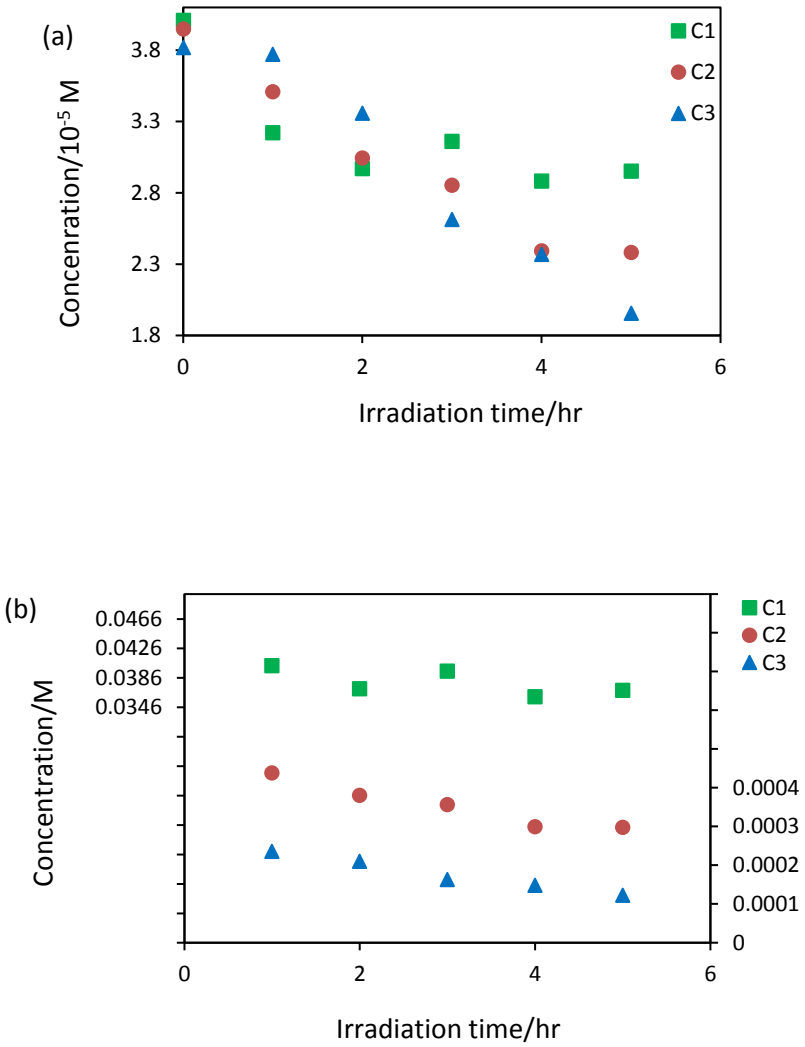

Figure 3.64: The change in the concentration of AZT with irradiation time in 2-propanol at different starting concentrations of C1 = 5.01 × 10^{-2}, C2 = 4.94 × 10^{-4} and C3 = 2.39 × 10^{-4} M. (a) The concentrations shown are for the diluted solutions analyzed, namely, C1 = 4.01 × 10^{-5} M, C2 = 3.95 × 10^{-5} M and C3 = 3.82 × 10^{-5} M. (b) The concentration of AZT remaining at different irradiation times as would have been present in the actual solutions irradiated.

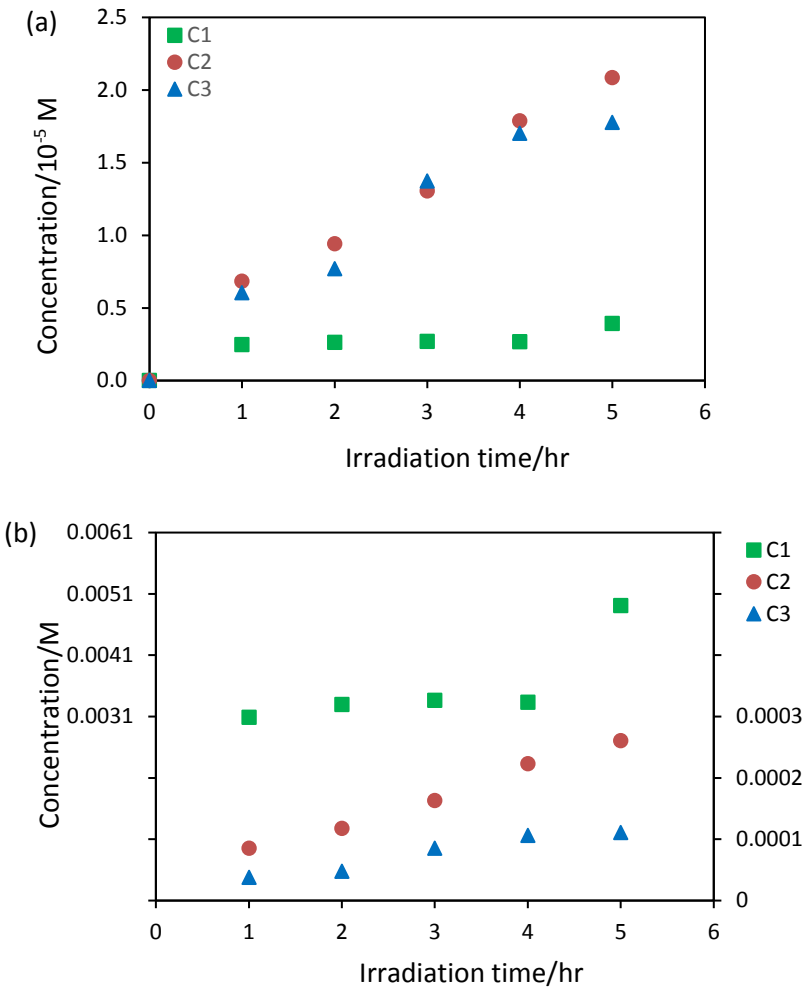

Figure 3.65: The concentration of thymine formed at different starting concentrations of AZT in 2-propanol of C1 = 5.01 × 10^{-2}, C2 = 4.94 × 10^{-4} and C3 = 2.39 × 10^{-4} M. (a) The concentrations shown are for the diluted solutions analyzed, namely, C1 = 4.01 × 10^{-5} M, C2 = 3.95 × 10^{-5} M and C3 = 3.82 × 10^{-5} M. (b) The concentration of AZT remaining at different irradiation times as would have been present in the actual solutions irradiated.

The photolysis of AZT in acetonitrile results in a loss of 0.394 mM of AZT after 5 hours of irradiation at 4.94 × 10^{-4} M as shown in **Fig. 3.66**. About 12.75 mM was destroyed at 5.01 × 10^{-2} M after 5 hours of irradiation and 0.139 mM was lost for 2.39 × 10^{-4} M.

The amount of thymine formed at different AZT initial concentrations of 5.01 × 10^{-2}, 4.94 × 10^{-4} and 2.39 × 10^{-4} M is shown in **Fig. 3.67**. It was observed that the concentration of thymine formed increases with the irradiation time for all three different starting

concentrations. However, it was observed that in the highest concentration the rate of photodegration was highest in the first 2 hours. For the intermediate concentration an increase in the formation of thymine was observed to show a photostationary state in the 2nd to the 4th hour and a rapid increase in the 5th hour of UV irradiation. About 0.120 mM of thymine was formed after 5 hours of UV-irradiation at low concentration, 0.280 mM was formed at the intermediate concentration and 5.063 mM was formed at the highest concentration.

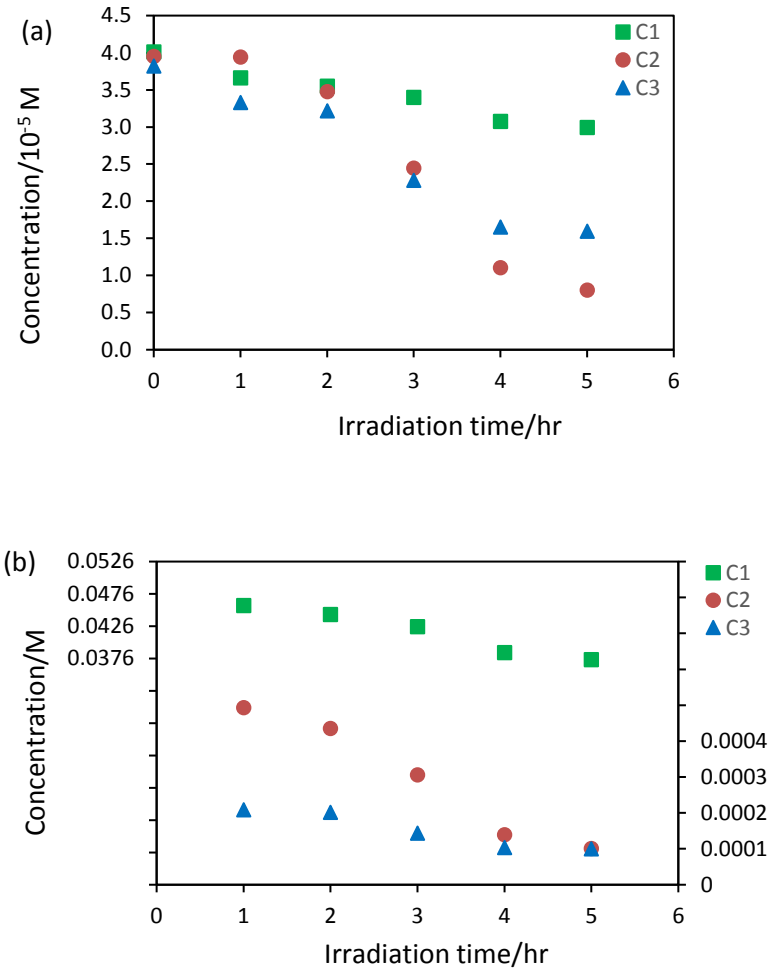

Figure 3.66: The change in the concentration of AZT with irradiation time in acetonitrile at different starting concentrations of C1 = 5.01 × 10^{-2}, C2 = 4.94 × 10^{-4} and C3 = 2.39 × 10^{-4} M. (a) The concentrations shown are for the diluted solutions analyzed, namely, C1 = 4.01 ×10^{-5} M, C2 = 3.95 × 10^{-5} M and C3 = 3.82 × 10^{-5} M. (b) The concentration of AZT remaining at different irradiation times as would have been present in the actual solutions irradiated.

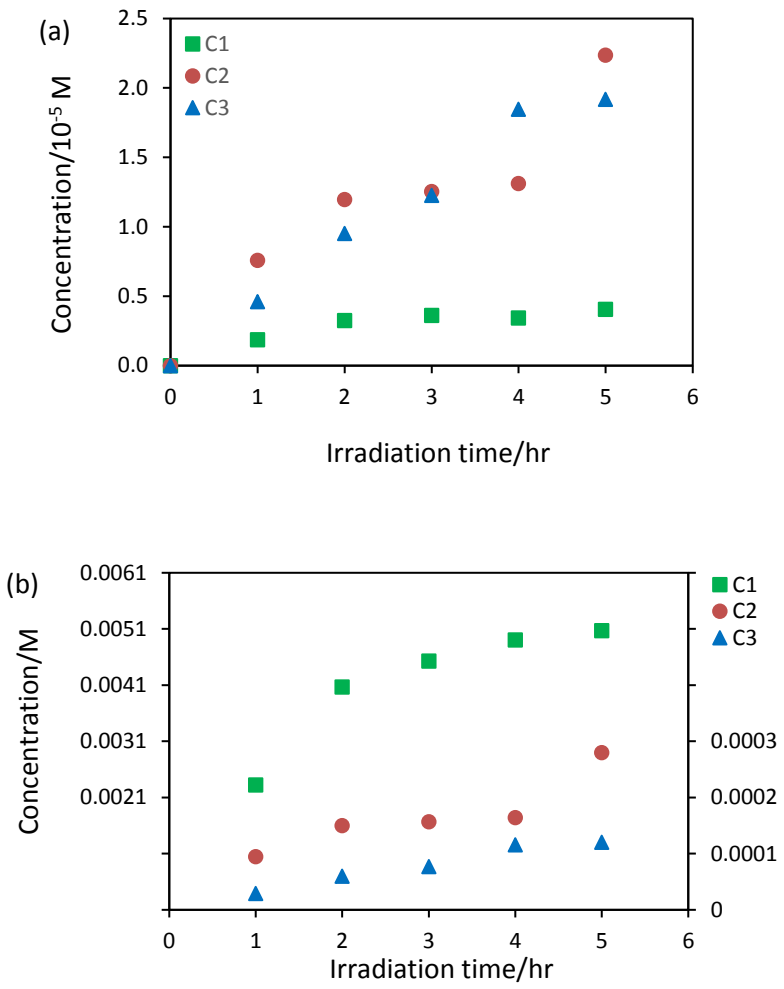

Figure 3.67: The concentration of thymine formed at different starting concentrations of AZT in acetonitrile of C1 = 5.01 × 10^{-2}, C2 = 4.94 × 10^{-4} and C3 = 2.39 × 10^{-4} M. (a) The concentrations shown are for the diluted solutions analyzed, namely, C1 = 4.01 × 10^{-5} M, C2 = 3.95 × 10^{-5} M and C3 = 3.82 × 10^{-5} M. (b) The concentration of AZT remaining at different irradiation times as would have been present in the actual solutions irradiated.

3.3.3. Quantification of AZT when irradiated at different pH conditions

Fig. 3.68 demonstrates the influence of pH on the photodegradation of AZT (4.94 × 10^{-4} M). After 5 hours of UV-exposure, the photolysis of AZT resulted in a loss of about 0.244 , 0.187 and 0.271 mM of the initial drug content at pH 3, 5 and 7, respectively. The rate of photodegradation of AZT occurred faster in the decreasing order: pH 7, pH 3 and pH 5.

Santos *et al.* reported a percentage degradation of 28.61 ± 0.96% AZT in both acidic and alkaline solution [87].

The formation of thymine in water at different pH solutions of 3, 5 and 7 is shown in **Fig. 3.69**. A significant increase in the concentration of thymine formed was observed under all conditions of pH. We also observe that thymine forms more in pH 5 followed by 3 and 7. These results did not with agree with the UV spectroscopy results presented in **Table 3.8** with respect to change the absorbance of the photodegraded AZT. This could be attributed to competing absorption by photoproducts as stated earlier.

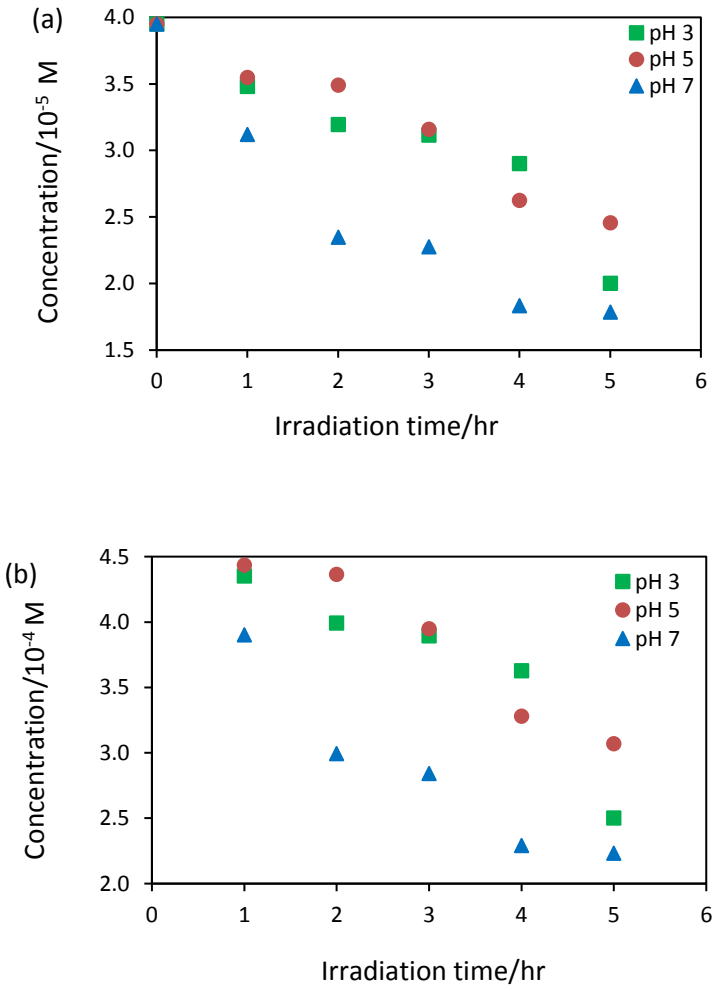

Figure 3.68: The concentration of AZT (4.94×10^{-4} M) photodegraded in water at different pH (3, 5 and 7) as observed (a) in the dilute solutions analysed and (b) in the actual solution irradiated.

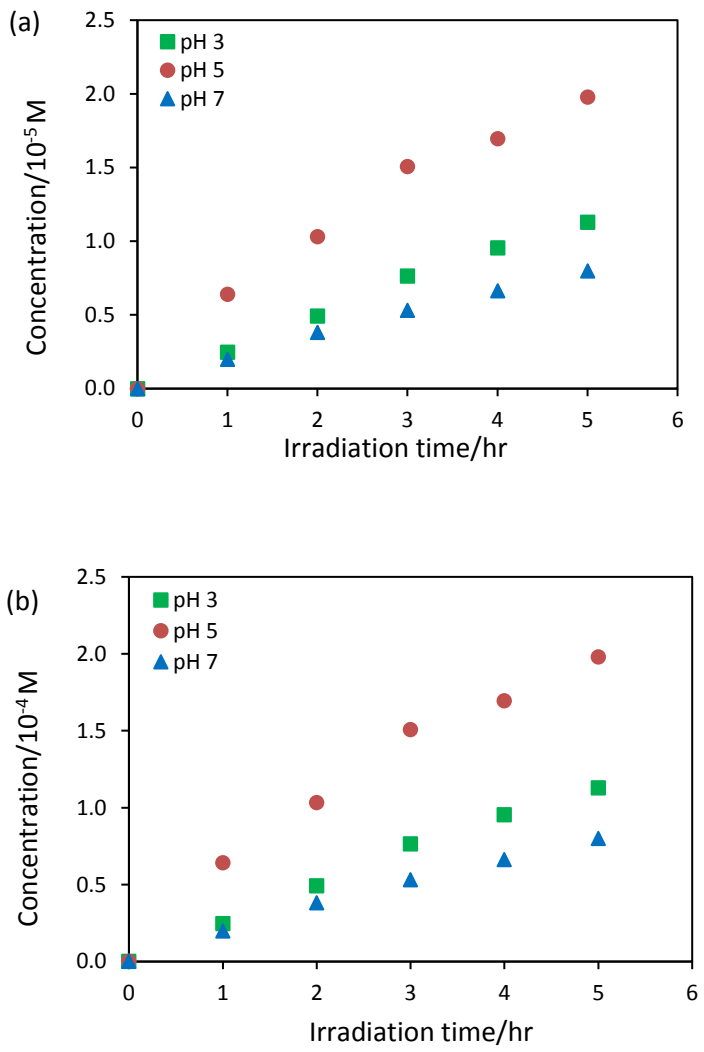

Figure 3.69: The concentration of thymine formed in water at different pH (3, 5 and 7) as observed (a) in the dilute solutions analysed and (b) in the actual solution irradiated.

Table 3.5: Summary of the percentage loss of AZT and thymine formed after 5 hours of irradiation.

% loss of AZT after 5 hours of irradiation								
	H_2O	**MeOH**	**EtOH**	**PrOH**	**ACN**	**pH 3**	**pH 5**	**pH 7**
C1	30	29	29	26	25			
C2	52	34	38	40	80	49	38	55
C3	58	50	32	49	58			
% thymine formed after 5 hours of irradiation								
C1	8.5	9.4	9.4	9.8	10			
C2	29	69	59	53	57	29	50	20
C3	30	38	47	46	50			

For some solutions the quantification indicated that more thymine was formed than AZT degraded (see **Table 3.5** shaded cells). Despite a thorough investigation of these anamolous results by carrying out repeat experiments, they also showed inconsistency in the percentage formation of thymine. The reason for this anomaly could not be ascertained.

3.4. Identification of the photoproducts

The photoproducts of AZT showed similar UV spectra and retention times in the HPLC analysis (see **Section 3.2**) for all different conditions of solvent, pH and concentration. Therefore, only one sample was analysed on LC-MS: the water sample. The photoproducts of AZT (4.94×10^{-4} M) in water obtained after 5 hours of irradiation were identified on a Shimadzu LC-MS 2020 Quadrupole MS in both positive and negative ESI modes. However, only positive mode was considered in this study because the negative mode only showed the AZT peak. The PDA chromatogram of AZT and its photoproducts is shown in **Fig. 3.70**.

The photoproducts P1 and thymine showed a shift in their retention times when eluted on the Shimadzu LC-MS system in variance to the elution times on the Agilent HPLC chromatograph. The HPLC retention time of the photoproduct P1 was 4.500 min and the retention time of thymine was 5.700 min on the Agilent HPLC system (see **Section 3.2**). However, on the Shimadzu LC-MS the two photoproducts switched positions, with thymine eluting earlier than photoproduct P1 (**Fig. 3.70**). This shift in the peak position could be due to change of instruments and columns.

The MS chromatogram of AZT and its photoproducts obtained on a Shimadzu LC-MS 2020 Quadrupole MS showed three peaks (P1, P2 and AZT) in the positive mode whereas in the negative mode only the peak of AZT was detected (**Fig. 3.71)**. The MS chromatogram obtained on a Waters Synapt G2 LC-MS detected P1 and AZT (**Fig. 3.72)**. Thymine (Thy) was not ionizable on both instruments and therefore was identified by spiking each sample with the standard and compared with the HPLC chromatogram of a thymine standard as described in **Section 3.2.3**.

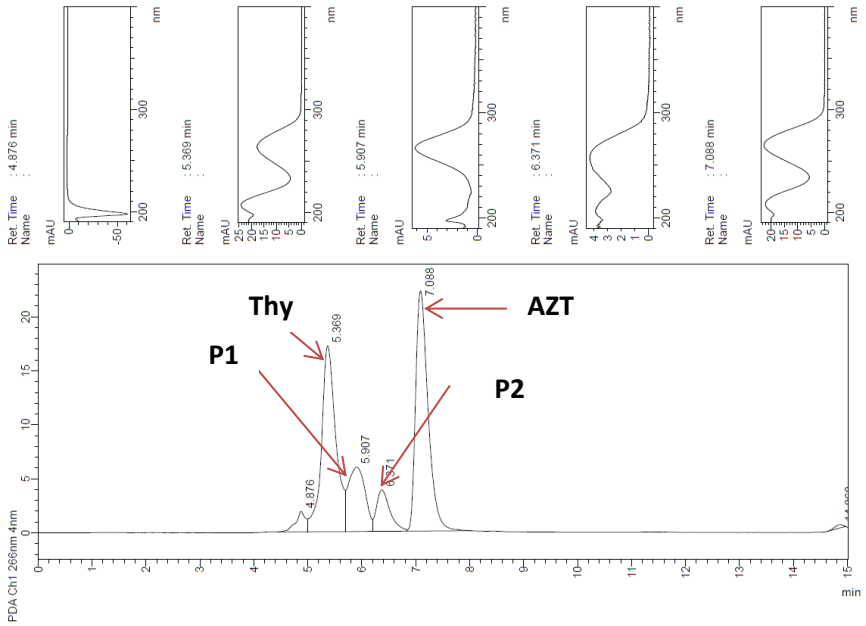

Figure 3.70: PDA chromatogram of AZT (4.94×10^{-4} M) and its photoproducts.

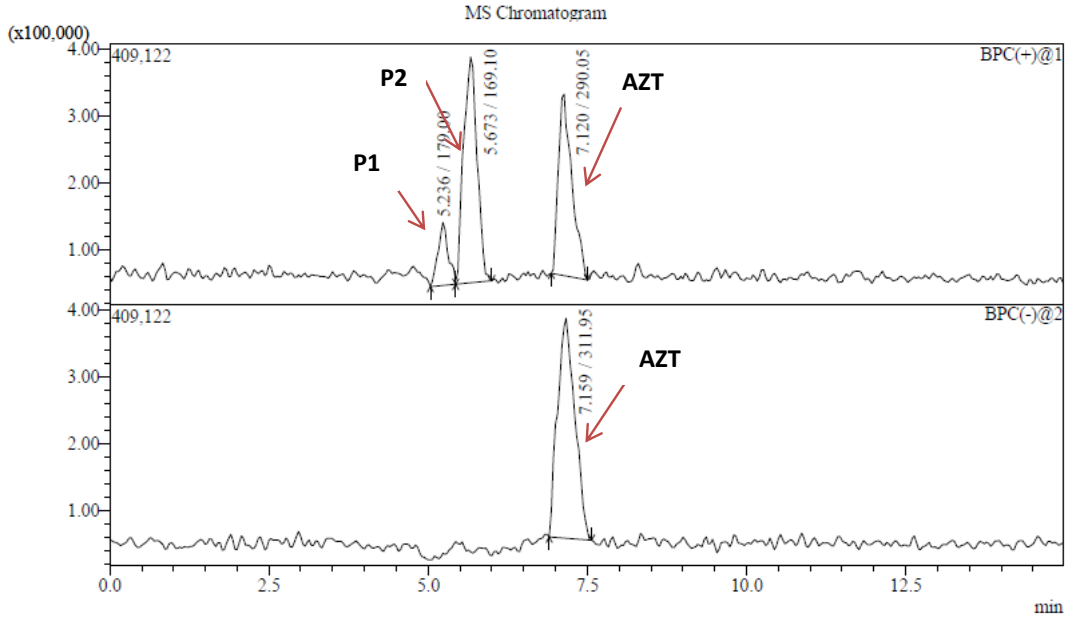

Figure 3.71: MS chromatogram of AZT and its photoproducts eluted on a Shimadzu Shim-pack GIST C18-HP (150 × 4.6 mm i.d., 3 µm particle size) column at 22 °C in the Shimadzu LC-MS 2020 Quadrupole MS instrument. The top chromatogram is in positive mode while the bottom one is in negative mode.

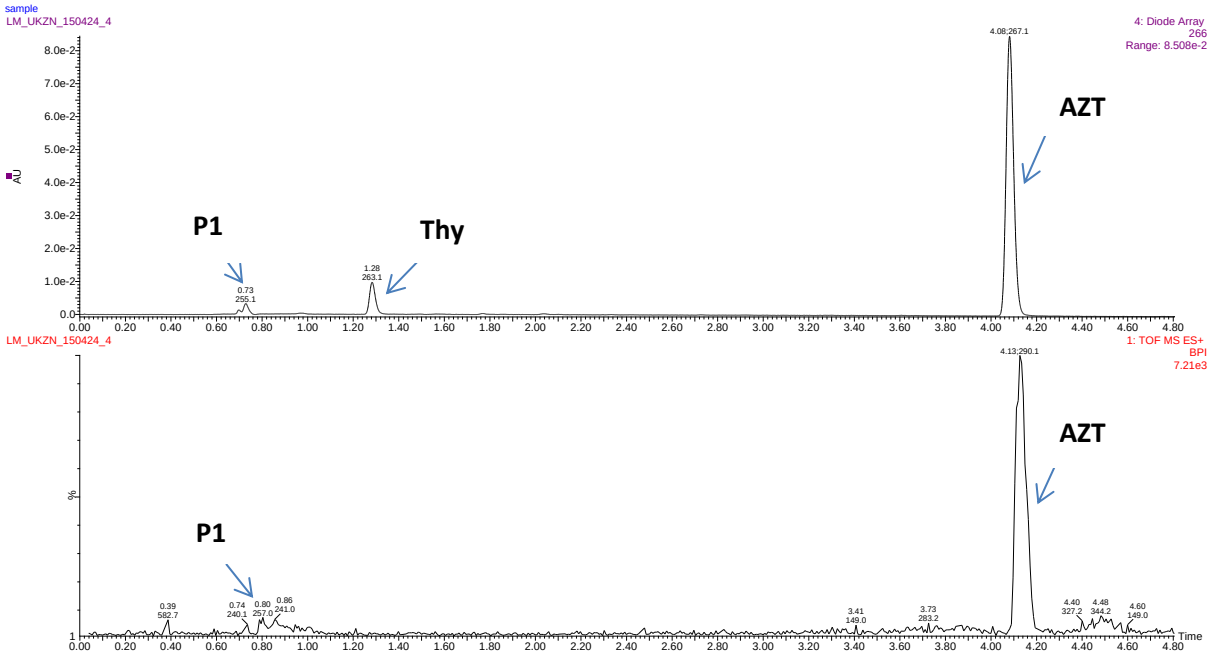

Figure 3.72: Chromatograms of AZT and its photoproducts obtained on a Waters Synapt G2 instrument. The mobile phase was methanol:water (60:40 v/v) and the detection wavelength was 266 nm. The top panel shows the PDA chromatogram and the bottom panel shows the MS chromatogram in positive mode.

AZT eluted at a retention time of 4.13 min (see **Fig. 3.72**) and showed a $[M + H]^+$ peak at *m/z* 391 on the mass spectrum and a base fragment at *m/z* 290 (**Fig. 3.73**). This molecular peak could arise from photo-induced dimerization of the photoproduct thymine (126) with a thymine moiety in undegraded AZT (267). The prominent fragment at *m/z* 290 is a sodium adduct of AZT (267 + 23).

The photoproduct (P1) with a retention time of 5.907 min (see **Fig. 3.70**) showed a $[M + H]^+$ peak at *m/z* 257 on the mass spectrum and a prominent fragment at *m/z* 179 (see **Fig. 3.74 (A)**). Although the peak was very small it was also confirmed from the MS chromatogram obtained from the Waters Synapt G2 LC-MS instrument (see **Fig. 3.72**). We propose that the photoproduct with *m/z* 257 results from the photo-induced elimination of molecular nitrogen to generate a nitrene as a reactive intermediate. The nitrene undergoes further intermolecular interaction with the solvent to form a hydroxylamine derivative as shown in **Scheme 3.1**. A similar photoproduct was reported by Iwamoto *et al.* [7] on UV-exposure of AZT. These authors reacted the hydroxylamine derivative formed with 2,3,5-triphenyl tetrazoliumchloride (TTC), reduced in alkali solution, known to form a purple colour [7]. The formation of the purple colour indicated the presence of the hydroxylamine moiety. The prominent peak at 179 results from the loss of the $C_2H_8NO_2$ fragment. Additionally, the proposed mechanism was informed by the fact that the UV spectrum of the photoproduct retains the same shape as the UV spectrum of AZT, therefore the thymine chromophore moiety is assumed to be retained.

In the case of the alcoholic solvents, methanol, ethanol, and 2-propanol, we assume addition of an alcoholic molecule in this position in place of the water molecule. The UV spectrum of the equivalent P1 photoproduct in acetonitrile showed a new absorption maximum at 355 nm in low and intermediate concentrations (see **Section 3.1.3**). In order to elucidate this new

absorption band Woodward-Fieser rules were employed to predict a suitable chromophore for that absorption. In this case we speculated that the photo-induced elimination of molecular nitrogen to generate a nitrene as a reactive intermediate, further undergoes intermolecular interaction with the solvent to form the new photoproduct (**Scheme 3.2**). Analysis of the chromophore is described as follows:

Base value for homoannular diene	= 253 nm
Alkyl substitutent or ring residue attached to parent diene	= 5 nm
Double bond extending conjugation	= 30 nm × 2 = 60 nm
O-Alkyl	= 6 nm
Exocyclic bond	= 5 nm
Alkyl substituent or ring residue in γ-position	= 18 nm
Total	= 347 nm

The calculated value of the absorption band (347 nm) is within the expected error range of the observed band at 355 nm, thus lending credence to the proposed structure in acetonitrile.

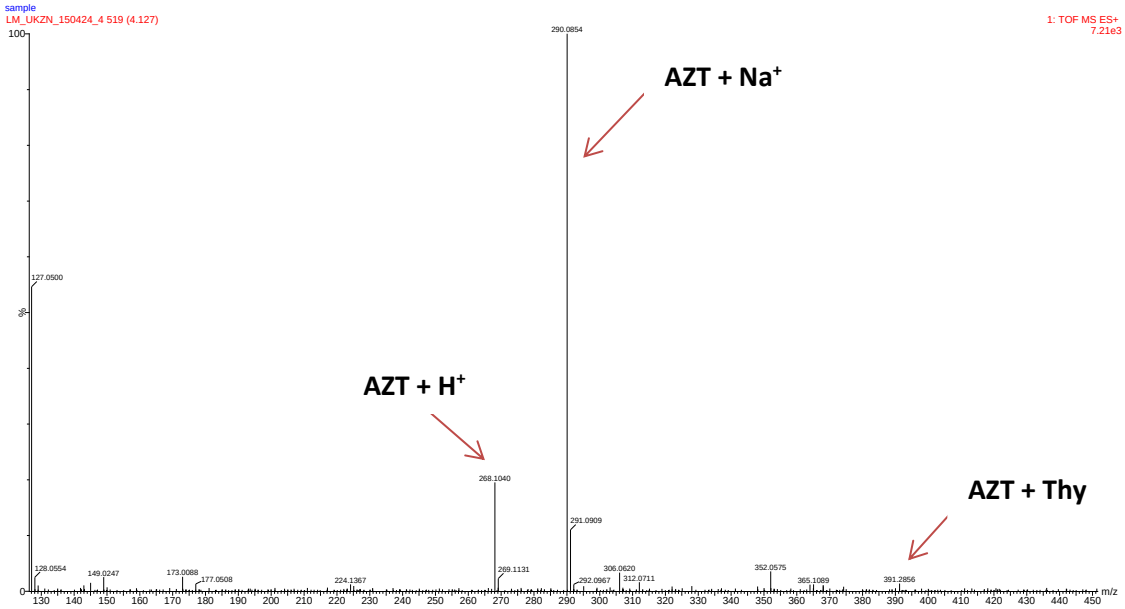

Figure 3.73: Mass spectrum of AZT obtained from the Waters Synapt G2 LC-MS instrument.

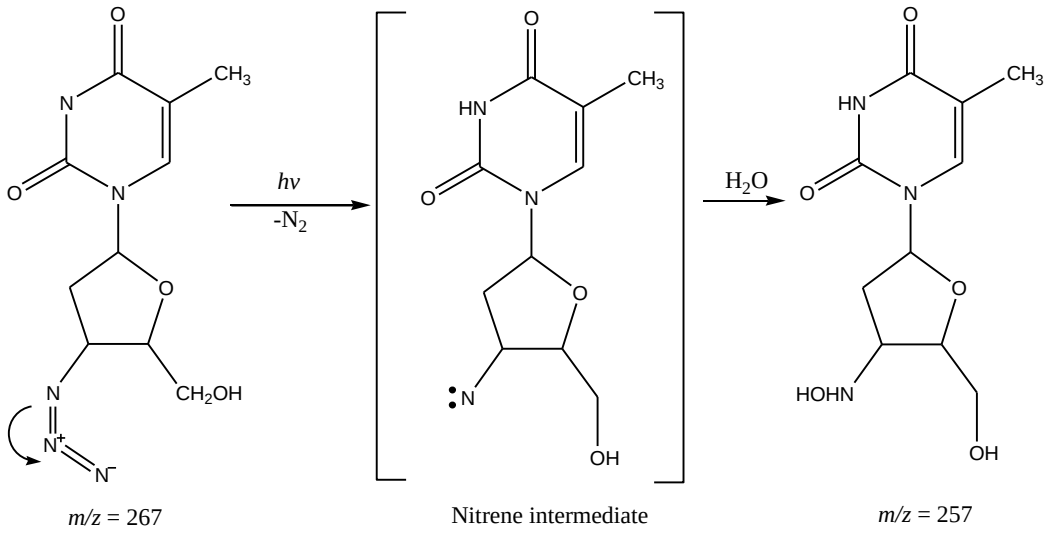

Scheme 3.1: The proposed mechanism for the formation of photoproduct P1 in water. In methanol, ethanol and 2-propanol, the HOH is replaced by the respective ROH.

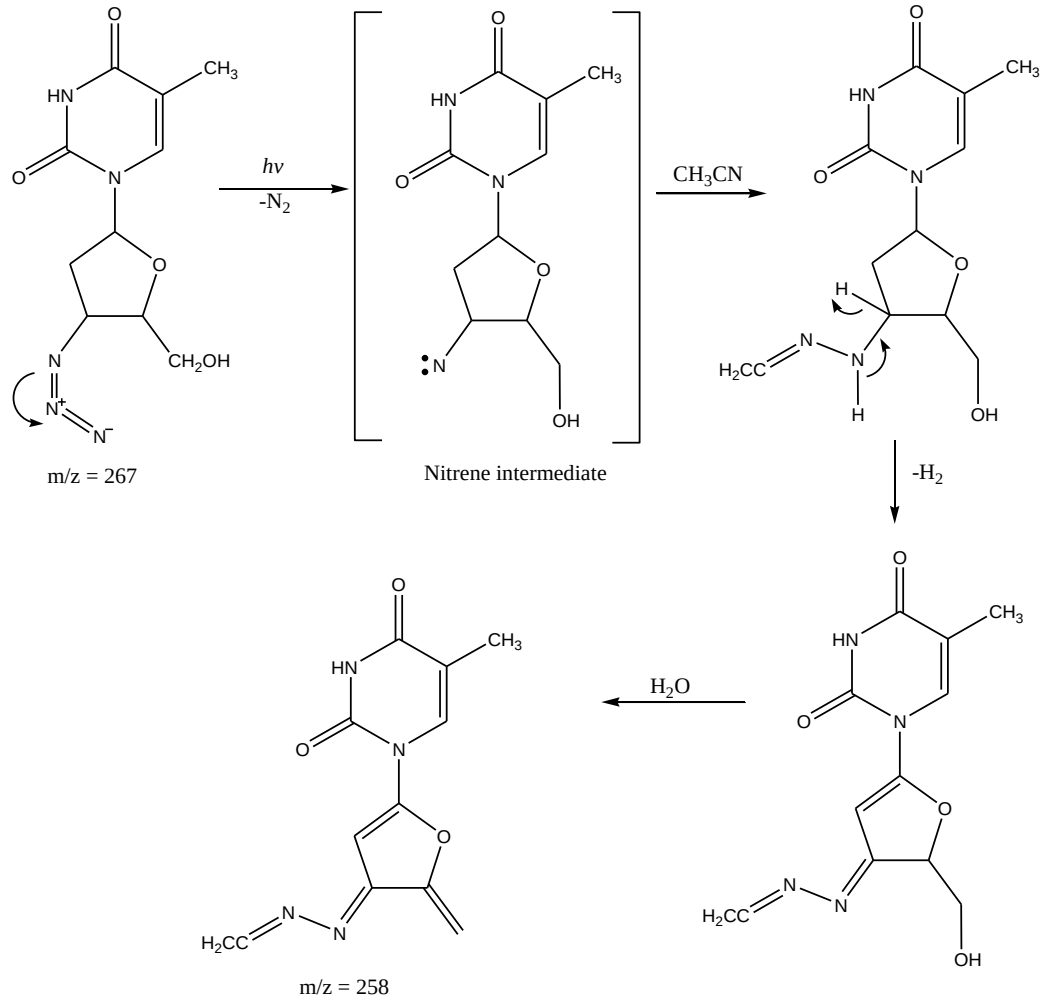

Scheme 3.2: The proposed mechanism for the formation of photoproduct P1 in acetonitrile.

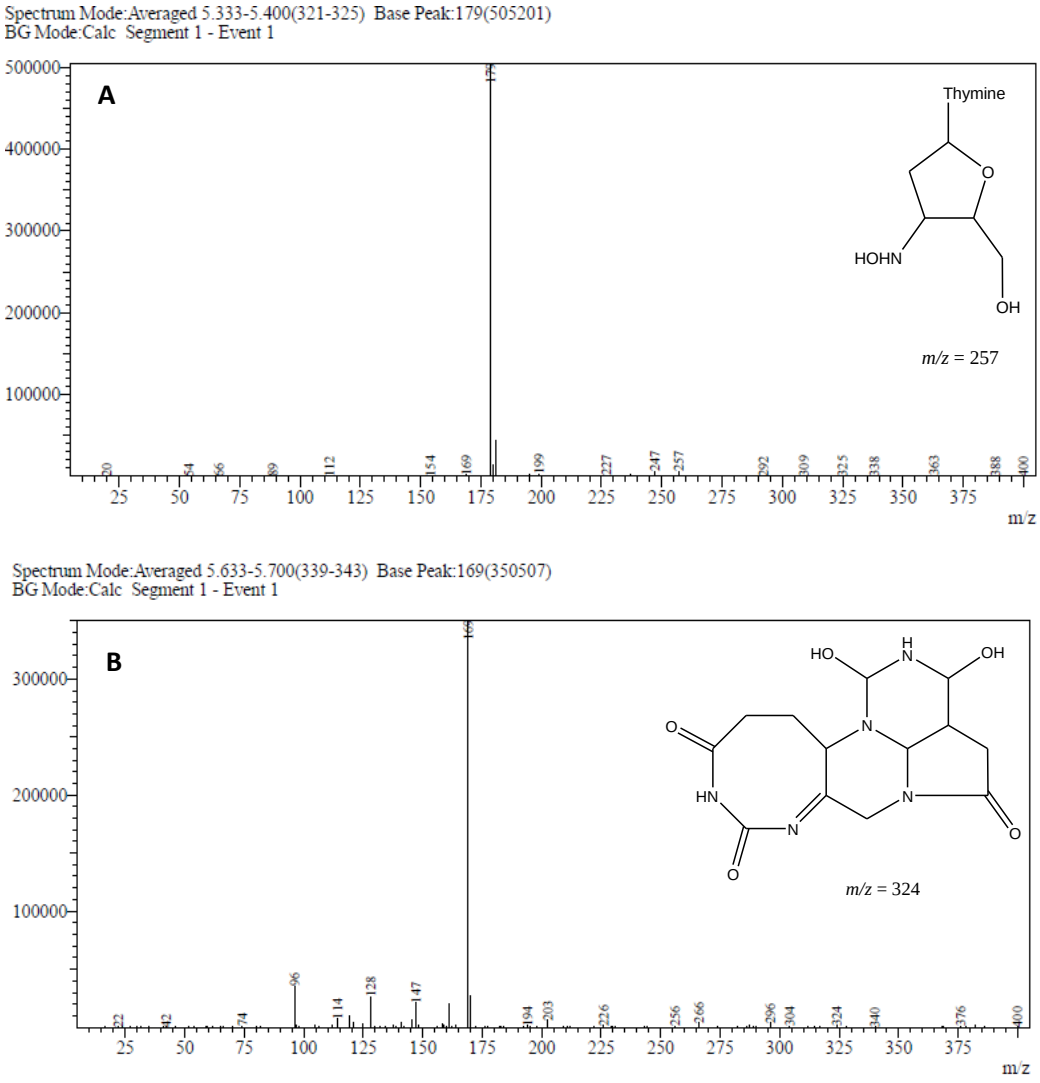

Figure 3.74: Mass spectra of photoproducts eluted on a Shimadzu Shim-pack GIST C18-HP (150 × 4.6 mm i.d., 3 µm particle size) column at 22 ºC in the Shimadzu LC-MS 2020 Quadrupole MS instrument. (A) photoproduct P1 and (B) photoproduct P2.

The photoproduct (P2) of AZT with a retention time of 6.371 min (see **Fig. 3.70**) showed a $[M + H]^+$ peak at *m/z* 324 with prominent fragments at *m/z* 296, 266, 169 and 114 (**Fig. 3.74)**. We propose that the peak at *m/z* 324 arises from the neutral loss of N_2 from the azido moiety which further undergoes Curtius rearrangement to form an isocyanate (see **Scheme 3.3**) [32]. A series of concerted excited state reactions are envisaged, coupled with a 4-membered ring closure which further undergoes ring expansion forming an 8-membered ring with the thymine moiety. The base peak at *m/z* 296 results from the elimination of a carbonyl group to

give the fragment-ion $C_{12}H_{17}N_5O_4$, whereas the base peaks at 266, 169, 114 result from the formation of $C_{10}H_{12}N_5O_4$, $C_7H_{11}N_3O_2$ and $C_4H_6N_2O_2$ respectively.

The photodegradation of AZT to thymine (retention time of 5.369 min, see **Fig. 3.70**) in water, methanol, ethanol and 2-propanol could be as a result of the loss of molecular nitrogen (N_2) accompanied by the concomitant intramolecular C-H insertion to form an aziridine moiety thus, occasioning a nucleophilic cleavage site. The angle-strained aziridine moiety may undergo a water induced ring opening to form the amide anion, which results in decomposition of the drug to thymine as the furanosyl moiety is cleaved (**Scheme 3.4**). The photodegradation of AZT to thymine in acetonitrile could also result from the loss of molecular nitrogen (N_2) accompanied by the concomitant intramolecular C-H insertion to form an aziridine moiety thus, occasioning a nucleophilic cleavage site. The angle-strained aziridine moiety may undergo a N-N π-overlapping with acetonitrile to give 1,3-dipolar resonance structures [120] which may further result in decomposition of thymine as the furanosyl moiety is cleaved (**Scheme 3.5**).

In summary, five photodegradation pathways were proposed to account for the photoproducts formed in protic and aprotic polar solvents.

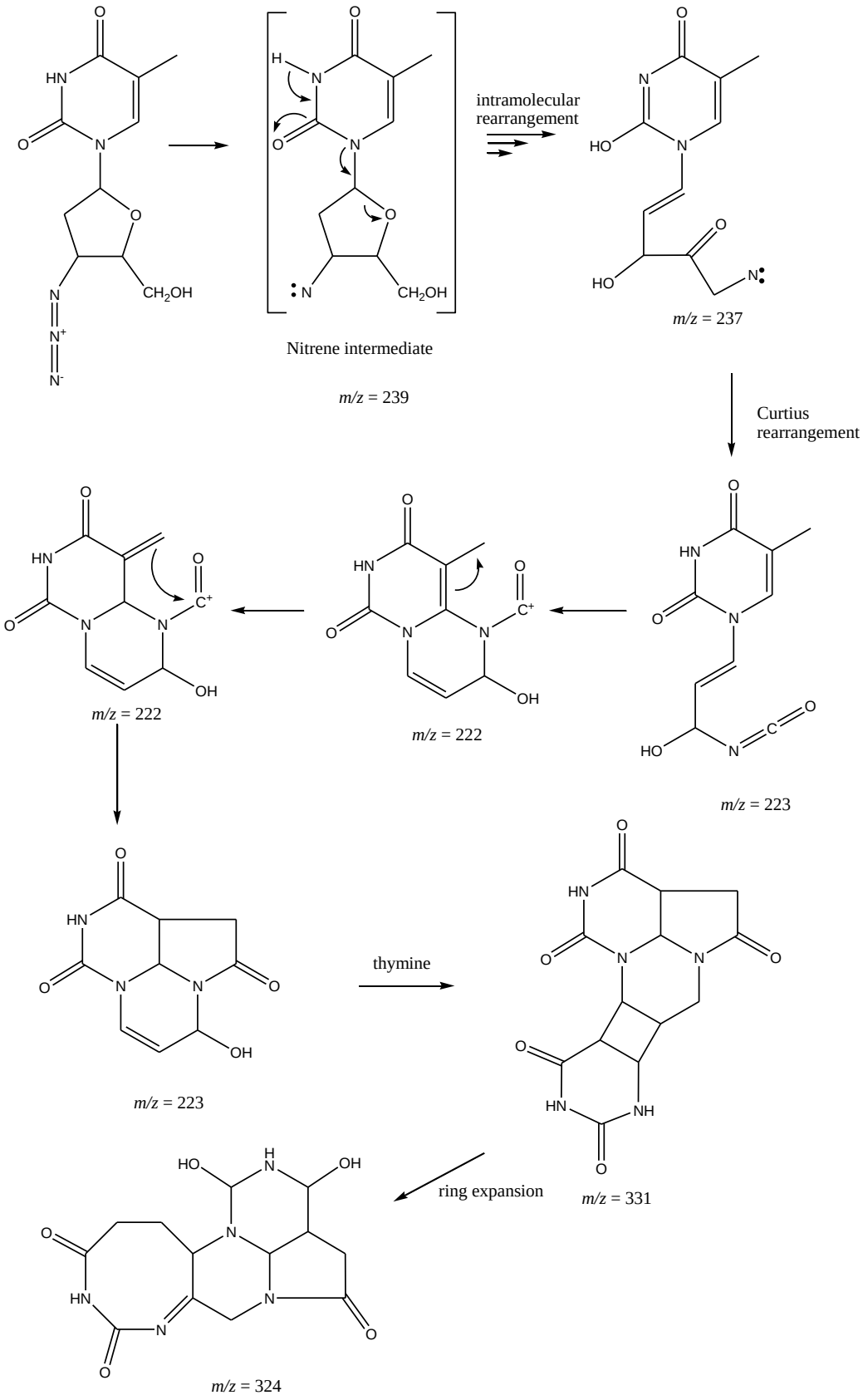

Scheme 3.3: The proposed mechanism for the formation of photoproduct P2 in water, methanol, ethanol, 2-propanol and acetonitrile.

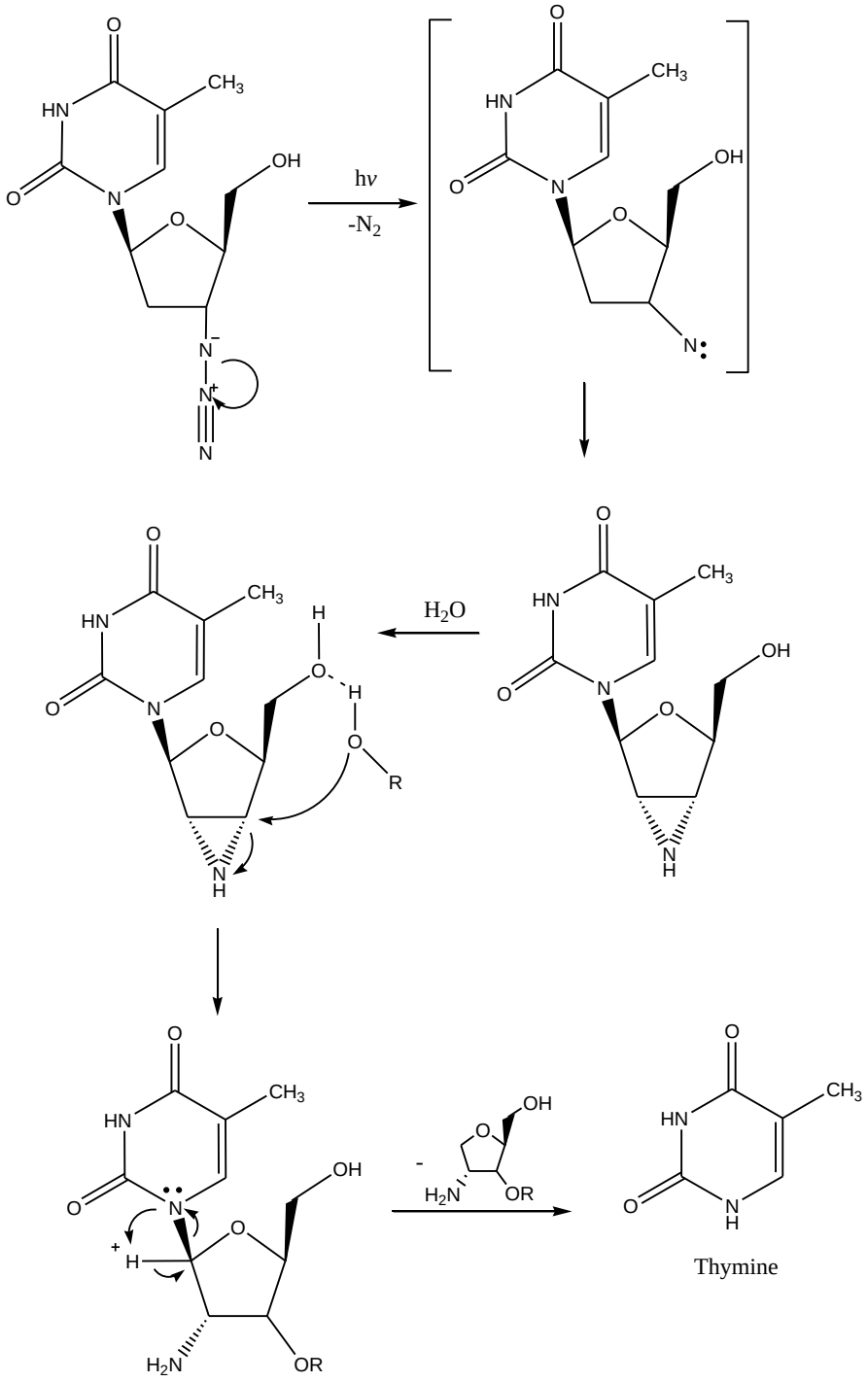

Scheme 3.4: Photodegradation pathway of AZT to thymine in water, methanol, ethanol and 2-propanol.

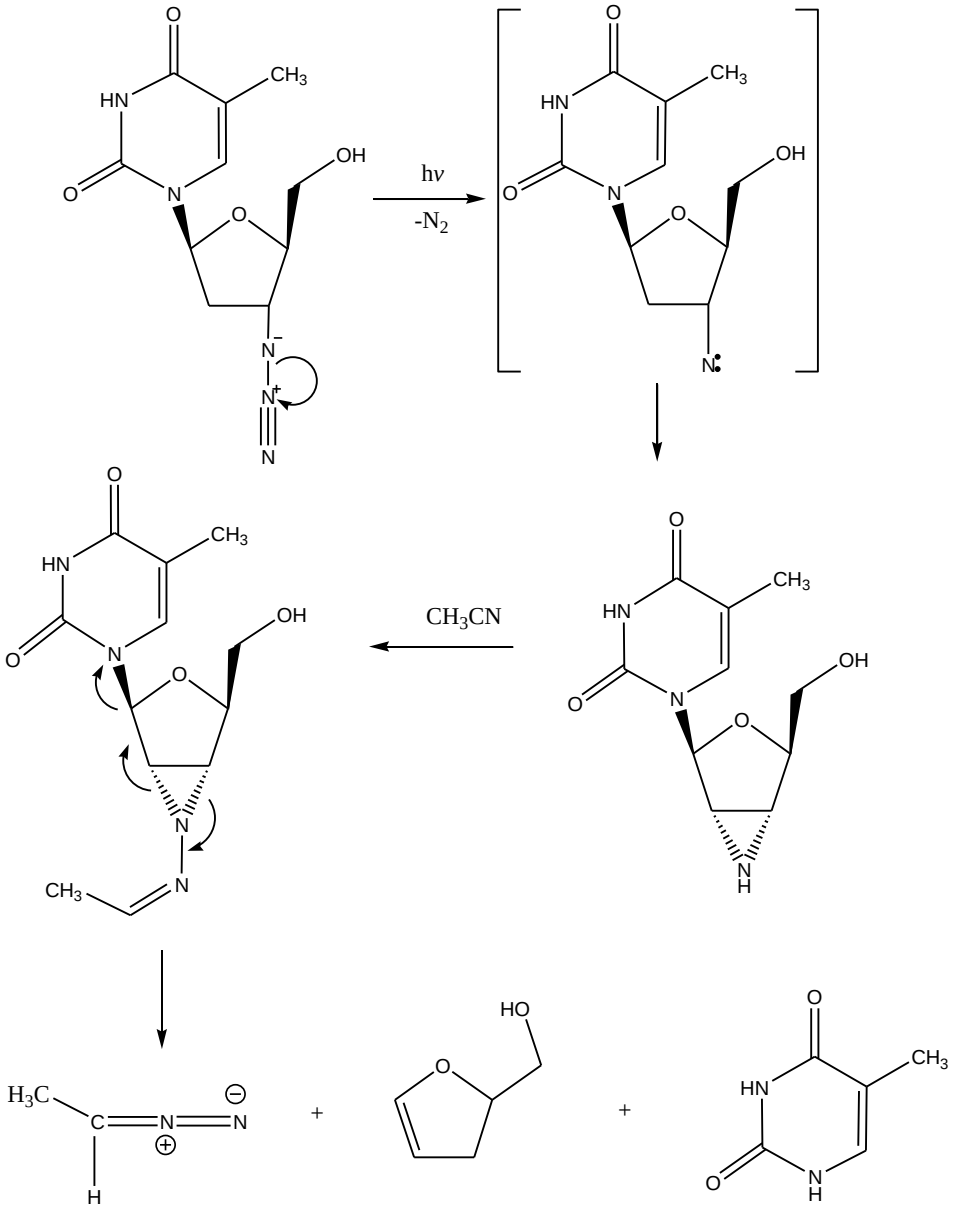

Scheme 3.5: Photodegradation pathway of AZT to thymine in acetonitrile.

CHAPTER 4

CONCLUSION

In this study the photochemical stability of AZT was studied under different conditions of solvent, pH and concentration. The photoproducts were monitored by UV/Vis spectroscopy and HPLC. Acetophenone was used as the internal standard for the quantification of AZT.

The results show that the photodegradation of AZT is strongly dependent on the solvent, the pH of the solution as well as on the initial concentration. The UV/Vis spectra of AZT upon photolysis showed a hyperchromic effect both at 213 and 265 nm in all of the different solvents, pH and concentration conditions. However, the change in absorbance was inconsistent with respect to irradiation time. We proposed that this could be attributed to competing absorption by the photoproducts formed during UV-exposure. The hypsochromic effect was also observed in all conditions of pH. A new absorption band at 355 nm was formed in acetonitrile which was predicted to be the result of elimination of nitrogen to generate a nitrene as a reactive intermediate, which may further undergo intermolecular interaction with the solvent to form new photoproducts.

The photodegradation products of AZT retained almost the same retention time and UV spectra under all the different conditions of solvent, pH and concentration. This indicates that the photoproducts formed have the same chromophore as AZT, which we propose to be a thymine moiety. Three photoproducts were formed at pH 5 and 7 and two photoproducts were formed at pH 3. For the effect of the initial concentration, three photoproducts were formed at the intermediate concentration (4.94×10^{-4} M) in all the different solvents, investigated. Three photoproducts were also formed at the lowest concentration (2.39×10^{-4} M) in all solvents, except in ethanol (two photoproducts were observed). Only one photoproduct was formed at high concentration (5.01×10^{-2} M) in water and acetonitrile and

two photoproducts were formed in alcoholic solutions (methanol, ethanol and 2-propanol). The HPLC peak area of AZT decreases with increase in irradiation time whereas the HPLC peak areas of the photoproducts increase with increase in irradiation time for all conditions of solvent, pH and concentration.

The photodegradation of AZT occurs faster as the dipole moment of the solvent increases in order: methanol < ethanol < water < acetonitrile, except for 2-propanol. The rate of photodegradation of AZT is more rapid at pH 7 than at pH 3 and 5. For water, methanol and 2-propanol, the rate of photodegradation was higher for the lowest concentration followed by the intermediate and highest concentration. For ethanol and acetonitrile, the rate of photodegradation was higher at the intermediate concentration followed by the lowest and highest concentrations. The mass spectral results revealed that the azido group was accountable for the photoreactivity of drug. Thymine was found to be the major photoproduct under all conditions of pH, solvent and concentration. Five photodegradation pathways mechanism were proposed to account for the photoproducts formed in protic and aprotic polar solvents.

4.1. Future work

This research should be furthered by investigating the following aspects:

1. The photochemical stability of AZT should be studied at low temperature in order determine whether the thymine moiety in AZT can form a dimer.

2. The photostability of AZT in the presence and absence of oxygen should be determined in different solvents, pH, and concentrations.

3. The kinetic rates of formation of the photoproducts and their quantum yields under different conditions should be measured.

REFERENCES

[1] H.H. Tonnesen, Photostability of drugs and drug formulations, CRC Press, Hoboken, 2004, pp. 1-2.

[2] I. Ahmad, S. Ahmed, Z. Anwar, M.A. Sheraz, M. Sikorski, Photostability and Photostabilization of Drugs and Drug Products, International Journal of Photoenergy, 2016 (2016) 1-19.

[3] V. Andrisano, C. Bertucci, A. Battaglia, V. Cavrini, Photostability of drugs: photodegradation of melatonin and its determination in commercial formulations, Journal of Pharmaceutical and Biomedical Analysis, 23 (2000) 15-23.

[4] E. De Clercq, Anti-HIV drugs: 25 compounds approved within 25 years after the discovery of HIV, International Journal of Antimicrobial Agents, 33 (2009) 307-320.

[5] D.W. Miller Jr, Fallacies in Modern Medicine: the HIV/AIDS Hypothesis, Journal of American Physicians and Surgeons, 20 (2015) 18-19.

[6] B.A. Diwan, C.W. Riggs, D. Logsdon, D.C. Haines, O.A. Olivero, J.M. Rice, S.H. Yuspa, M.C. Poirier, L.M. Anderson, Multiorgan transplacental and neonatal carcinogenicity of 3′-azido-3′-deoxythymidine in mice, Toxicology and Applied Pharmacology, 161 (1999) 82-99.

[7] T. Iwamoto, Y. Hiraku, S. Oikawa, H. Mizutani, M. Kojima, S. Kawanishi, Oxidative DNA damage induced by photodegradation products of 3′-azido-3′-deoxythymidine, Archives of Biochemistry and Biophysics, 416 (2003) 155-163.

[8] F.-X. Zhou, Z.-K. Liao, J. Dai, J. Xiong, C.-H. Xie, Z.-G. Luo, S.-Q. Liu, Y.-F. Zhou, Radiosensitization effect of zidovudine on human malignant glioma cells, Biochemical and Biophysical Research Communications, 354 (2007) 351-356.

[9] L. Celewicz, A. Jóźwiak, P. Ruszkowski, H. Laskowska, A. Olejnik, A. Czarnecka, M. Hoffmann, B. Hładoń, Synthesis and anticancer activity of 5′-chloromethylphosphonates of

3′-azido-3′-deoxythymidine (AZT), Bioorganic & Medicinal Chemistry, 19 (2011) 6375-6382.

[10] J.M. Pezzuto, M.E. Johnson, H.R. Manasse, Biotechnology and pharmacy, Springer Science & Business Media, British, 2013, pp. 253-254.

[11] C.-Y. Wu, L.Z. Benet, Predicting drug disposition via application of BCS: transport/absorption/elimination interplay and development of a biopharmaceutics drug disposition classification system, Pharmaceutical Research, 22 (2005) 11-23.

[12] L. Menendez-Arias, Mechanisms of resistance to nucleoside analogue inhibitors of HIV-1 reverse transcriptase, Virus Research, 134 (2008) 124-146.

[13] M.A. Raviolo, J.S. Trinchero-Hernández, G. Turk, M.C. Briñón, Synthesis and antiretroviral evaluation of derivatives of zidovudine, Journal of the Brazilian Chemical Society, 20 (2009) 1870-1877.

[14] M. Blessy, R.D. Patel, P.N. Prajapati, Y.K. Agrawal, Development of forced degradation and stability indicating studies of drugs—A review, Journal of Pharmaceutical Analysis, 4 (2014) 159-165.

[15] M. Brandl, R. Strickley, T. Bregante, G. Leo, T.W. Chan, Degradation of 4′-azidothymidine in aqueous solution, International Journal of Pharmaceutics, 93 (1993) 75-83.

[16] T. Huybrechts, M. Hermans, B. Van Hoof, G. Winderickx, C. De Neef, S. Hostyn, S. Vrielynck, W. Vermeulen, Photochemical stability of 4'-azido-2'-deoxy-2'-methylcytidine hydrochloride: structural elucidation of major degradation products by LC-MS and NMR analysis, Journal of Pharmaceutical and Biomedical Analysis, 70 (2012) 231-244.

[17] T. Douki, A. Reynaud-Angelin, J. Cadet, E. Sage, Bipyrimidine photoproducts rather than oxidative lesions are the main type of DNA damage involved in the genotoxic effect of solar UVA radiation, Biochemistry, 42 (2003) 9221-9226.

[18] A. Sosnik, D.A. Chiappetta, Á.M. Carcaboso, Drug delivery systems in HIV pharmacotherapy: What has been done and the challenges standing ahead, Journal of Controlled Release, 138 (2009) 2-15.

[19] S. Liu, S. Kokot, G. Will, Photochemistry and chemometrics—An overview, Journal of Photochemistry and Photobiology C: Photochemistry Reviews, 10 (2009) 159-172.

[20] R. Kumar, M. Yusuf, Chromones and bischromones: an account of photoinduced reactions, Arkivoc, 9 (2006) 239-264.

[21] E. Coyle, Green Photochemistry: The synthesis of fine chemicals with sunlight, PhD Thesis, Dublin City University, Dublin, 2010.

[22] P. Klán, J. Wirz, Photochemistry of organic compounds: From concepts to practice, John Wiley & Sons, 2009, pp. 26-28.

[23] R.P. Wayne, Photochemistry, Butterworths, London, 1970, pp. 8-9.

[24] G.R. Allen, Laser pyrolysis of selected halogenated compounds with $W(CO)_6$, PhD Thesis, The University of Auckland, Auckland, 2000.

[25] N. Gritsan, M. Platz, Photochemistry of azides: the azide/nitrene interface, John Wiley and Sons: Chichester, UK, 2010, pp. 311-364.

[26] G. L'abbe, Decomposition and addition reactions of organic azides, Chemical Reviews, 69 (1969) 345-363.

[27] V. Desikan, Y. Liu, J.P. Toscano, W.S. Jenks, Photochemistry of sulfilimine-based nitrene precursors: Generation of both singlet and triplet benzoylnitrene, The Journal of Organic Chemistry, 72 (2007) 6848-6859.

[28] S. Fantauzzi, A. Caselli, E. Gallo, Nitrene transfer reactions mediated by metallo-porphyrin complexes, Dalton Transactions, (2009) 5434-5443.

[29] J. Wang, J. Kubicki, G. Burdzinski, J.C. Hackett, T.L. Gustafson, C.M. Hadad, M.S. Platz, Early Events in the Photochemistry of 2-Naphthyl Azide from Femtosecond UV/Vis

Spectroscopy and Quantum Chemical Calculations: Direct Observation of a Very Short-Lived Singlet Nitrene, The Journal of Organic Chemistry, 72 (2007) 7581-7586.

[30] A. Reiser, F. Willets, G. Terry, V. Williams, R. Marley, Photolysis of aromatic azides. Part 4.—Lifetimes of aromatic nitrenes and absolute rates of some of their reactions, Transactions of the Faraday Society, 64 (1968) 3265-3275.

[31] R.O. Kan, Organic Photochemistry, McGraw-Hill, New York, 1966, pp. 248 -249.

[32] S. Bräse, C. Gil, K. Knepper, V. Zimmermann, Organic azides: an exploding diversity of a unique class of compounds, Angewandte Chemie International Edition, 44 (2005) 5188-5240.

[33] K. Komodziński, J. Nowak, J. Lepczyńska, J. Milecki, B. Skalski, Photochemistry of 6-azidopurine ribonucleoside in aqueous solution, Tetrahedron Letters, 53 (2012) 2316-2318.

[34] K. Komodziński, Z. Gdaniec, B. Skalski, Photochemical Behavior of 2-Azidopurine Tri-O-Acetylribonucleoside in Aqueous Solution: Unprecedented Transformation into 1-(5′-O-Acetyl-β-D-Ribofuranosyl)-5-[(2-Oxo-1,3,5-Oxadiazocan-4-Ylidene)Amino]-1H-Imidazole-4-Carbaldehyde, Nucleosides, Nucleotides and Nucleic Acids, 34 (2015) 235-245.

[35] D. Polshakov, S. Rai, R.M. Wilson, E.T. Mack, M. Vogel, J.A. Krause, G. Burdzinski, M.S. Platz, Photoaffinity labeling with 8-azidoadenosine and its derivatives: chemistry of closed and opened adenosine diazaquinodimethanes, Biochemistry, 44 (2005) 11241-11253.

[36] S. Gourdain, A. Martinez, C. Petermann, D. Harakat, P. Clivio, Unraveling the photochemistry of the 5-azido-2′-deoxyuridine photoaffinity label, The Journal of Organic Chemistry, 74 (2009) 6885-6887.

[37] C. Zhou, J. Chen, Q. Xie, X. Wei, Y. Zhang, Z. Fu, Photolysis of three antiviral drugs acyclovir, zidovudine and lamivudine in surface freshwater and seawater, Chemosphere, 138 (2015) 792-797.

[38] M.S. Chen, P.K. Chang, W.H. Prusoff, Photochemical studies and ultraviolet sensitization of *Escherichia coli* thymidylate kinase by various halogenated substrate analogs, Journal of Biological Chemistry, 251 (1976) 6555-6561.

[39] F. Peyrane, M. Cesario, P. Clivio, Photochemical ring expansion of 4-azidouracil: a route to 5 H-1, 3, 5-triazepin-2, 4-dione in the nucleoside series, The Journal of Organic Chemistry, 71 (2006) 1742-1745.

[40] B.T. Hill, M.S. Platz, Matrix isolation photolysis study of tetrazolo [1,5-b] pyridazine, Physical Chemistry Chemical Physics, 5 (2003) 1051-1058.

[41] M. Cerro-Lopez, N.P. Gritsan, Z. Zhu, M.S. Platz, A matrix isolation spectroscopy and laser flash photolysis study of 2-pyrimidylnitrene, The Journal of Physical Chemistry A, 104 (2000) 9681-9686.

[42] M.D. Shetlar, J. Chung, The Cyclobutane Dimers of 2′-Deoxyuridine, 2′-Deoxycytidine, 5-Methyl-2′-Deoxycytidine and 5-Bromo-2′-Deoxyuridine, Photochemistry and Photobiology, 88 (2012) 1236-1247.

[43] B.E. Billinghurst, S.A. Oladepo, G.R. Loppnow, Initial excited-state structural dynamics of thymine derivatives, The Journal of Physical Chemistry B, 116 (2012) 10496-10503.

[44] G. Boros, E. Miko, H. Muramatsu, D. Weissman, E. Emri, G.T. van der Horst, A. Szegedi, I. Horkay, G. Emri, K. Karikó, Identification of cyclobutane pyrimidine dimer-responsive genes using UVB-irradiated human keratinocytes transfected with in vitro-synthesized photolyase mRNA, PloS One, 10 (2015) 1-19.

[45] J.-S. Taylor, DNA, sunlight, and skin cancer, Journal of Chemical Education, 67 (1990) 835-841.

[46] A. Knips, M. Zacharias, Influence of a *cis, syn*-cyclobutane pyrimidine dimer damage on DNA conformation studied by molecular dynamics simulations, Biopolymers, 103 (2015) 215-222.

[47] R.P. Rastogi, A. Kumar, M.B. Tyagi, R.P. Sinha, Molecular mechanisms of ultraviolet radiation-induced DNA damage and repair, Journal of Nucleic Acids, (2010) 1-32.

[48] J. Yamamoto, K. Nishiguchi, K. Manabe, C. Masutani, F. Hanaoka, S. Iwai, Photosensitized [2+2] cycloaddition of N-acetylated cytosine affords stereoselective formation of cyclobutane pyrimidine dimer, Nucleic Acids Research, 39 (2011) 1165-1175.

[49] T. Douki, The variety of UV-induced pyrimidine dimeric photoproducts in DNA as shown by chromatographic quantification methods, Photochemical and Photobiological Sciences, 12 (2013) 1286-1302.

[50] J.L. Alderfer, S.D. Soni, A.V. Arakali, J.C. Wallace, UV irradiation of nucleic acids: characterization of photoproducts of thymidylyl-(3'-5′)-2′-deoxy-5-fluorouridine, Photochemistry and Photobiology, 57 (1993) 770-776.

[51] T. Douki, M. Court, J. Cadet, Electrospray–mass spectrometry characterization and measurement of far-UV-induced thymine photoproducts, Journal of Photochemistry and Photobiology B: Biology, 54 (2000) 145-154.

[52] K. Heil, D. Pearson, T. Carell, Chemical investigation of light induced DNA bipyrimidine damage and repair, Chemical Society Reviews, 40 (2011) 4271-4278.

[53] C.l. Desnous, D. Guillaume, P. Clivio, Spore photoproduct: a key to bacterial eternal life, Chemical Reviews, 110 (2009) 1213-1232.

[54] M.D. Shetlar, J. Chung, The (5-4) and (6-4) Adducts of 1-Methylthymine and Their Dewar Valence Isomers, Photochemistry and Photobiology, 87 (2011) 802-817.

[55] D.M. Ames, G. Lin, Y. Jian, J. Cadet, L. Li, Unusually large deuterium discrimination during spore photoproduct formation, The Journal of Organic Chemistry, 79 (2014) 4843-4851.

[56] K. Vandana, Studies of DNA base radical cations using anthraquinone photosensitization and radiation induced precursors of adenine nitrogen centred radicals, PhD Thesis, Mahatma Gandhi University, India, 2010.

[57] I. Saito, H. Sugiyama, T. Matsuura, Photoreaction of thymidine with alkylamines. Application to selective removal of thymine from DNA, Journal of the American Chemical Society, 105 (1983) 956-962.

[58] M.D. Shetlar, J. Chung, Opened-Ring Adducts of 5-Methylcytosine and 1, 5-Dimethylcytosine with Amines and Water and Evidence for an Opened-Ring Hydrate of 2′-Deoxycytidine, Photochemistry and Photobiology, 87 (2011) 818-832.

[59] M.D. Shetlar, K. Hom, V.J. Venditto, Photohydrate-Mediated Reactions of Uridine, 2′-Deoxyuridine and 2′-Deoxycytidine with Amines at Near Neutral pH, Photochemistry and Photobiology, 89 (2013) 869-877.

[60] T.I. Sølling, E.W.G. Diau, C. Kötting, S. De Feyter, A.H. Zewail, Femtochemistry of Norrish Type-I Reactions: IV. Highly Excited Ketones—Experimental, ChemPhysChem, 3 (2002) 79-97.

[61] V. Ramamurthy, X.-G. Lei, N.J. Turro, T.J. Lewis, J.R. Scheffer, Photochemistry of macrocyclic ketones within zeolites: competition between Norrish type I and type II reactivity, Tetrahedron Letters, 32 (1991) 7675-7678.

[62] S. Jockusch, H.-J. Timpe, W. Schnabel, N. Turro, Photoreduction of organic dyes in ketone amine systems, Journal of Photochemistry and Photobiology A: Chemistry, 96 (1996) 129-136.

[63] A. Albini, E. Fasani, Drugs, Photochemistry and Photostability, Royal Society of Chemistry, Cambridge, UK, 1998, pp. 4-47.

[64] D.E. Moore, S. Roberts-Thomson, D. Zhen, C.C. Duke, Photochemical studies on the antiinflammatory drug diclofenac, Photochemistry and Photobiology, 52 (1990) 685-690.

[65] J. Hemmens Violet, Photochemical sensitization by azathioprine and its metabolites. II. Azathioprine and nitroimidazole metabolites, Photochemistry and Photobiology, 43 (1986) 257-262.

[66] D. Budac, Photodecarboxylation: mechanism and synthetic utility, Journal of Photochemistry and Photobiology A: Chemistry, 67 (1992) 135-166.

[67] A.-B. Wu, Photolysis of indomethacin in methanol, Tetrahedron Letters, 38 (1997) 621-627.

[68] F. Vargas, C. Rivas, R. Machado, Z. Sarabia, Photodegradation of benzydamine: Phototoxicity of an isolated photoproduct on erythrocytes, Journal of Pharmaceutical Sciences, 82 (1993) 371-372.

[69] S. Caffieri, S. Dall'Acqua, I. Castagliuolo, P. Brun, G. Miolo, UVB photolysis of hydrocortisone 21-acetate, Journal of Pharmaceutical and Biomedical Analysis, 47 (2008) 771-777.

[70] J. Iqbal, A. Gupta, A. Husain, Photochemistry of clobetasol propionate, a steroidal anti-inflammatory drug, Arkivoc,, 11 (2006) 91-98.

[71] G. Wright, Photooxidation of reserpine, Journal of Pharmaceutical Sciences, 61 (1972) 299-300.

[72] J. Pawlaczyk, Photochemistry of photodynamic compounds. VII. Identification of certain products of sulfanilamide photolysis in aqueous solutions, Acta Poloniae Pharmaceutica, 31 (1974) 71-75.

[73] J. Pawlaczyk, Photochemistry of photodynamic compounds. V. Kinetics of sulfanilamide-35S photolysis in aqueous solutions, Acta Poloniae Pharmaceutica, 32 (1975) 465-469.

[74] D.E. Moore, M.P. Fallon, C.D. Burt, Photo-oxidation of tetracycline—a differential pulse polarographic study, International Journal of Pharmaceutics, 14 (1983) 133-142.

[75] S.I.S. Mubarak, Some aspects of the photochemical degradation of chloramphenicol, Pharmaceutica Acta Helvetiae, 57 (1982) 226-230.

[76] D.E. Moore, B.J. Wilkins, Common products from gamma-radiolysis and ultraviolet photolysis of metronidazole, International Journal of Radiation Applications and Instrumentation. Part C. Radiation Physics and Chemistry, 36 (1990) 547-550.

[77] V. Shetty Bhasker, Degradation of dacarbazine in aqueous solution, Journal of Pharmaceutical and Biomedical Analysis, 10 (1992) 675-683.

[78] J. Iqbal, Photooxidation of acyclovir in aqueous solution, Pharmazie, 60 (2005) 574-576.

[79] R. Frith, Application of clomiphene photolysis to assays based on analysis of the derived phenanthrenes, Journal of Chromatography A, 367 (1986) 260-266.

[80] R.T. Swasono, Photolytic decomposition of hydrochlorothiazide, Journal of Pharmaceutical Sciences, 72 (1983) 180-183.

[81] Y. Fu, Photooxidation of troglitazone, a new antidiabetic drug, Photochemistry and Photobiology, 63 (1996) 615-620.

[82] T. Doyle, Spectrophotometric study of dienestrol photoisomerization, Photochemistry and Photobiology, 27 (1978) 3-8.

[83] L.E. Piñero-Santiago, C. García, V. Lhiaubet-Vallet, J. Trzcionka, R. Oyola, K. Torres, J. Leguillú, M.A. Miranda, Photooxidation Mechanism of Levomepromazine in Different Solvents, Photochemistry and Photobiology, 89 (2013) 1479-1489.

[84] S. Dall'Acqua, D. Vedaldi, A. Salvador, Isolation and structure elucidation of the main UV-A photoproducts of vandetanib, Journal of Pharmaceutical and Biomedical Analysis, 84 (2013) 196-200.

[85] A. Dunge, A.K. Chakraborti, S. Singh, Mechanistic explanation to the variable degradation behaviour of stavudine and zidovudine under hydrolytic, oxidative and

photolytic conditions, Journal of Pharmaceutical and Biomedical Analysis, 35 (2004) 965-970.

[86] A. Dunge, N. Sharda, B. Singh, S. Singh, Validated specific HPLC method for determination of zidovudine during stability studies, Journal of Pharmaceutical and Biomedical Analysis, 37 (2005) 1109-1114.

[87] J.V.d. Santos, L.A.B.d. Carvalho, M.E. Pina, Development and validation of a RP-HPLC method for the determination of zidovudine and its related substances in sustained-release tablets, Analytical Sciences, 27 (2011) 283-289.

[88] M.I.R. Santoro, A.M. Taborianski, A.K. Singh, E.R. Kedor-Hackmann, Stability-indicating methods for quantitative determination of zidovudine and stavudine in capsules, Química Nova, 29 (2006) 240-244.

[89] S. Kumar, Spectroscopy of organic compounds, Cosmic Rays, 10 (2006) 4-36.

[90] H. Hamid, Preliminary Introduction of Spectroscopy, (2008).

[91] G.J. Mturi, An investigation of the photostabilisation of sunscreen absorbers by plant polyphenols, MSc Thesis, University of KwaZulu-Natal, Durban, 2005.

[92] J. Atanu Kumar, HPLC: Highly Accessible Instrument in Pharmaceutical Industry for Effective Method Development, Pharmaceutica Analytica Acta, 3 (2012) 2-9.

[93] S. Patwekar, R. Sakhare, N.N. Nilesh, HPLC method development and validation-A general concept, International Journal of Chemical and Pharmaceutical Sciences, 6 (2015) 1-14.

[94] M.-I. Aguilar, HPLC of Peptides and Proteins, Humana press Inc., New Jersey, 2004, pp. 9-22.

[95] B.L. Kedrowski, T. Shors, Methods to isolate anti-microbials from fruit or seed extracts, US20140004214, (2013) 1-22.

[96] R. Sajjanwar, S. Bhaskaran, K. Kakati, S.K. Jha, Simultaneous estimation of pyrantel pamoate, praziquantel and febantel by high perfomance liquid chromatography using dual wavelength, Journal of Applied Pharmaceutical Research, XI (2014) 32-43.

[97] T. Kupiec, Quality-control analytical methods: High-performance liquid chromatography, International Journal of Pharmaceutical Compounding, 8 (2004) 223-227.

[98] B.G. Jadhav, A.M. Jadhav, A.R. Shirode, V.J. Kadam, A Comprehensive Review for the Learners and Users: Preparative High Performance Liquid Chromatography, International Journal of Chemical and Pharmaceutical Analysis, 1 (2014) 121-129.

[99] K. Kimata, K. Iwaguchi, S. Onishi, K. Jinno, R. Eksteen, K. Hosoya, M. Araki, N. Tanaka, Chromatographic characterization of silica C18 packing materials. Correlation between a preparation method and retention behavior of stationary phase, Journal of Chromatographic Science, 27 (1989) 721-728.

[100] M. Swartz, HPLC detectors: a brief review, Journal of Liquid Chromatography & Related Technologies, 33 (2010) 1130-1150.

[101] L.R. Snyder, J.J. Kirkland, J.W. Dolan, Introduction to modern liquid chromatography, John Wiley & Sons, Canada, 2011, pp. 165-166.

[102] V.R. Meyer, Practical high-performance liquid chromatography, John Wiley & Sons, U.K., 2013, pp. 109-111.

[103] B. Matuszewski, M. Constanzer, C. Chavez-Eng, Strategies for the assessment of matrix effect in quantitative bioanalytical methods based on HPLC-MS/MS, Analytical Chemistry, 75 (2003) 3019-3030.

[104] H. Li, H. Li, X. Liu, B. Chen, Analysis of volatile flavor compounds in top fermented wheat beer by headspace sampling-gas chromatography, International Journal of Agricultural and Biological Engineering, 5 (2012) 67-75.

[105] K.M. Usher, S.W. Hansen, J.S. Amoo, A.P. Bernstein, M.E.P. McNally, Precision of Internal Standard and External Standard Methods in High Performance Liquid Chromatography, LC GC Chromatography online, 33 (2015) 40-46.

[106] P. Araujo, F. Couillard, E. Leirnes, K. Ask, A. Bøkevoll, L. Frøyland, Experimental design considerations in quantification experiments by using the internal standard technique: Cholesterol determination by gas chromatography as a case study, Journal of Chromatography A, 1121 (2006) 99-105.

[107] S. Lindsay, D. Kealey, Acol, High performance liquid chromatography, Published on behalf of ACOL, London by Wiley, Chichester [West Sussex], 1987, p. 236.

[108] M. Baumann, I.R. Baxendale, An overview of the synthetic routes to the best selling drugs containing 6-membered heterocycles, Beilstein Journal of Organic Chemistry, 9 (2013) 2265-2319.

[109] T. Gustavsson, N. Sarkar, Á. Bányász, D. Markovitsi, R. Improta, Solvent Effects on the Steady-state Absorption and Fluorescence Spectra of Uracil, Thymine and 5-Fluorouracil, Photochemistry and Photobiology, 83 (2007) 595-599.

[110] K. Polewski, S. Kniat, D. Slawinska, Gallic acid, a natural antioxidant, in aqueous and micellar environment: spectroscopic studies, Current Topics in Biophysics, 26 (2002) 217-227.

[111] C. Reichardt, T. Welton, Solvents and solvent effects in organic chemistry, John Wiley & Sons, Germany, 2003, pp. 389-445.

[112] F.A. Carey, R.J. Sundberg, Advanced Organic Chemistry: Part A: Structure and Mechanisms, Springer Science & Business Media, Virginia, 2007, pp. 230-231.

[113] M.J. Kamlet, J.L.M. Abboud, M.H. Abraham, R. Taft, Linear solvation energy relationships. 23. A comprehensive collection of the solvatochromic parameters, .pi.*,

.alpha., and .beta., and some methods for simplifying the generalized solvatochromic equationca, The Journal of Organic Chemistry, 48 (1983) 2877-2887.

[114] C. Reichardt, Solvatochromic dyes as solvent polarity indicators, Chemical Reviews, 94 (1994) 2319-2358.

[115] W.C. Mahoney, M.A. Hermodson, Separation of large denatured peptides by reverse phase high performance liquid chromatography. Trifluoroacetic acid as a peptide solvent, Journal of Biological Chemistry, 255 (1980) 11199-11203.

[116] A. Budruev, D. Sinjagina, S. Scobeleva, Photocyclization of 2-azidobenzophenone, 16 th International Electronic Conference on Synthetic Organic Chemistry (1-30 November 2012) ECSOC-16.

[117] K. Gallicano, Antiretroviral-drug concentrations in semen, Antimicrobial Agents and Chemotherapy, 44 (2000) 1117-1118.

[118] N.E. Mircescu, A. Varvescu, K. Herman, V. Chiş, N. Leopold, Surface-enhanced Raman and DFT study on zidovudine, Journal of Spectroscopy, 26 (2011) 311-315.

[119] A. Adhikary, D. Khanduri, V. Pottiboyina, C.T. Rice, M.D. Sevilla, Formation of Aminyl Radicals on Electron Attachment to AZT: Abstraction from the Sugar Phosphate Backbone versus One-Electron Oxidation of Guanine, The Journal of Physical Chemistry B, 114 (2010) 9289-9299.

[120] M.H. Akhtar, Electrocyclic reactions of aziridines, PhD Thesis, Simon Fraser University, Canada, 1970.

APPENDIX A: HPLC ANALYSIS

Table A 1: Peak areas of AZT and photoproducts for different solvents and concentrations as obtained for the diluted solutions analysed.

Irradiation time/hr	P1	Thy	P2	AZT
Water				
C1 = 5.01 × 10^{-2} M (values for diluted conc analyzed = 4.01 × 10^{-5} M)				
0	-	-	-	928.7
1	-	70.80	-	900.8
2	-	96.70	-	884.9
3	-	106.2	-	875.4
4	-	123.1	-	869.1
5	-	124.6	-	842.0
C2 = 4.94 × 10^{-4} M (values for diluted conc analyzed = 3.95 × 10^{-5} M)				
0	-	-	-	922.6
1	76.60	85.40	-	807.9
2	158.5	138.3	9.180	736.5
3	199.1	208.4	12.00	647.5
4	229.7	256.8	9.200	585.5
5	214.7	309.3	20.60	527.0
C3 = 2.39 × 10^{-4} M (values for diluted conc analyzed = 3.82 × 10^{-5} M)				
0	-	-	-	922.6
1	91.50	90.00	6.900	830.7
2	169.4	175.6	8.900	707.8
3	256.6	238.5	7.200	646.7
4	279.4	290.4	-	486.8
5	290.2	331.9	7.620	433.0
Irradiation time/hr	**P1**	**Thy**	**P2**	**AZT**
Methanol				
C1 = 5.01 × 10^{-2} M (values for diluted conc analyzed = 4.01 × 10^{-5} M)				
0	-	-	-	1238
1	-	84.50	5.900	1210
2	-	137.8	9.700	1156
3	-	182.2	8.820	1112
4	-	200.5	11.10	1094
5	-	140.3	12.00	1094
C2 = 4.94 × 10^{-4} M (values for diluted conc analyzed = 3.95 × 10^{-5} M				
0	-	-	-	1020
1	85.60	127.7	10.00	969.8
2	81.90	187.5	9.900	824.0
3	108.7	334.74	12.60	736.6

4	114.9	445.5	16.80	696.4
5	122.9	448.6	16.30	596.4
C3 = 2.39 × 10^{-4} M (values for diluted conc analyzed = 3.82 × 10^{-5} M)				
0	-	-	-	1020
1	35.10	101.6	6.900	901.3
2	51.60	202.1	8.900	825.7
3	68.10	302.0	7.200	750.1
4	84.60	402.7	12.20	674.6
5	74.00	450.7	7.850	649.1
Irradiation time/hr	**P1**	**Thy**	**P2**	**AZT**
Ethanol				
C1 = 5.01 × 10^{-2} M (values for diluted conc analyzed = 4.01 × 10^{-5} M)				
0	-	-	-	1093
1	-	63.40	10.80	1023
2	-	88.90	6.500	953.1
3	-	91.50	8.500	950.5
4	-	97.40	8.800	944.6
5	-	103.8	9.500	866.1
C2 = 4.94 × 10^{-4} M (values for diluted conc analyzed = 3.95 × 10^{-5} M)				
0	-	-	-	834.6
1	60.50	116.2	-	787.0
2	76.40	152.9	18.28	718.9
3	128.8	253.6	23.13	654.7
4	164.4	300.8	18.82	522.4
5	204.0	386.8	35.77	460.8
C3 = 2.39 × 10^{-4} M (values for diluted conc analyzed = 3.82 × 10^{-5} M)				
0	-	-	-	834.6
1	56.50	121.3	-	828.8
2	112.4	185.2	-	728.0
3	144.0	239.8	-	631.5
4	181.5	312.9	-	550.0
5	283.2	424.7	-	439.1
Irradiation time/hr	**P1**	**Thy**	**P2**	**AZT**
2-propanol				
C1 = 5.01 × 10^{-2} M (values for diluted conc analyzed = 4.01 × 10^{-5} M)				
0	-	-	-	1100
1	-	117.9	-	1035
2	-	108.4	9.200	919.0
3	-	136.5	5.700	896.1
4	-	131.3	9.200	890.9
5	-	91.91	9.500	823.4

C2 = 4.94 × 10^{-4} M (values for diluted conc analyzed = 3.95 × 10^{-5} M)				
0	-	-	-	1238
1	45.80	105.7	-	1000
2	47.80	183.6	6.900	905.1
3	69.40	281.7	17.60	812.5
4	75.50	336.8	15.70	699.3
5	101.0	393.4	12.70	638.4
C3 = 2.39 × 10^{-4} M (values for diluted conc analyzed = 3.82 × 10^{-5} M)				
0	-	-	-	875.6
1	74.10	150.6	6.200	765.0
2	112.0	256.6	5.500	719.2
3	133.2	346.3	8.800	567.5
4	159.4	448.0	18.67	499.4
5	199.3	492.5	14.70	426.4
Irradiation time/hr	**P1**	**Thy**	**P2**	**AZT**
Acetonitrile				
C1 = 5.01 × 10^{-2} M (values for diluted conc analyzed = 4.01 × 10^{-5} M)				
0	-	-	-	1018
1	-	61.10	-	956.9
2	-	73.80	-	944.4
3	-	86.50	-	842.6
4	-	103.2	-	825.8
5	-	114.9	-	963.6
C2 = 4.94 × 10^{-4} M (values for diluted conc analyzed = 3.95 × 10^{-5} M)				
0	-	-	-	1042
1	138.7	138.7	46.90	928.1
2	157.7	157.7	53.50	907.1
3	223.9	223.9	61.30	824.7
4	338.0	288.5	67.20	755.7
5	425.0	360.0	75.10	688.5
C3 = 2.39 × 10^{-4} M (values for diluted conc analyzed = 3.82 × 10^{-5} M)				
0	-	-	-	962.1
1	61.36	97.52	6.700	797.1
2	195.0	227.9	8.900	724.5
3	182.5	288.5	12.90	525.6
4	178.5	331.0	27.54	445.0
5	376.1	362.2	14.15	492.2

Table A 2: Peak areas of AZT and photoproducts at different pH in water.

Irradiation time/hr	P1	Thy	P2	AZT
pH 3				
0	-	-	-	908.5
1	30.20	99.50	-	754.2
2	63.70	126.7	-	706.4
3	70.90	201.6	-	657.9
4	154.5	303.3	-	479.5
5	170.5	329.4	-	426.2
pH 5				
0	-	-	-	906.0
1	72.80	117.5	-	831.3
2	191.2	223.9	8.100	731.8
3	257.4	273.6	10.60	609.6
4	303.1	314.3	16.70	517.4
5	332.4	360.7	12.50	454.1
pH 7				
0	-	-	-	941.9
1	88.70	106.6	9.200	809.5
2	173.3	154.0	11.80	754.6
3	291.0	243.2	12.10	608.4
4	353.6	298.0	23.30	549.0
5	394.6	343.7	25.60	485.4

APPENDIX B: QUANTIFICATION

Table B 1: Quantification of AZT in different solvents, concentrations and pH.

Response factor = 6.1382							
Conc.(IS) = 2.081×10^{-5} M							
Initial conc 1. = 4.008×10^{-5} M							
Initial conc 2. = 3.952×10^{-5} M							
Initial conc 3. = 3.824×10^{-5} M							
Irradiation time/hr	**Peak area of AZT**	**Peak area of IS**	**Area ratio**	**Conc. ratio**	**Conc. AZT in the diluted sample/10^{-5} M**	**Conc. AZT in the original sample/M**	**Loss in AZT/M**
Water							
C1 = 5.01×10^{-2} M							
1	835.9	85.7	9.754	1.589	3.307	4.13E-02	8.77E-03
2	782.3	85.8	9.118	1.485	3.091	3.86E-02	1.15E-02
3	782.3	86.2	9.075	1.479	3.077	3.85E-02	1.16E-02
4	780.4	85.3	9.149	1.490	3.101	3.88E-02	1.13E-02
5	716.8	86.8	8.258	1.345	2.800	3.50E-02	1.51E-02
C2 = 4.94×10^{-4} M							
1	770.6	84.3	9.141	1.489	3.140	3.87E-04	1.07E-04
2	727.0	91.1	7.980	1.300	2.706	3.38E-04	1.56E-04
3	646.3	87.4	7.395	1.205	2.507	3.13E-04	1.81E-04
4	583.5	88.0	6.631	1.080	2.248	2.81E-04	2.13E-04
5	489.1	86.6	5.648	0.920	1.915	2.39E-04	2.55E-04
C3 = 2.39×10^{-4} M							
1	786.8	85.2	9.235	1.504	3.131	1.96E-04	4.33E-05
2	699.9	89.5	7.820	1.274	2.651	1.66E-04	7.33E-05
3	645.8	91.6	7.050	1.149	2.390	1.49E-04	8.96E-05
4	634.7	90.5	7.013	1.142	2.378	1.49E-04	9.04E-05
5	425.0	90.6	4.691	0.764	1.590	9.94E-05	1.40E-04
Irradiation time/hr	**Peak area of AZT**	**Peak area of IS**	**Area ratio**	**Conc. ratio**	**Conc. AZT in the diluted sample/10^{-5} M**	**Conc. AZT in the original sample/M**	**Loss in AZT/M**
Methanol							
C1 = 5.01×10^{-2} M							
1	889.2	87.5	10.16	1.656	3.445	4.31E-02	7.03E-03
2	740.9	78.6	9.426	1.536	3.196	3.99E-02	1.02E-02
3	739.0	83.8	8.819	1.437	2.990	3.74E-02	1.27E-02
4	709.8	83.2	8.531	1.390	2.892	3.62E-02	1.39E-02
5	664.7	79.0	8.414	1.371	2.853	3.57E-02	1.44E-02
C2 = 4.94×10^{-4} M							
1	720.0	72.8	9.890	1.611	3.353	4.19E-04	7.49E-05
2	525.9	62.3	8.441	1.375	2.862	3.58E-04	1.36E-04
3	565.4	67.2	8.414	1.371	2.852	3.57E-04	1.37E-04

4	639.0	85.4	7.482	1.219	2.537	3.17E-04	1.77E-04
5	513.4	66.6	7.709	1.256	2.613	3.27E-04	1.67E-04
C3 = 2.39 × 10^{-4} M							
1	832.8	76.2	10.93	1.781	3.705	2.32E-04	7.42E-06
2	552.0	73.0	7.562	1.232	2.564	1.60E-04	7.88E-05
3	498.0	73.9	6.739	1.098	2.285	1.43E-04	9.62E-05
4	423.4	69.0	6.136	0.100	2.080	1.30E-04	1.09E-04
5	390.2	69.6	5.606	0.913	1.901	1.19E-04	1.20E-04
Irradiation time/hr	**Peak area of AZT**	**Peak area of IS**	**Area ratio**	**Conc. ratio**	**Conc. AZT in the diluted sample/10^{-5} M**	**Conc. AZT in the original sample/M**	**Loss in AZT/M**
Ethanol							
C1 = 5.01 × 10^{-2} M							
1	754.7	80.9	9.329	1.52	2.865	3.95E-02	1.06E-02
2	729.8	80.5	9.066	1.477	3.163	3.84E-02	1.17E-02
3	707.4	78.0	9.069	1.478	3.074	3.84E-02	1.17E-02
4	736.0	86.3	8.528	1.389	3.075	3.61E-02	1.40E-02
5	642.2	76.0	8.450	1.377	2.891	3.58E-02	1.43E-02
C2 = 4.94 × 10^{-4} M							
1	763.3	72.5	10.53	1.715	3.560	4.46E-04	4.78E-05
2	727.5	74.8	9.726	1.585	3.299	4.12E-04	8.18E-05
3	575.8	72.6	7.931	1.292	2.688	3.36E-04	1.58E-04
4	559.2	74.7	7.486	1.220	2.539	3.17E-04	1.77E-04
5	474.6	65.2	7.279	1.186	2.468	3.08E-04	1.86E-04
C3 = 2.39 × 10^{-4} M							
1	726.2	71.7	10.13	1.65	3.424	2.15E-04	2.44E-05
2	707.8	69.7	10.15	1.655	3.441	2.15E-04	2.38E-05
3	630.0	71.4	8.824	1.437	2.990	1.87E-04	5.20E-05
4	518.3	66.5	7.794	1.270	2.641	1.65E-04	7.39E-05
5	549.9	71.6	7.680	1.251	2.604	1.63E-04	7.63E-05
Irradiation time/hr	**Peak area of AZT**	**Peak area of IS**	**Area ratio**	**Conc. ratio**	**Conc. AZT in the diluted sample/10^{-5} M**	**Conc. AZT in the original sample/M**	**Loss in AZT/M**
2-propanol							
C1 = 5.01 × 10^{-2} M							
1	771.0	81.1	9.507	1.549	3.223	4.03E-02	9.81E-03
2	702.8	80.2	8.763	1.428	2.971	3.71E-02	1.30E-02
3	723.7	77.6	9.326	1.519	3.162	3.95E-02	1.06E-02
4	702.5	82.6	8.505	1.386	2.883	3.60E-02	1.41E-02
5	674.1	77.4	8.709	1.419	2.953	3.69E-02	1.32E-02
C2 = 4.94 × 10^{-4} M							
1	762.0	73.6	10.35	1.687	3.526	4.39E-04	5.52E-05
2	704.9	78.5	8.980	1.463	3.044	3.81E-04	1.13E-04
3	639.0	75.9	8.419	1.372	2.855	3.57E-04	1.37E-04

4	511.1	72.4	7.059	1.150	2.394	2.99E-04	1.95E-04
5	522.8	74.4	7.027	1.145	2.383	2.98E-04	1.96E-04
C3 = 2.39 × 10^{-4} M							
1	765.3	68.8	11.12	1.812	3.763	2.36E-04	3.30E-06
2	719.2	72.6	9.906	1.614	3.360	2.10E-04	2.91E-05
3	567.5	73.6	7.710	1.256	2.614	1.63E-04	7.56E-05
4	499.4	71.5	6.985	1.138	2.366	1.48E-04	9.10E-05
5	426.4	73.9	5.770	0.940	1.956	1.22E-04	1.17E-04
Irradiation time/hr	**Peak area of AZT**	**Peak area of IS**	**Area ratio**	**Conc. ratio**	**Conc. AZT in the diluted sample/10^{-5} M**	**Conc. AZT in the original sample/M**	**Loss in AZT/M**
Acetonitrile							
C1 = 5.01 × 10^{-2} M							
1	880.0	81.5	10.80	1.759	3.661	4.58E-02	4.34E-03
2	783.1	74.8	10.47	1.706	3.549	4.44E-02	5.73E-03
3	749.1	74.7	10.03	1.634	3.400	4.25E-02	7.60E-03
4	692.6	76.3	9.077	1.479	3.077	3.85E-02	1.16E-02
5	600.1	68.0	8.825	1.438	2.992	3.74E-02	1.27E-02
C2 = 4.94 × 10^{-4} M							
1	928.1	79.8	11.63	1.895	3.933	4.93E-04	1.13E-06
2	800.5	78.1	10.25	1.670	3.458	4.34E-04	5.96E-05
3	600.3	83.2	7.215	1.175	2.448	3.06E-04	1.88E-04
4	251.6	77.1	3.263	0.532	1.105	1.38E-04	3.56E-04
5	184.4	78.0	2.364	0.385	0.800	1.00E-04	3.94E-04
C3 = 2.39× 10^{-4} M							
1	812.9	82.7	9.830	1.601	3.333	2.08E-04	3.07E-05
2	724.5	76.3	9.495	1.547	3.221	2.01E-04	3.78E-05
3	530.4	78.7	6.740	1.098	2.285	1.43E-04	9.62E-05
4	384.3	78.8	4.877	0.795	1.653	1.03E-04	1.36E-04
5	377.0	80.1	4.707	0.767	1.596	9.97E-05	1.39E-04
Irradiation time/hr	**Peak area of AZT**	**Peak area of IS**	**Area ratio**	**Conc. ratio**	**Conc. AZT in the diluted sample/10^{-5} M**	**Conc. AZT in the original sample/M**	**Loss in AZT/M**
pH 3							
C2 = 4.94 × 10^{-4} M							
1	820.2	79.9	10.27	1.672	3.480	4.35E-04	5.90E-05
2	713.1	75.7	9.420	1.535	3.194	3.99E-04	9.48E-05
3	659.6	71.8	9.187	1.497	3.114	3.89E-04	1.05E-04
4	688.0	80.4	8.557	1.394	2.901	3.63E-04	1.31E-04
5	487.4	82.6	5.901	0.961	2.000	2.50E-04	2.44E-04
pH 5							
C2 = 4.94 × 10^{-4} M							
1	815.1	77.9	10.46	1.705	3.547	4.43E-04	5.06E-05
2	687.7	66.8	10.30	1.677	3.490	4.36E-04	5.77E-05
3	590.5	63.4	9.314	1.517	3.158	3.95E-04	9.93E-05

4	515.5	66.6	7.740	1.261	2.624	3.28E-04	1.66E-04
5	450.5	62.2	7.243	1.180	2.455	3.07E-04	1.87E-04
pH 7							
C2 = 4.94 × 10^{-4} M							
1	703.1	76.4	9.203	1.499	3.120	3.90E-04	1.04E-04
2	532.1	76.9	6.919	1.127	2.346	2.93E-04	2.01E-04
3	502.3	74.9	6.706	1.093	2.274	2.84E-04	2.10E-04
4	425.8	78.8	5.404	0.880	1.832	2.29E-04	2.65E-04
5	435.0	82.6	5.266	0.858	1.785	2.23E-04	2.71E-04

Table B 2: Formation of thymine at different solvent, concentration and pH.

Response factor = 5.9884						
Conc.(IS) = 2.081×10^{-5} M						
Initial conc 1. = 4.01×10^{-5} M						
Initial conc 2. = 3.95×10^{-5} M						
Initial conc 3. = 3.82×10^{-5} M						
Irradiation time/hr	**Peak area of Thy**	**Peak area of IS**	**Area ratio**	**Conc. ratio**	**Conc. Thy in the diluted sample/10^{-5} M**	**Conc. Thy formed in the original sample/M**
Water						
C1 = 5.01×10^{-2} M						
1	43.3	85.7	0.505	0.084	0.176	2.19E-03
2	70.4	85.8	0.821	0.137	0.285	3.56E-03
3	98.7	86.2	1.145	0.191	0.398	4.97E-03
4	85.8	85.3	1.006	0.168	0.350	4.37E-03
5	85.6	86.8	0.986	0.165	0.343	4.28E-03
C2 = 4.94×10^{-4} M						
1	56.0	84.3	0.664	0.111	0.231	2.89E-05
2	128	91.1	1.407	0.235	0.489	6.11E-05
3	209	87.4	2.394	0.400	0.832	1.04E-04
4	238	88.0	2.699	0.451	0.938	1.17E-04
5	288	86.6	3.324	0.555	1.155	1.44E-04
C3 = 2.39×10^{-4} M						
1	64.2	85.2	0.754	0.126	0.262	1.64E-05
2	149	89.5	1.665	0.278	0.579	3.62E-05
3	166	91.6	1.808	0.302	0.628	3.93E-05
4	268	90.5	2.961	0.495	1.029	6.43E-05
5	298	90.6	3.284	0.548	1.141	7.13E-05
Irradiation time/hr	**Peak area of Thy**	**Peak area of IS**	**Area ratio**	**Conc. ratio**	**Conc. Thy in the diluted sample/10^{-5} M**	**Conc. Thy formed in the original sample/M**
Methanol						
C1 = 5.01×10^{-2} M						
1	80.4	87.5	0.919	0.153	0.319	3.99E-03
2	83.7	78.6	1.065	0.178	0.370	4.63E-03
3	83.2	83.8	0.993	0.166	0.345	4.31E-03
4	83.8	83.2	1.007	0.168	0.350	4.38E-03
5	85.3	79	1.080	0.180	0.375	4.69E-03
C2 = 4.94×10^{-4} M						
1	68.6	72.8	0.942	0.157	0.678	8.47E-05
2	158	62.3	2.533	0.423	1.00	1.26E-04
3	225	67.2	3.354	0.560	1.33	1.66E-04
4	233	85.4	2.722	0.455	1.66	2.08E-04

5	273	66.6	4.104	0.685	2.75	3.43E-04
C3 = 2.39 × 10^{-4} M						
1	90.7	76.2	1.190	0.199	0.414	2.59E-05
2	139	73.0	1.908	0.319	0.663	4.14E-05
3	196	73.9	2.654	0.443	0.922	5.76E-05
4	241	69.0	3.497	0.584	1.215	7.60E-05
5	288	69.6	4.142	0.692	1.440	9.00E-05
Irradiation time/hr	**Peak area of Thy**	**Peak area of IS**	**Area ratio**	**Conc. ratio**	**Conc. Thy in the diluted sample/10^{-5} M**	**Conc. Thy formed in the original sample/M**
Ethanol						
C1 = 5.01 × 10^{-2} M						
1	65.0	80.9	0.803	0.134	0.279	3.49E-03
2	82.7	80.5	1.027	0.172	0.357	4.46E-03
3	69.4	78	0.890	0.149	0.309	3.86E-03
4	96.7	86.3	1.121	0.187	0.389	4.87E-03
5	82.6	76	1.087	0.181	0.378	4.72E-03
C2 = 4.94 × 10^{-4} M						
1	144	72.5	1.985	0.331	0.690	8.62E-05
2	185	74.8	2.477	0.414	0.861	1.08E-04
3	283	72.6	3.894	0.650	1.353	1.69E-04
4	352	74.7	4.714	0.787	1.638	2.05E-04
5	439	65.2	6.738	1.125	2.341	2.93E-04
C3 = 2.39 × 10^{-4} M						
1	95.9	71.7	1.338	0.223	0.465	2.90E-05
2	170	69.7	2.443	0.408	0.849	5.31E-05
3	248	71.4	3.472	0.580	1.207	7.54E-05
4	337	66.5	5.063	0.845	1.759	1.10E-04
5	372	71.6	5.191	0.867	1.804	1.13E-04
Irradiation time/hr	**Peak area of Thy**	**Peak area of IS**	**Area ratio**	**Conc. ratio**	**Conc. Thy in the diluted sample/10^{-5} M**	**Conc. Thy formed in the original sample/M**
2-propanol						
C1 = 5.01 × 10^{-2} M						
1	57.7	81.1	0.711	0.119	0.247	3.09E-03
2	60.9	80.2	0.759	0.127	0.264	3.30E-03
3	60.1	77.6	0.774	0.129	0.269	3.36E-03
4	63.4	82.6	0.768	0.128	0.267	3.33E-03
5	87.5	77.4	1.130	0.189	0.393	4.91E-03
C2 = 4.94 × 10^{-4} M						
1	145	73.6	1.967	0.329	0.684	8.55E-05
2	213	78.5	2.712	0.453	0.942	1.18E-04
3	285	75.9	3.759	0.628	1.306	1.63E-04
4	373	72.4	5.145	0.859	1.788	2.23E-04
5	447	74.4	6.001	1.002	2.086	2.61E-04

C3 = 2.39 × 10^{-4} M						
1	120	68.8	1.743	0.291	0.606	3.79E-05
2	161	72.6	2.215	0.370	0.770	4.81E-05
3	291	73.6	3.950	0.660	1.373	8.58E-05
4	350	71.5	4.900	0.818	1.703	1.06E-04
5	378	73.9	5.116	0.854	1.778	1.11E-04
Irradiation time/hr	**Peak area of Thy**	**Peak area of IS**	**Area ratio**	**Conc. ratio**	**Conc. Thy in the diluted sample/10^{-5} M**	**Conc. Thy formed in the original sample/M**
Acetonitrile						
C1 = 5.01 × 10^{-2} M						
1	43.5	81.5	0.534	0.089	0.185	2.32E-03
2	70.0	74.8	0.936	0.156	0.325	4.07E-03
3	77.8	74.7	1.042	0.174	0.362	4.52E-03
4	75.6	76.3	0.990	0.165	0.344	4.91E-03
5	79.3	68.0	1.166	0.195	0.405	5.07E-03
C2 = 4.94 × 10^{-4} M						
1	174	79.8	2.180	0.364	0.758	9.47E-05
2	269	78.1	3.446	0.575	1.197	1.50E-04
3	300	83.2	3.605	0.602	1.253	1.57E-04
4	291	77.1	3.776	0.630	1.312	1.64E-04
5	502	78.0	6.437	1.075	2.237	2.80E-04
C3 = 2.39 × 10^{-4} M						
1	110	82.7	1.324	0.221	0.460	2.88E-05
2	209	76.3	2.739	0.457	0.952	5.95E-05
3	278	78.7	3.531	0.590	1.227	7.67E-05
4	419	78.8	5.316	0.888	1.847	1.15E-04
5	442	80.1	5.517	0.921	1.917	1.20E-04
Irradiation time/hr	**Peak area of Thy**	**Peak area of IS**	**Area ratio**	**Conc. ratio**	**Conc. Thy in the diluted sample/10^{-5} M**	**Conc. Thy formed in the original sample/M**
pH 3						
C2 = 4.94 × 10^{-4} M						
1	56.6	79.9	0.708	0.118	0.246	3.08E-05
2	107	75.7	1.415	0.236	0.492	6.15E-05
3	158	71.8	2.200	0.367	0.764	9.55E-05
4	221	80.4	2.745	0.458	0.954	1.19E-04
5	268	82.6	3.249	0.543	1.129	1.41E-04
pH 5						
1	144	77.9	1.843	0.308	0.641	8.01E-05
2	198	66.8	2.970	0.496	1.032	1.29E-04
3	275	63.4	4.336	0.724	1.507	1.88E-04
4	325	66.6	4.877	0.814	1.695	2.12E-04
5	354	62.2	5.695	0.951	1.979	2.47E-04
pH 7						

1	43.8	76.4	0.573	0.096	0.199	2.49E-05
2	84.2	76.9	1.095	0.183	0.380	4.76E-05
3	114	74.9	1.526	0.255	0.530	6.63E-05
4	150	78.8	1.909	0.319	0.663	8.29E-05
5	190	82.6	2.299	0.384	0.799	9.99E-05